EnergyChem 5 (2023) 100107

Contents lists available at ScienceDirect

EnergyChem

journal homepage: www.sciencedirect.com/journal/energychem

Microenvironment effect of covalent organic frameworks on chemical catalysis

Qingyan Pan [a], Zepeng Lei [b], Yingjie Zhao [a,*], Wei Zhang [b,*]

[a] College of Polymer Science and Engineering, Qingdao University of Science and Technology, 53 Zhengzhou Road, 266000 Qingdao, China
[b] Department of Chemistry, University of Colorado Boulder, Boulder, CO 80309, United States

ARTICLE INFO

Keywords:
Covalent organic frameworks
Organocatalysis
Asymmetric organocatalysis
Confined effect
Microenvironment

ABSTRACT

Inspired by enzymatic catalysis, a variety of covalent organic frameworks (COFs), which have precisely engineered microenvironments enabled by the well-defined porous channels and cavities with catalytically active sites built in, have been developed to mimic the catalytic process of enzymes. The structure diversity and customizability of COFs make them an ideal platform for studying the catalyst structure-activity relationship in heterogeneous catalysis and obtaining a thorough understanding of the catalytic mechanisms. In this review, we summarize the recent progress in the development of COF materials for catalysis applications, with a particular focus on their microenvironment effects. Representative examples of organocatalysis, asymmetric organocatalysis, and metal-supported catalysis utilizing the microenvironment effect enabled by diversified COF materials are discussed. Finally, we outline the key fundamental issues to be addressed and provide our perspectives on the future of COF-based catalysis.

1. Introduction

Enzymatic catalysis in nature provides an exemplary illustration of selectively controlled reactions that are achieved through the utilization of protein pockets with exceptional efficiency [1,2]. This natural process has inspired the development of porous materials such as the inorganic zeolites [3–6], mesoporous silicas [7–10], metal-organic frameworks (MOFs) [10–22], and covalent organic frameworks (COFs) [23–26] that mimic the catalytic process of enzymes by utilizing porous structures containing channels and cavities with reactive sites. COFs, as a class of crystalline porous organic materials that contain no metal cluster nodes, have witnessed rapid developments since the pioneering work by Yaghi and co-workers reported in 2005 [27–29]. Such frameworks offer a unique combination of advantages, including those of traditional inorganic porous materials, such as well-defined structures, high surface area, and heterogeneous catalytic ability, as well as those of porous organic polymers, such as chemical diversity, structural stability, and customizability [23,25]. This allows for a variety of applications, such as gas storage/separation, which utilize the confined channels for precise molecule recognition within COFs, and the introduction of abundant catalytic active sites installed within the skeletons due to the tunability [24,30]. Nevertheless, COFs with these benefits make them an ideal platform for gaining a thorough understanding of the mechanisms involved in heterogeneous catalysts [25,30-32]. Numerous studies, along with several notable reviews, have explored the potential of COFs as promising materials for various catalytic applications, including organocatalysis [33–35], electrocatalysis [32,36], and photocatalysis [37–40].

The regular channels derived from the highly ordered structures of the COFs provide a special and stable microenvironment for the chemical reaction to occur inside the channels. The characteristics of the microenvironment, such as physical dimension, active sites located in the channels, and even the chirality, can be tuned through chemical synthesis and modification. A detailed discussion of the characteristics of COFs for catalysis – the influence of the microenvironment created by the well-defined structures of COFs, has yet to be conducted. To be more specific, the concept of the microenvironment has been widely accepted and utilized in the field of zeolites, but in COF materials, the study of the microenvironment effect in catalysis is still in its nascent stage. Many studies have shown that the microenvironment plays a key role in COF-catalyzed reactions. The precisely engineered microenvironments enabled by the highly ordered channels decorated with functional groups undoubtedly make these materials perfect candidates for emulating enzymatic catalysis in nature. The specific locations in the

* Corresponding author.
E-mail addresses: yz@qust.edu.cn (Y. Zhao), wei.zhang@colorado.edu (W. Zhang).

https://doi.org/10.1016/j.enchem.2023.100107

Available online 13 October 2023

catalyst possessing catalytic activity are called active sites, which could come from either the COF structures themselves or the post-introduced active substances such as metal species. To construct these catalytic active COFs, both the linkers and nodes could be designed to *in-situ* integrate the active sites into the frameworks. Alternatively, these active sites could also be introduced through the post-synthetic method. In addition, some active metal nanoparticles (MNPs) and enzymes could also be physically loaded in the pores of the COFs. The size of the channel, the shape of the pore, and the active site can be well-controlled through rational design and bottom-up synthesis, leading to the formation of "nanoreactors". Therefore, microenvironment effects could be systematically studied since the reaction occurs within the "nanoreactor".

In industrially relevant processes, heterogeneous catalysts have been extensively used due to their easy operation and recoverability [41]. Research on traditional heterogeneous catalysts usually focuses on catalytic performance, including selectivity, turnover numbers, and reusability. The exact porous structures, such as channels or cavities, usually receive less attention due to the difficulties in studying them at the molecular level. Although heterogeneous catalysis at the molecular level, such as microporous structures containing pores of less than 2 nm, can be realized in zeolites, the limited diversity in elemental composition and structure impedes studies of the structure-activity relationship (Scheme 1). Meanwhile, despite porous organic polymers [42,43] have been reported for catalysis application, the exact catalytic sites and their spatial distributions are still not well understood due to their amorphous nature (Scheme 1). Constructing catalytically identical microenvironments with those active sites in well-defined highly ordered structures still represents a grand challenge.

COFs, as a novel class of crystalline organic porous materials, offer significant advantages in terms of structural diversity. By using the "toolbox" of organic synthesis, the pore sizes, functional groups, and porous structures can be tuned at the molecular level (Scheme 1). In addition, the highly ordered framework can usually provide well-defined channels with specific active sites. These characteristics make COFs an excellent platform for studying heterogeneous catalysis. The superiorities of heterogeneous nature and uniform catalytic sites (microenvironment) are well integrated into the system of COFs.

To utilize the advantages of COFs and realize these functions, the diversified design of COFs is critical. The understanding of both the structure-activity relationship and the key role of the microenvironment depends on the rational design of diversified COF structures. The design of COFs materials should be topologically feasible. The combination of the planar C2, C3, C4, C6 symmetric building blocks are commonly used in constructing 2D COFs, while the tetrahedral C4 building blocks are mainly employed in constructing 3D COFs [44–46]. In terms of the linkages, COFs can be constructed using a variety of chemistries such as B—O bonds [27,47-49], C═N bonds [50,51], oxazole[52,53], thiazole [54,55], vinylene [56,57], sp^2 C═C [58,59], hydroxyimine or hydroxyamine [60,61,62], aryl ether [63], pyrazine [64,65], dioxin [66], imidazole [67], aromatic thieno[3,2-c]pyridine [68], cyanurate [69], etc. Over the past two decades, significant advances have been made not only in the design and synthesis of building blocks for COFs but also in the chemistry used for constructing diverse COF materials. Thousands of COF materials have been successfully prepared and have found applications in a wide range of fields, such as adsorption/separation, gas storage, catalysis, sensing, energy storage, and drug delivery.

The incorporation of catalytically active sites into the COF backbones is critical to the design of COFs-based catalysts. And a wide variety of organic moieties with different catalytic functionalities can be readily integrated into COFs structures. Therefore, to create COFs with catalytic activity, it is essential to employ rational design and introduce functional groups into building blocks. Through the bottom-up design strategy, the building blocks are connected in a pre-designed manner to construct 2D or 3D frameworks and directly immobilize the functionalities or active sites on the pore surface within COFs. This *in-situ* approach offers precise active sites, high functional group density, and uniform distribution of active sites in COFs. On the other hand, specific functionalities can be introduced into COFs through post-synthetic modification. Using this strategy, various active sites can be installed on the COF backbones, avoiding the possible dissolution of catalytic sites or decreased framework crystallinity during *in-situ* COF synthesis. However, this approach usually leads to smaller quantities of active sites. Also, the post-introduced active sites are sometimes unfavorable for high crystallinity and porosity of the parent COFs. Thus, the post-modified strategy, also called the "two-step" synthetic strategy, is commonly adopted to incorporate the catalytic sites within the COFs if the as-prepared COFs possess excellent stability and rigidity.

Besides the characteristics of the uniform pores and channels in the COFs materials, the π-conjugated structures in COFs endow them with excellent semiconductor properties. Therefore, COFs have also exhibited efficient electro/photo-catalytic activities. As we know, electro/photo-catalysis represents a straightforward and efficient avenue for converting electro/photo-energy into chemicals, which is essential for realizing sustainable clean energy in the future. COFs-based electro/photo-catalyst have gained significant attention due to their utility in a diverse range of reactions, including but not limited to organic reaction [52,70,71], hydrogen evolution reaction (HER) [72–75], hydrogen oxidation reaction (HOR) [76,77], oxygen evolution reaction (OER) [78,79], oxygen reduction reaction (ORR) [80–82], nitrogen reduction reaction (NRR) [83–85], and carbon dioxide reduction reaction (CO_2RR) [86–88]. The realization of electro/photo-catalytic activities is rooted in the semiconductor properties of COF materials, such as band gap and carrier transport characteristics, as well as the adsorption capacity to the substrates. These properties are directly related to the highly conjugated 2D or 3D structures and regular channels in COFs. To date, several

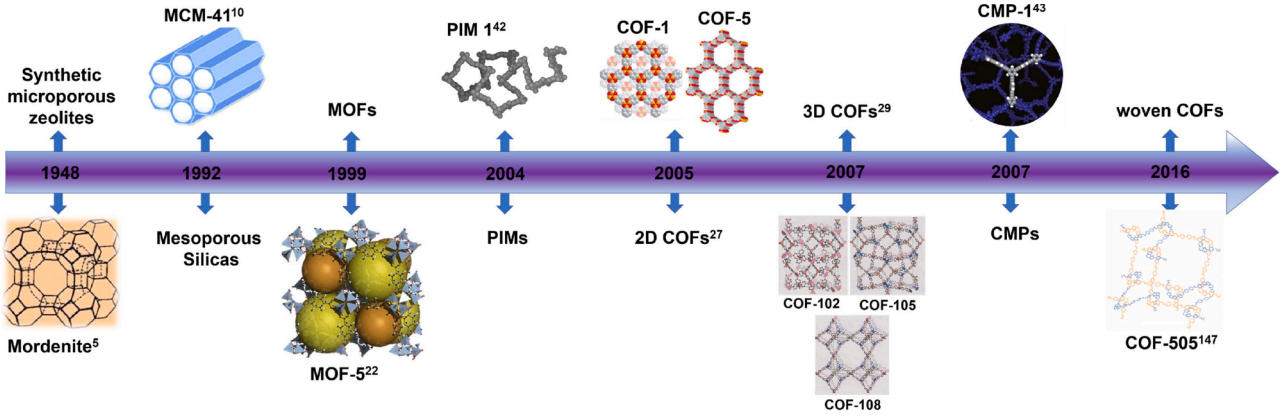

Scheme 1. Milestones in the history of porous materials.

excellent reviews have been reported for COFs-based electro/-photo-catalysis in detail. Thus, we will not discuss this in depth here and focus on organocatalysis through the microenvironment of COFs.

In this review, we summarize the recent progress in the development of COF materials for catalysis applications, with a particular focus on their microenvironment effects. Examples of the microenvironment effect for the chemical reaction and the formation of reactive metal species as the catalyst are presented. Finally, we outline the key fundamental issues to be addressed and provide our perspectives on future COFs catalysis.

2. Organocatalysis

2.1. Active sites pre-installed in monomers

The catalytically active sites in COFs can derive from either the *in-situ* formed linkages or the building blocks themselves. Most of the linkages in the COFs are limited to imine bonds which highly restrict the variety of microenvironments for catalytic reactions. The pre-designed building blocks with active catalytic sites are more frequently adopted. Achieving good crystallinity while retaining the active sites within COFs represents a challenge. The catalytic sites pre-installed in the monomer usually influence the framework crystallinity. In addition, the commonly adopted harsh solvothermal conditions for the polymerization are also

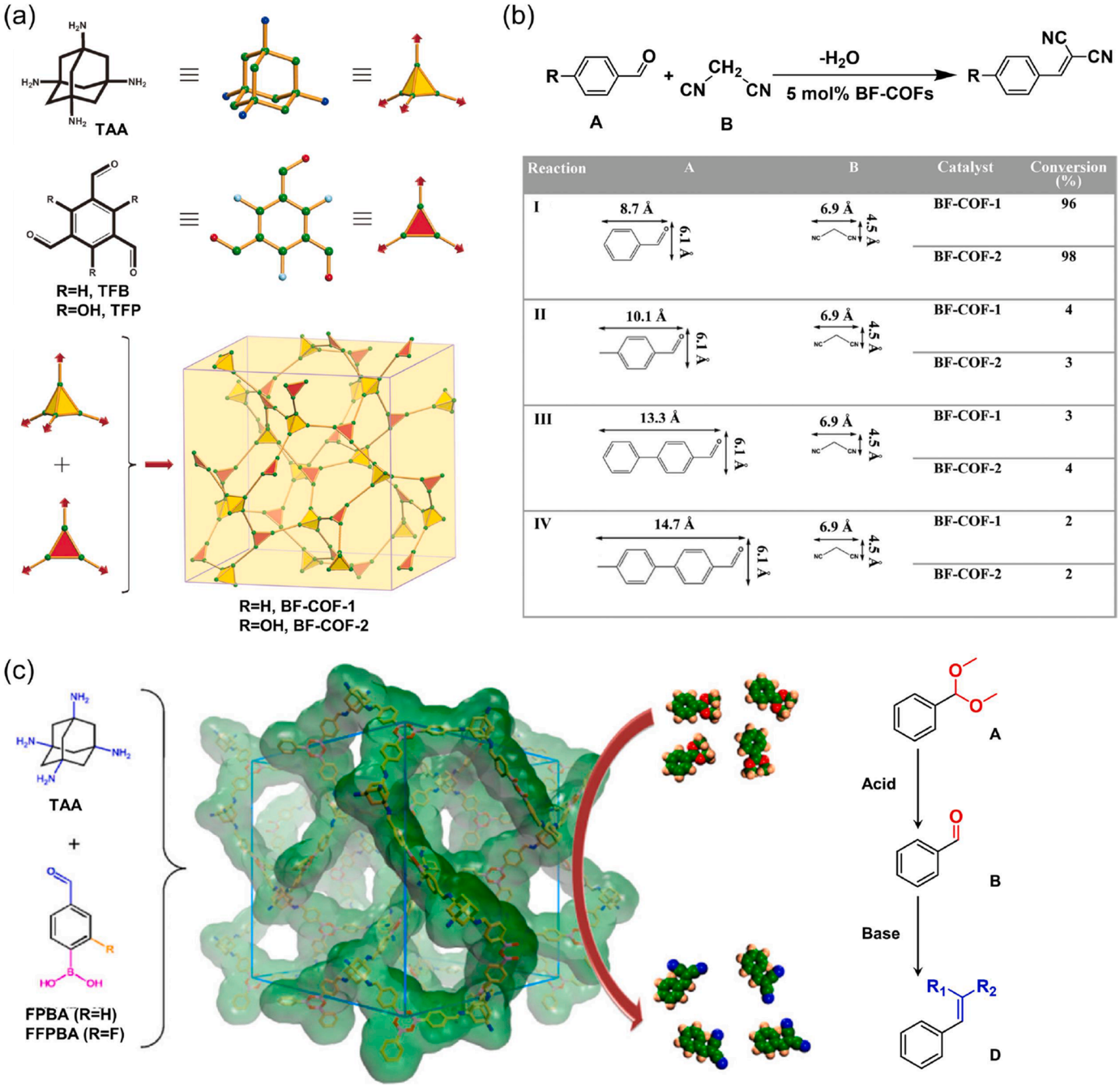

Reaction	A	B	Catalyst	Conversion (%)
I	8.7 Å × 6.1 Å	6.9 Å × 4.5 Å	BF-COF-1	96
			BF-COF-2	98
II	10.1 Å × 6.1 Å	6.9 Å × 4.5 Å	BF-COF-1	4
			BF-COF-2	3
III	13.3 Å × 6.1 Å	6.9 Å × 4.5 Å	BF-COF-1	3
			BF-COF-2	4
IV	14.7 Å × 6.1 Å	6.9 Å × 4.5 Å	BF-COF-1	2
			BF-COF-2	2

Fig. 1. (a) Schematic representation of the strategy for preparing **BF-COF-1** and **BF-COF-2**. (b) The catalytic activities of **BF-COFs** in the Knoevenagel condensation reactions with different-sized substrates. Reproduced with permission [89]. Copyright 2014, Wiley-VCH. (c) Condensation of **TAA** and **FPBA** or **FFPBA** to give 3D COFs with dual linkages and the catalysis of one-pot cascade reactions. Reproduced with permission [90]. Copyright 2016, American Chemical Society.

unfavorable to the active catalytic sites.

Yan and co-workers reported two 3D microporous base-functionalized COFs (**BF-COF-1** and **BF-COF-2**), which show clear size-selective catalysis performance for Knoevenagel condensation reactions [89]. The COFs were designed and synthesized by combining tetrahedral C4 symmetric **TAA** and planar triangular C3 symmetric **TFB** or **TFP** building blocks via solvothermal Schiff-base reaction (Fig. 1a). The two COFs showed a narrow pore width (8.3 Å for **BF-COF-1** and 8.1 Å for **BF-COF-2**). Given their microporosity and the basicity of the linkages in the 3D COFs, the catalytic performance was then explored. Specifically, the Knoevenagel reaction with the substrates of different sizes was employed to estimate the catalytic activity and size selectivity of the obtained 3D COFs (Fig. 1b). The experimental results indicate that only the products with a smaller size than the windows of the **BF-COFs** can reach a high yield (96–98%). Notably, the 3D COFs-based catalysts are inactive for the larger substrates which will lead to large products (2%−4% yield). It is suggested that the reactions occur in the channels of the **BF-COFs**. The highly efficient size selectivity arises from the effect of the confined microenvironment provided by the pores within 3D COFs. These results indicate that 3D COFs can act as promising novel catalysts with size-selectivity. The same group further reported another 3D COF example for bifunctional cascade catalysis [90]. Dual linkages of the boroxine ring and imine group were simultaneously introduced to construct two 3D COFs (**DL-COF-1** and **DL-COF-2**) (Fig. 1c). Encouraged by the ordered channels, high surface areas, and the catalytic acidic and basic sites in the 3D COFs, the catalytic activities for the acid-base catalyzed one-pot cascade reactions were then explored. The bifunctional 3D COFs exhibit high activities in acid-base catalyzed one-pot cascade reactions. Up to 98% conversion was obtained.

Besides the active linkages, the building blocks are more commonly used as catalytic sites. Banerjee and co-workers reported a catechol-porphyrin-based 2D COF (**2,3-DhaTph**) consisting of both acidic and basic sites in the backbone structure, which acted as a bifunctional heterogeneous catalyst for the cascade reaction [91]. Catechols act as weak acidic sites, and porphyrin units, together with the imine linkages, act as the basic sites in the COFs. Both catechol and porphyrin are also the building blocks used for constructing the 2D COFs (Fig. 2a). The high crystallinity of the 2D COFs provides precise information on the framework structure and position of the antagonist catalytic sites. Considering the bifunctional structure of the 2D COFs, the acid–base catalyzed one-pot deprotection of acetal groups followed by Knoevenagel condensation cascade reactions were chosen to demonstrate the catalytic activity of these 2D COFs (Fig. 2b). An excellent isolated yield (96%) was obtained for the desired product 2-benzylidenemalononitrile (**3a**). The authors further synthesized **2,3-DmaTph** as a control catalyst, which has only porphyrin centers without the catecholic–OH as acidic sites (Fig. 2a). The PXRD patterns of the two obtained COFs both showed good crystallinity. However, the control reaction gives only a 52% yield of product **3a**. The substrate scope was explored using several substituted dimethyl acetal reactants, and slightly decreased conversions (~80%) were observed. The significant activity of the **2,3-DhaTph** catalyst is ascribed to the ordered and periodic distribution of the acidic and basic sites in the backbone of the COF structure.

Zhang and co-workers reported a squaramide-based 2D COF (**COF-SQ**) with good crystallinity and high porosity [92]. A diamino monomer **1** functionalized with a squaramide core was designed to prepare **COF-SQ** directly through the condensation reaction with monomer **2**, in which the framework itself is catalytic because of the presence of squaramide (Fig. 3a). **COF-SQ** showed good catalytic performance for the Michael addition reaction (Fig. 3b). In addition, as three important

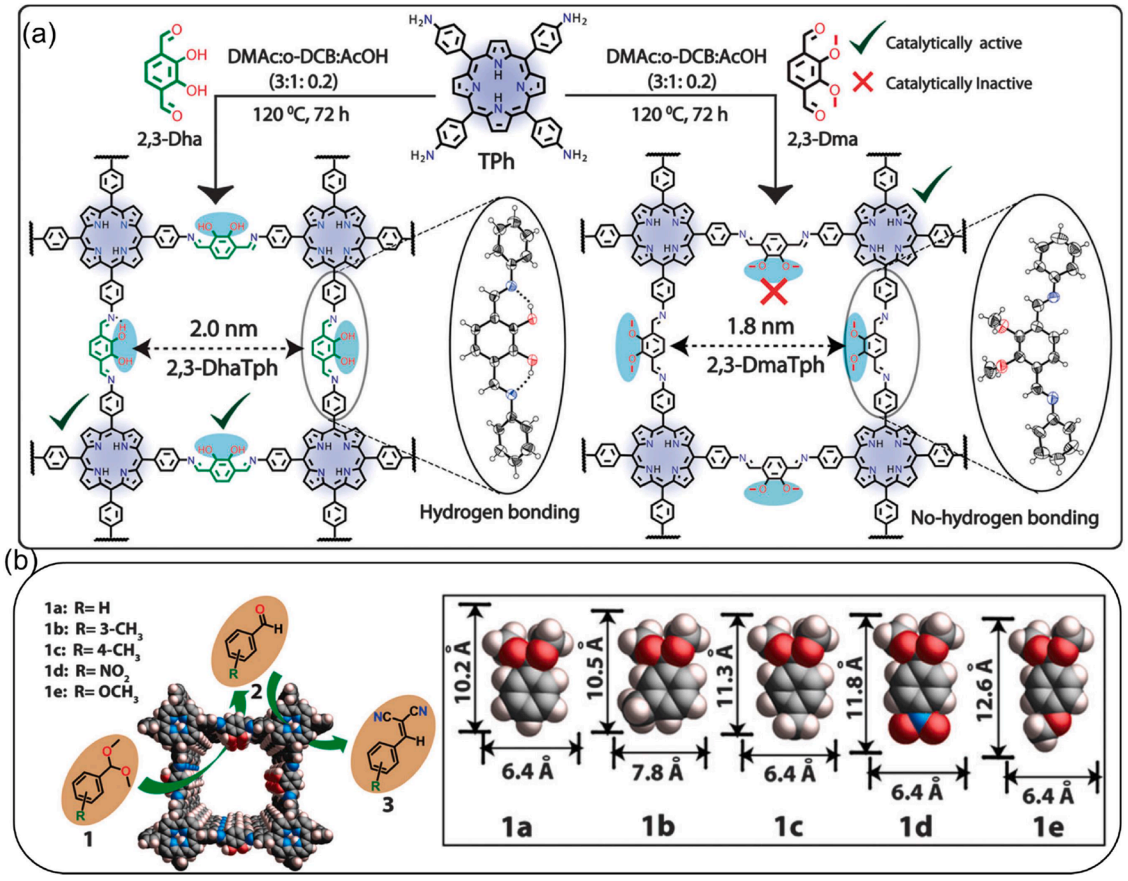

Fig. 2. (a) The synthesis of **2,3-DhaTph** and **2,3-DmaTph**. (b) The catalytic activity towards acid–base catalyzed reaction with various reactants. Reproduced with permission [91]. Copyright 2015, Royal Society of Chemistry.

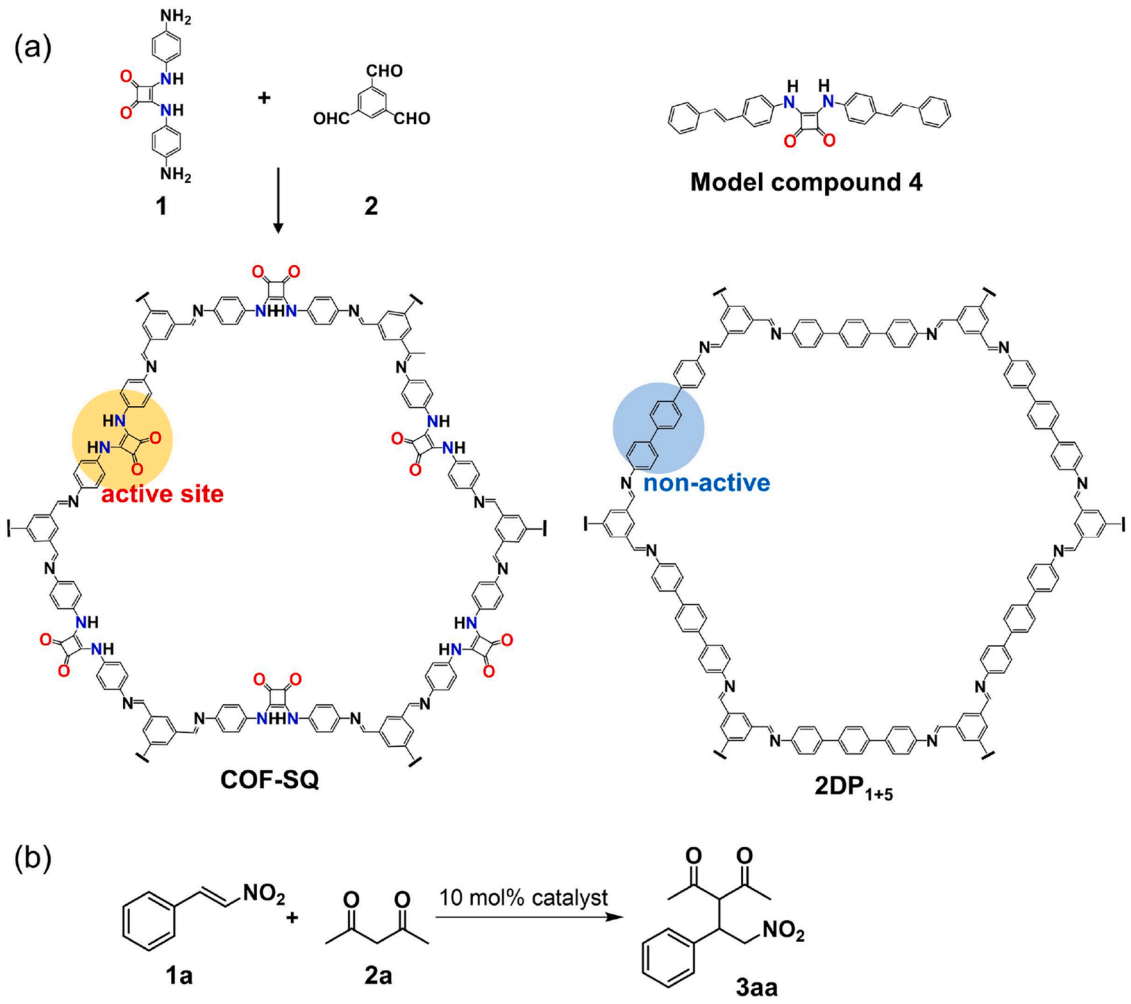

Fig. 3. (a) Synthesis of **COF-SQ** by condensation of monomers **1** and **2**. (b) The catalytic activities of **COF-SQ** in the Michael addition reaction. Reproduced with permission [92]. Copyright 2019, Royal Society of Chemistry.

control samples, monomer **1**, model compound **4**, and **2DP$_{1+5}$** all exhibited lower activities than **COF-SQ** (Fig. 3a). The good catalytic activity of **COF-SQ** is due to the combination of the following two key factors: the uniformly distributed catalytic sites and the highly ordered framework structure. The highly ordered open meso-sized channels allow efficient access of the monomers to the uniformly distributed active sites. The transport of reactants and products was facilitated, thus leading to high catalytic performance.

The weak interactions between the building blocks and the substrate can also favor the catalytic process, which has also been widely observed in enzyme catalysis. Jiang and co-workers reported a pyrene-anthracene-based 2D COF (**Py-An COF**) (Fig. 4a) [93]. The pyrene units are located at the vertices, while the anthracene units are on the edges. Notably, the ordered anthracene columnar π-walls and uniform pores enable the COF to be a heterogeneous catalyst for the Diels-Alder reaction (Fig. 4d). The columnar π-walls within **Py-An COF** act as catalytic beds allowing the organic transformations to occur inside the 1D channels (Fig. 4b). The C–H···π interactions between the π-walls of COF and the 9-hydroxymethylanthracene substrate enhanced the reactant concentration within the pores of the COF and thus accelerated the reaction (Fig. 4c). The channels in the COF are similar to the pockets in enzymes. This is a typical example of a catalytic chemical reaction under the microenvironment effect of the COF backbone structure.

The confined effect provided by the microenvironment of the COF-based catalysts can improve the chemoselectivity and minimize side reactions. A 2D COF (**TFP-DABA**) with reactive sulfonic pendant groups was reported by Zhao and co-workers [94]. The COF was synthesized from **TFP** and **DABA** through imine condensation. The subsequent irreversible enol-to-keto tautomerization strengthened the chemical bond and improved its stability. The well-defined 1D channels and uniformly distributed sulfonic acid groups within the channels are beneficial to the exploration of its catalytic application in fructose dehydration (Fig. 5a, b). **TFP-DABA** showed superior catalytic activity with remarkable yields of products (97% for HMF), excellent chemoselectivity and recyclability. The incorporation of reactive pendant groups (sulfonic acid groups) into the monomer as catalytic sites was proved to be effective in constructing COFs-based catalysts.

Zhao and co-workers reported a 2D COF example with reactive carboxylic acid pendant groups in the backbone [95]. **TPF** containing two carboxylic acid groups was chosen as one of the monomers. The imine condensation reaction and the subsequent enol-to-keto tautomerization led to the formation of **OH-COOH-COF** (Fig. 5c). The framework catalytic activity in the synthesis of L-lactide was then evaluated. The confined effect of the microenvironment in the COFs facilitates the dimerization of the L-lactic acid to L-lactide with an excellent yield of ~80% and avoids the formation of oligomers (Fig. 5d, e). The catalytic process is very similar to enzymatic catalysis, in which the selectivity of the product is controlled by the enzyme pocket. The microenvironment created by the confinement and the available active sites in the COF channels enabled the cyclic dimerization and avoided oligomerization.

Dong and co-workers installed the pendant groups with ionic moieties on the pore wall of 2D COFs and prepared an allyl-imidazolium

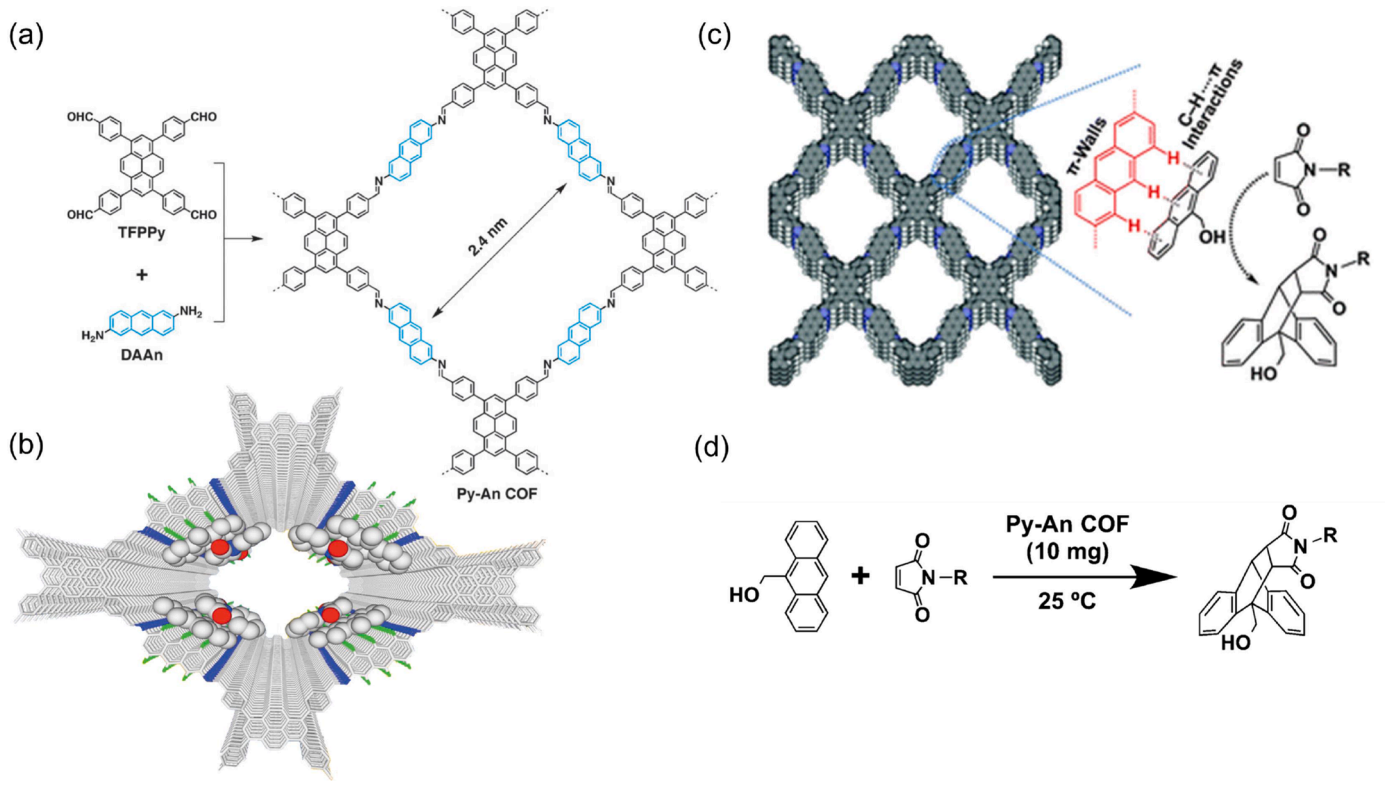

Fig. 4. (a) Synthesis of **Py-An COF** by condensation of monomers **TFPPy** and **DAAn**. (b) Schematic representation of the substrates inside of the channels. (c) The catalytic mechanism of the Diels–Alder reaction occurs inside the channels. (d) The catalytic Diels–Alder reaction of **Py-An COF**. Reproduced with permission [93]. Copyright 2015, Royal Society of Chemistry.

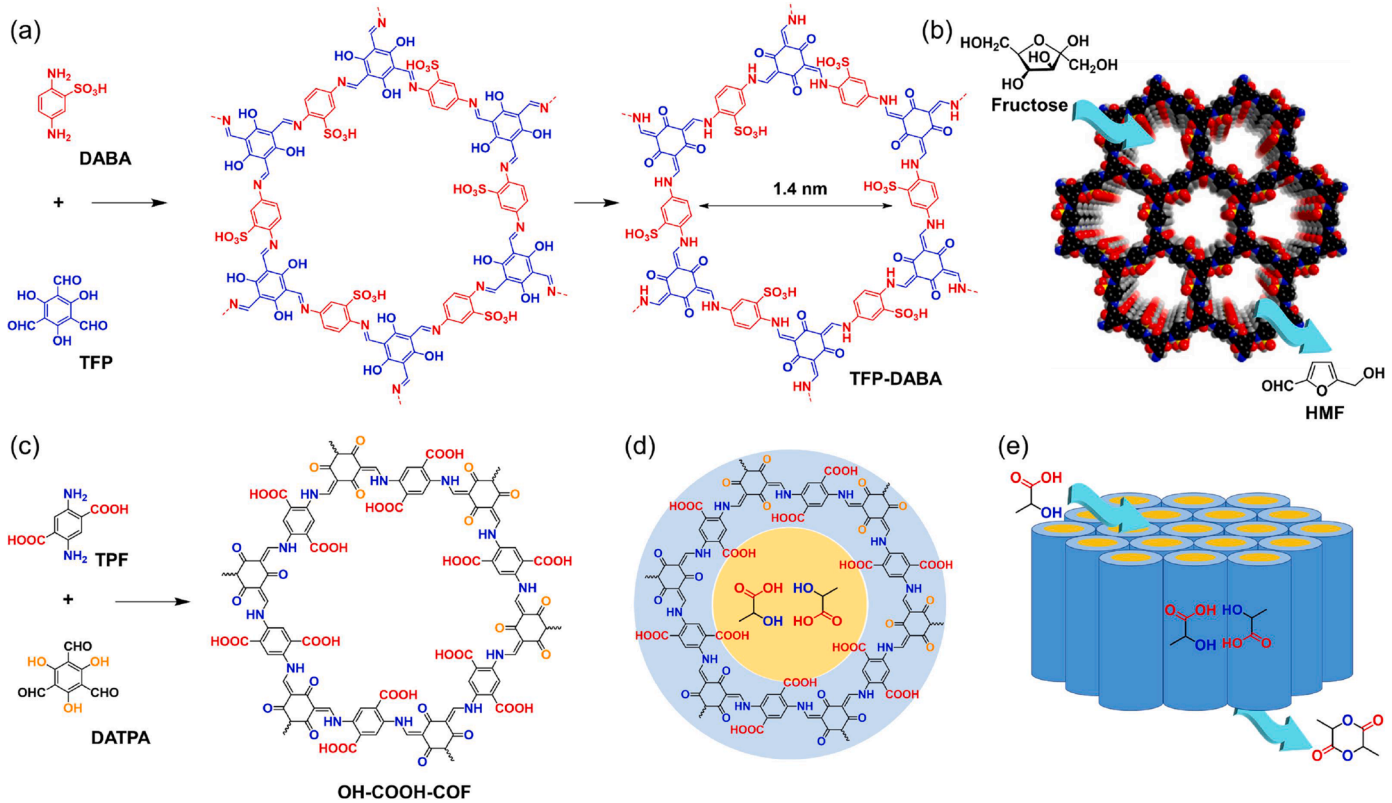

Fig. 5. (a) Synthetic scheme of **TFP-DABA** by Schiff base condensation and enol-to-keto tautomerization. (b) Schematic diagram of the catalytic process from Fructose to HMF. Reproduced with permission [94]. Copyright 2015, Wiley-VCH. (c) Synthetic scheme and chemical structures of **OH-COOH-COF**. Schematic diagram of the catalytic process: Top view (d) and side view (e). Reproduced with permission [95]. Copyright 2023, Royal Society of Chemistry.

ionic liquid-decorated 2D COF (**COF-IL**) via the condensation reaction of predesigned zwitter ionic monomer (**IL-ADH**) and **Tp** (Fig. 6a, c) [96]. **COF-IL** exhibits highly selective adsorption for CO_2, and thus was considered to be a highly active catalyst for CO_2 transformation through cycloaddition with epoxides. The CO_2 cycloaddition with substituted epoxides was adopted to evaluate the catalytic performance of **COF-IL**. Relatively high cycloaddition yields were obtained (Fig. 6b). The large channels and abundant imidazolium moieties in **COF-IL** channels play critical roles in the highly efficient CO_2 cycloaddition reaction. Notably, the long chain substituted epoxide of 1,2-epoxyoctadecane as substrate (Fig. 6b, entry 7) led to only a 7% yield. The relatively low yield may result from the limited diffusion of the substrate in the channel of the framework due to the unsuitable size caused by the long alkyl chain. This provides clear evidence indicating the reaction occurs inside the COF channels.

2.2. *Active sites installed via post-functionalization of COFs*

Besides the *in-situ* synthesis or bottom-up approaches, attaching active sites to the COF structures can also be realized through a post-synthetic approach. Despite the availability of a variety of building blocks containing active sites for the design of COFs, achieving crystallinity usually requires a significant amount of effort. For example, the direct construction of COFs by using monomers containing large catalytic functional groups is challenging since the hindrance of catalytic sites usually influences the crystallinity, and the harsh solvothermal conditions are generally detrimental to the catalytic sites. In such cases, developing approaches that allow systematic engineering of the modification for the COF becomes necessary. The post-synthetic approach endows COFs with tailor-made porous channels to meet specific catalysis requirements. The size and shape of the channels can be adjusted for substrate adsorption and encapsulation. Thus, the post-functionalization of highly ordered open-channel structures also provides an intriguing motif for exploring the microenvironment catalytic effect.

Jiang and co-workers reported a post-synthetic pore surface engineering that allows the post-modification of COF with functional organic moieties [97]. **N_3-COF-5** containing azide units in the channels was prepared by a three-component reaction system with **N_3-BDBA, BDBA**, and **HHTP**. The molar ratio of **N_3-BDBA** to **BDBA** is tunable from 0 to 100%, thus leading to the different contents of the N_3-appended wall.

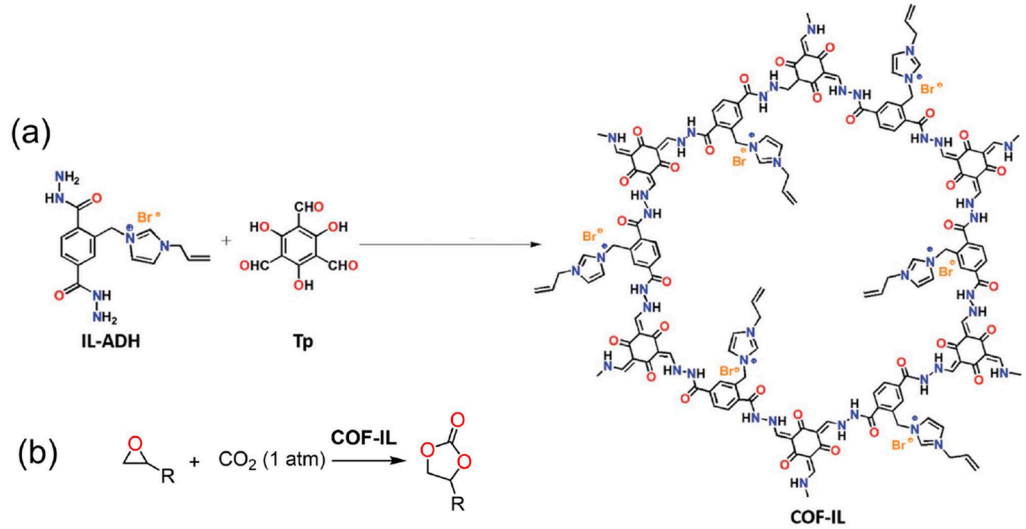

Entry	Substrate	COF-IL[b] (mol%)	T (°C)	t (h)	Yield[c] (%)
1		3.0	80	48	98
2		3.0	80	48	98
3		3.0	80	48	~100
4		3.0	80	48	97
5		3.0	80	48	89
6		3.0	80	48	71
7		3.0	80	48	7

Fig. 6. (a) Synthesis of **COF-IL** and its idealized structure. (b) CO_2 cycloaddition with substituted epoxides catalyzed by **COF-IL**. (c) The structure of **COF-IL** and the assuming 2D eclipsed stacking. Reproduced with permission [96]. Copyright 2019, Royal Society of Chemistry.

The further quantitative click reaction with alkyne derivatives successfully introduces various functional groups through the formation of 1,2,3-triazole rings (Trz) linkages leading to **RTrz-COF-5** (Fig. 7a). The strategy was further successfully applied to the construction of a tetragonal metallophthalocyanine-based COF (**N_3-NiPc-COF**) and the corresponding post-modified **RTrz-NiPc-COF** (Fig. 7b). Although no further catalytic applications were explored, this strategy offers a pathway for the preparation of COFs with large functional groups in the channels. Such COFs are usually difficult to achieve through direct synthesis.

The multi-component strategy developed by Jiang is favorable for constructing the COF precursors for post-modification. The built-in active sites for further reaction are well controlled. The crystallinity loss through the excessive introduction of catalytic moieties can be avoided. Thus, the diversified functional groups were installed successfully to the channels of the COFs. Gao and co-workers reported an ionic liquid immobilized COF through the post-synthetic approach [98]. Pyrene-based and imine-linked 2D COFs (**[HO]$_{X\%}$-Py-COFs**) were initially prepared through the condensation of **DHPA, PyTTA**, and **PA** at various molar ratios (Fig. 8a). X% represented the reactive phenol contents on the channel walls of **[HO]$_{X\%}$-Py-COFs**. The subsequent post-synthetic Williamson ether reaction successfully realized the immobilization of ionic liquids onto the backbones of the COFs. The introduction of ionic moieties can change the microenvironment of the cavities in COFs, such as the polarity, positive or negative charge, and size, which results in special properties for the substrate and catalytic performance. The obtained ionic **[Et$_4$NBr]$_{50\%}$-Py-COFs** exhibit effective catalysis for *N*-formylation reactions from different amines and CO_2. As an important control, the **[HO]$_{50\%}$-Py-COFs** show much lower activity than **[Et$_4$NBr]$_{50\%}$-Py-COFs** due to the absence of active ionic sites. The highly ordered open channels and the presence of ionic sites in **[Et$_4$NBr]$_{X\%}$-Py-COFs** allow efficient formylation reactions to occur under mild conditions (Fig. 8b).

Another similar example was reported by Han and co-workers [99]. A zwitterionic 2D COF (**[BE]$_{X\%}$-TD-COFs**) was prepared by attaching betaine groups (**BE**) to the channels of the frameworks (Fig. 8c). The

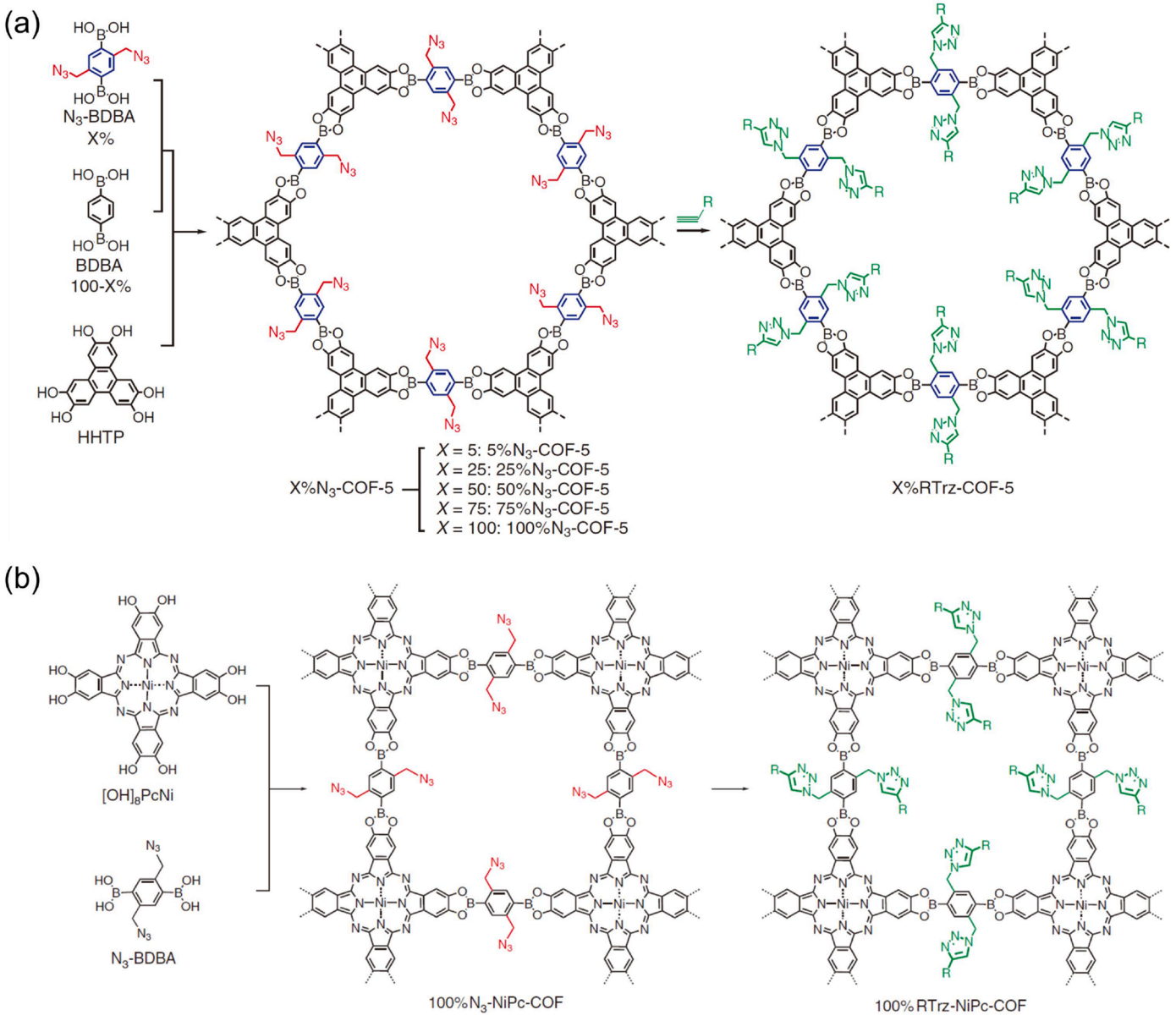

Fig. 7. (a) The general strategy for the synthesis of **N_3-COF-5** and the corresponding **RTrz-COF-5**. (b) The synthesis of **N_3-NiPc-COF** and the corresponding **RTrz-NiPc-COF**. Reproduced with permission [97]. Copyright 2011, Springer Nature.

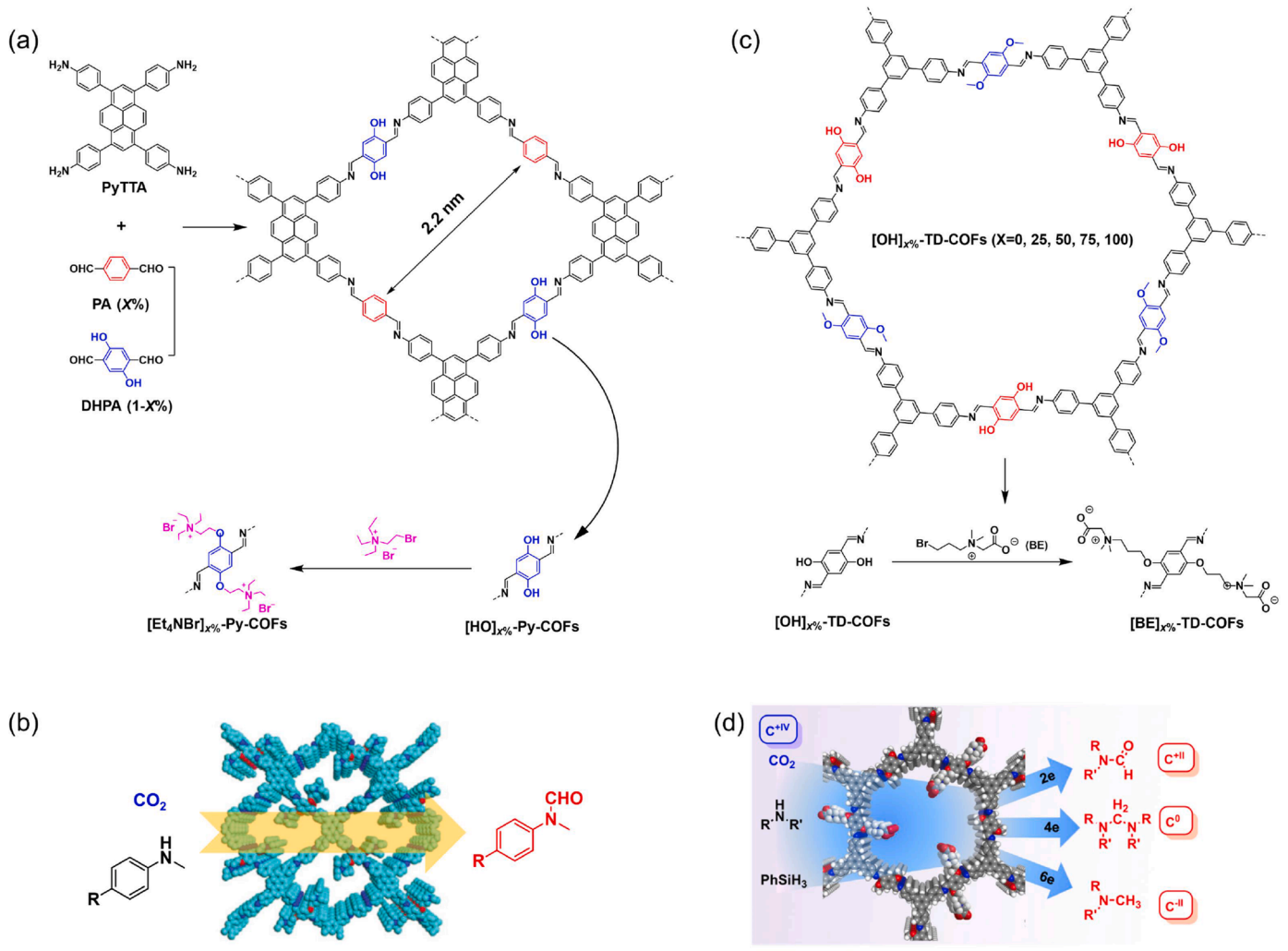

Fig. 8. (a) Synthesis of **[HO]$_{X_{\%}}$-Py-COFs** and its post-modified **[Et$_4$NBr]$_{X_{\%}}$-Py-COFs**. (b) The **[Et$_4$NBr]$_{50\%}$-Py-COFs** catalyzed the formylation of amines **1** with CO_2 and $PhSiH_3$. Reproduced with permission [98]. Copyright 2016, Royal Society of Chemistry. (c) Synthesis of **[OH]$_{X\%}$-TD-COFs** and its post-modified **[BE]$_{X\%}$-TD-COFs**. (d) The **[BE]$_{X\%}$-TD-COFs** catalyzed the hierarchical reduction of CO_2 with the amine to afford formamide, aminal, and methylamine. Reproduced with permission [99]. Copyright 2018, American Chemical Society.

uniform catalytic site distribution and 1D mass transport are beneficial to the catalysis of hierarchical reduction of CO_2 with amine and hydrosilane (Fig. 8d). High efficiency and selectivity in catalyzing hierarchical (two-, four-, and six-electron) reduction of CO_2 with amine and $PhSiH_3$ to produce formamide, aminal, and methylamine were achieved.

Most of the prepared COFs are based on imine linkage, which suffers from poor chemical stability under harsh conditions. In this case, Dong and co-workers prepared a quinoline-linked **COF-IM** containing imidazole groups via a three-component one-pot Povarov reaction (Fig. 9a) [100]. **COF-IM** was then converted to sulfonic acid-functionalized **COF-IM-SO$_3$H** by the reaction with 1,3-propane sultone, followed by protonation (Fig. 9a, c). The catalytic activity of the **COF-IM-SO$_3$H** was examined to catalyze the Biginelli reaction with various substrates (Fig. 9b). Excellent yields (90−98%) were obtained for a wide range of substrates. Notably, the substrates with large sizes, such as 2-naphthaldehyde and 4-phenylbenzaldehyde, gave a moderate 60% yield due to the limited diffusion within the channels of the COFs. This further proved the occurrence of the reaction inside the channels. The confined microenvironments with strong acidity provided by the **COF-IM-SO$_3$H** play key roles in catalyzing the Biginelli reaction.

Considering the atomically designable and well-confined channels in COF materials, they are highly attractive supports for enzyme immobilization. The confined channels and the easy modulation of the specific microenvironments allow for efficient mass transfer and conformational confinement for the stabilization of enzymes. Recently, Wang, Zhang, and co-workers reported a covalent immobilization of enzymes inside the channels of COFs by a post-synthetic method [101]. The **[OH]$_{x\%}$-TD-COFs** (x% represents the molar percentage of **DHTA**) with 1D channels were prepared first through the multi-component strategy (Fig. 10). The first post-synthetic modification was achieved by the Williamson ether reaction, yielding the epoxy-integrated **[EP]$_{y\%}$-TD-COFs** (y% represents the molar percentage of epoxy functionalized **DHTA**). The as-synthesized COFs with a tunable density of epoxy units featured size-matched channels for the enzyme cytochrome *c* (Cyt *c*) immobilization. The second post-synthetic modification anchored Cyt *c* in the **[EP]$_{y\%}$-TD-COFs** channels through covalent bonds between epoxy groups and nucleophilic groups from the enzyme and led to the enzyme immobilized **Cyt *c*⊂[EP]$_{y\%}$-TD-COFs**. The catalytic performance of **Cyt *c*⊂[EP]$_{y\%}$-TD-COFs** was evaluated in the oxidation of **ABTS** (2,2′-azinobis-(3-ethylbenzthiazoline-6-sulphonate)). The higher catalytic activity of **Cyt *c*⊂[EP]$_{y\%}$-TD-COFs** was observed and compared to the corresponding physically adsorbed one and the free Cyt *c* as references. Through the mechanism study, it was confirmed that the covalent bonding between the enzymes and the confined channels of the COF could induce conformational perturbation and result in more

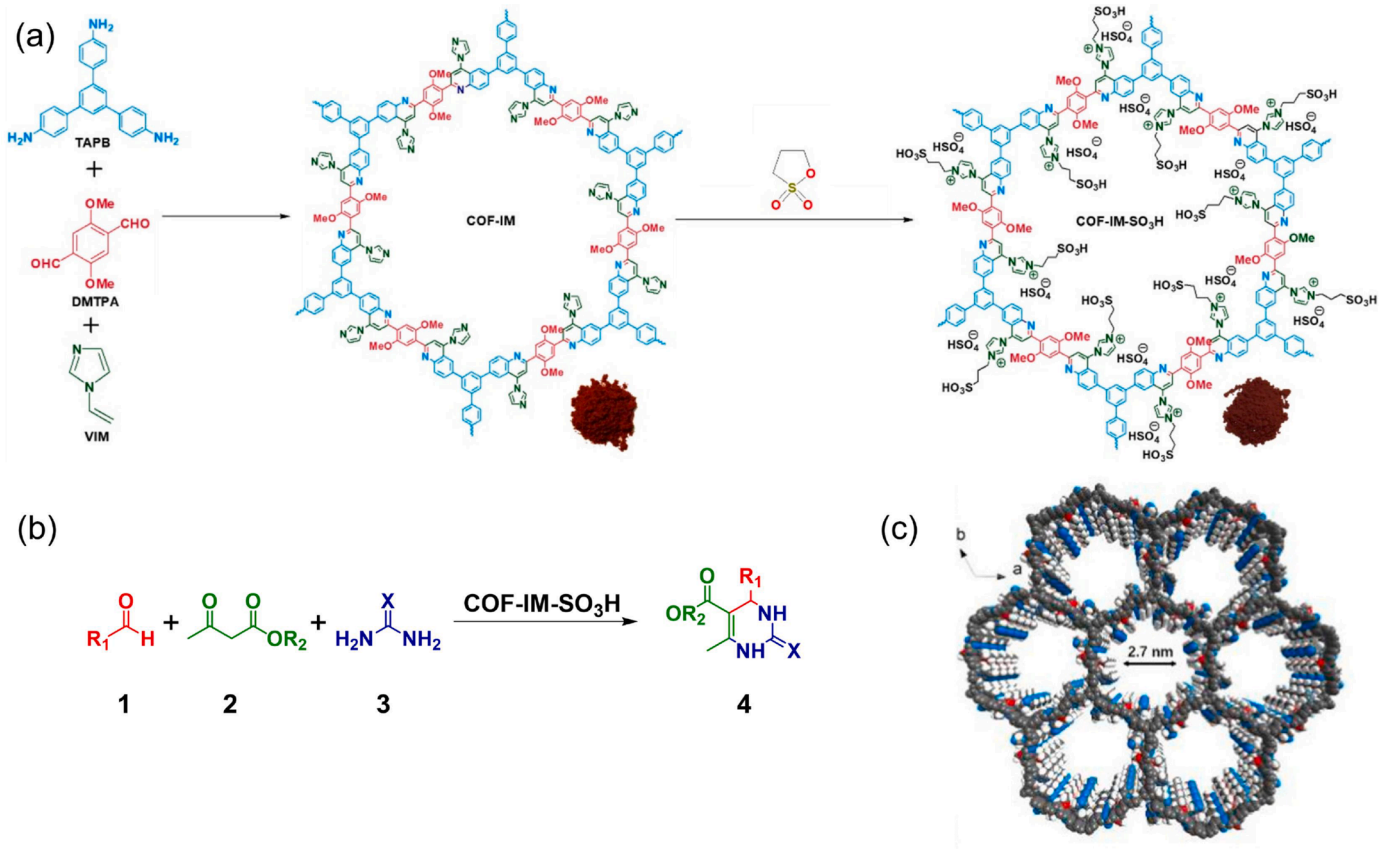

Fig. 9. (a) The synthesis of the quinoline-linked **COF-IM** and the corresponding post-synthetic **COF-IM-SO$_3$H**. (b) **COF-IM-SO$_3$H** catalyzed the Biginelli reactions of aromatic aldehyde, ethyl acetoacetate, urea or thiourea. (c) A graphical representation of **COF-IM-SO$_3$H**. Reproduced with permission [100]. Copyright 2021, American Chemical Society.

accessible active sites, which promoted the catalytic activity of the enzymes.

Compared to the direct synthesis of COF materials using the monomers containing pendant groups as active sites, it is relatively easy to achieve the crystallinity through the post-synthetic method for the parent COFs with modifiable groups, and a lot of trial-and-error efforts could thus be avoided. Once the parent COFs are synthesized successfully, a variety of the post-modified COFs could be easily obtained, while the reaction types for the post-modification are limited to some highly efficient reactions with almost quantitative conversion yields. On the other hand, retaining the crystallinity and porosity is important in the post-synthetic process considering the influence of the reaction on the structure order. Decrease in the PXRD intensity and the BET surface areas frequently occur during the post-synthetic process but sometimes it is difficult to determine whether the structures are destroyed or if only the channels within COFs are partially occupied.

3. Asymmetric organocatalysis

Crystalline porous COF materials are highly desired for heterogeneous asymmetric catalysis applications due to their well-defined and highly ordered structures. The previously reported chiral porous polymers with amorphous topologies have been proven to be less controlled in their chiral catalysis functions [103–106]. As discussed in Section 1, the crystallinity, porosity, and functionality must all be considered. More importantly, the designed building blocks should be rigid, symmetric, and readily connect with chiral ligands via chemical reactions. In addition, the chemical structures, electronic properties, and spatial configurations of the chiral ligands in the as-prepared COFs should also be considered. The uniformly distributed catalytically active chiral moieties in the rigid channels need to provide a microenvironment with chiral confined space, thus leading to successful asymmetric catalysis towards optically pure products. Similarly, the design strategies are also divided into direct synthesis and post-synthetic modification (Fig. 11) [102]. Incorporating chiral functional groups into the monomer for the construction of COFs is usually unfriendly to the crystallinity and stability. The bulkiness of chiral catalytic sites usually influences the framework crystallinity because of the conflicting requirements of symmetry for crystallinity and asymmetry for chirality. Besides, the harsh solvothermal conditions are generally detrimental to the chiral catalytic sites. Therefore, the direct synthesis from chiral monomers is facing significant challenges. In comparison, the post-synthetic modification of the COFs skeleton with chiral functional moieties is more straightforward. However, this approach also has its disadvantages, including uneven distribution and less loading content of chiral moieties. Undoubtedly, the chiral-functionalized COFs with well-defined microenvironment is important to the study of chiral reaction mechanism and kinetic process. We here classify the asymmetric catalysis content into two parts based on the different synthetic strategies. Some examples of chiral COFs will not be discussed here because these are not for asymmetric catalysis applications.

3.1. *Active sites pre-installed in monomers*

Wang and co-workers report a direct construction of chiral-functionalized COFs by using chiral building blocks [102]. The use of a rigid scaffold is key to this work. The linear-structured 4,4′-diamino-*p*-terphenyl (**1**) was chosen as the backbone, which could be easily converted into imidazole-functionalized intermediate (**2**) and then to the chiral building block (**3**) (Fig. 12a). Two chiral COFs, **LZU-72** and

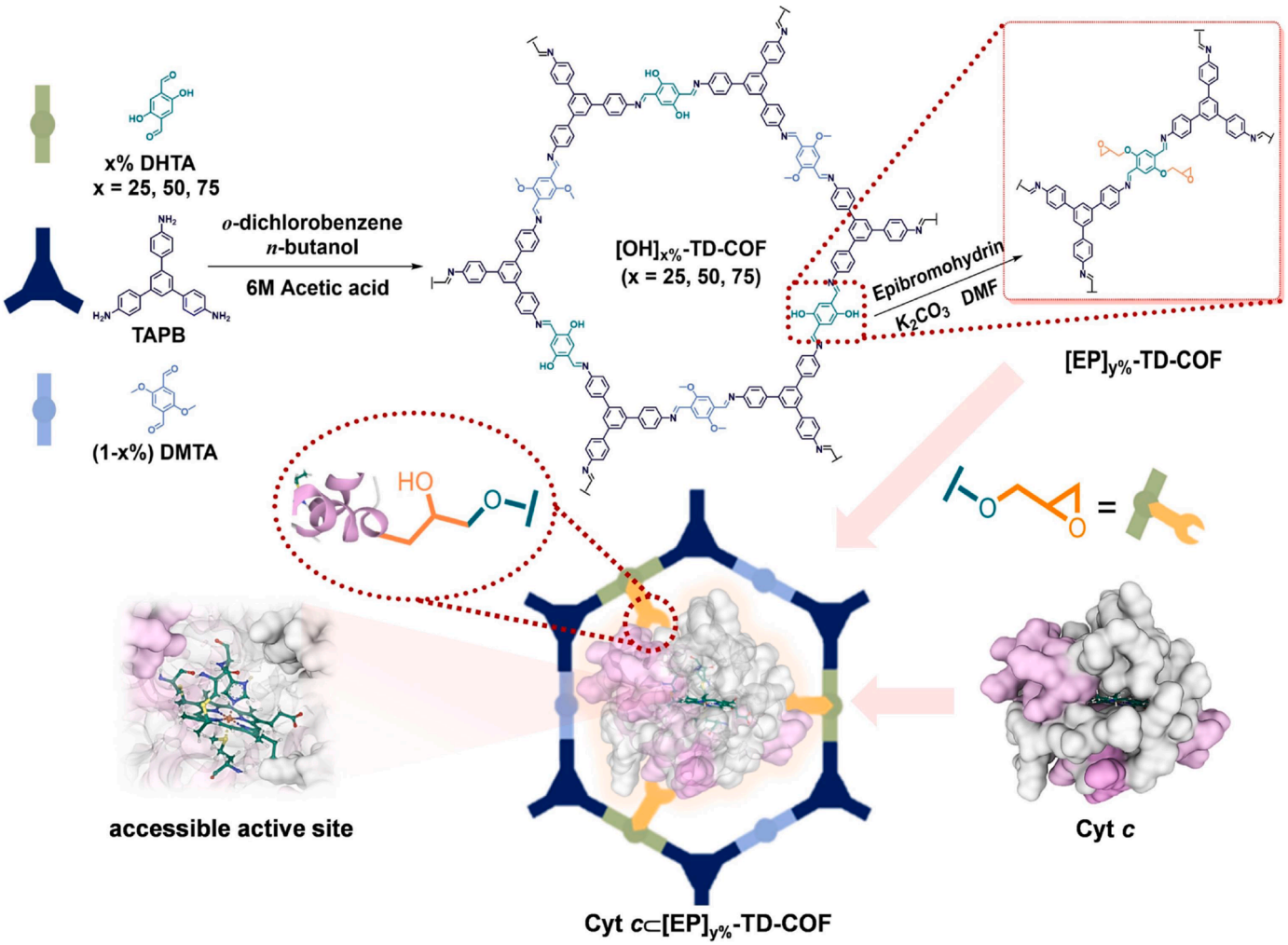

Fig. 10. The synthesis of **[OH]$_{x\%}$-TD-COFs** and post-synthesized **[EP]$_{y\%}$-TD-COFs**, and the further covalent immobilized **Cyt *c*⊂ [EP]$_{y\%}$-TD-COFs**. Reproduced with permission [101]. Copyright 2021, Wiley-VCH.

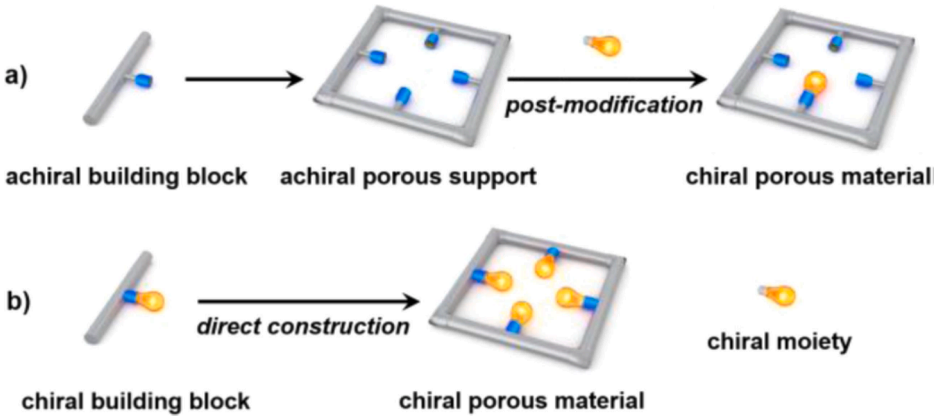

Fig. 11. General strategies for constructing chiral porous materials: (a) post-modification of achiral porous supports with chiral moieties, and (b) direct construction from chiral building blocks. Reproduced with permission [102]. Copyright 2016, American Chemical Society.

LZU-76 were successfully prepared from the direct condensation of *N*-Boc-protected **3** with **4** or **5**, respectively (Fig. 12b). **LZU-76** shows higher stability under acidic conditions due to the presence of robust β-ketoenamine linkages. The catalytic activity of **LZU-76** was examined in asymmetric aldol reactions with excellent enantioselectivity (Fig. 12c). The rigid monomer ensures the crystallinity of the obtained COFs. In addition, the formed aligned channels provide efficient access to the chiral-pyrrolidine sites for the realization of asymmetric catalysis and facilitate the transport of reactants and products. The same group further made a combinatorial library for high-throughput screening and structure-activity investigation, considering the former study is only suitable for a specific target. A series of chiral COFs for parallel

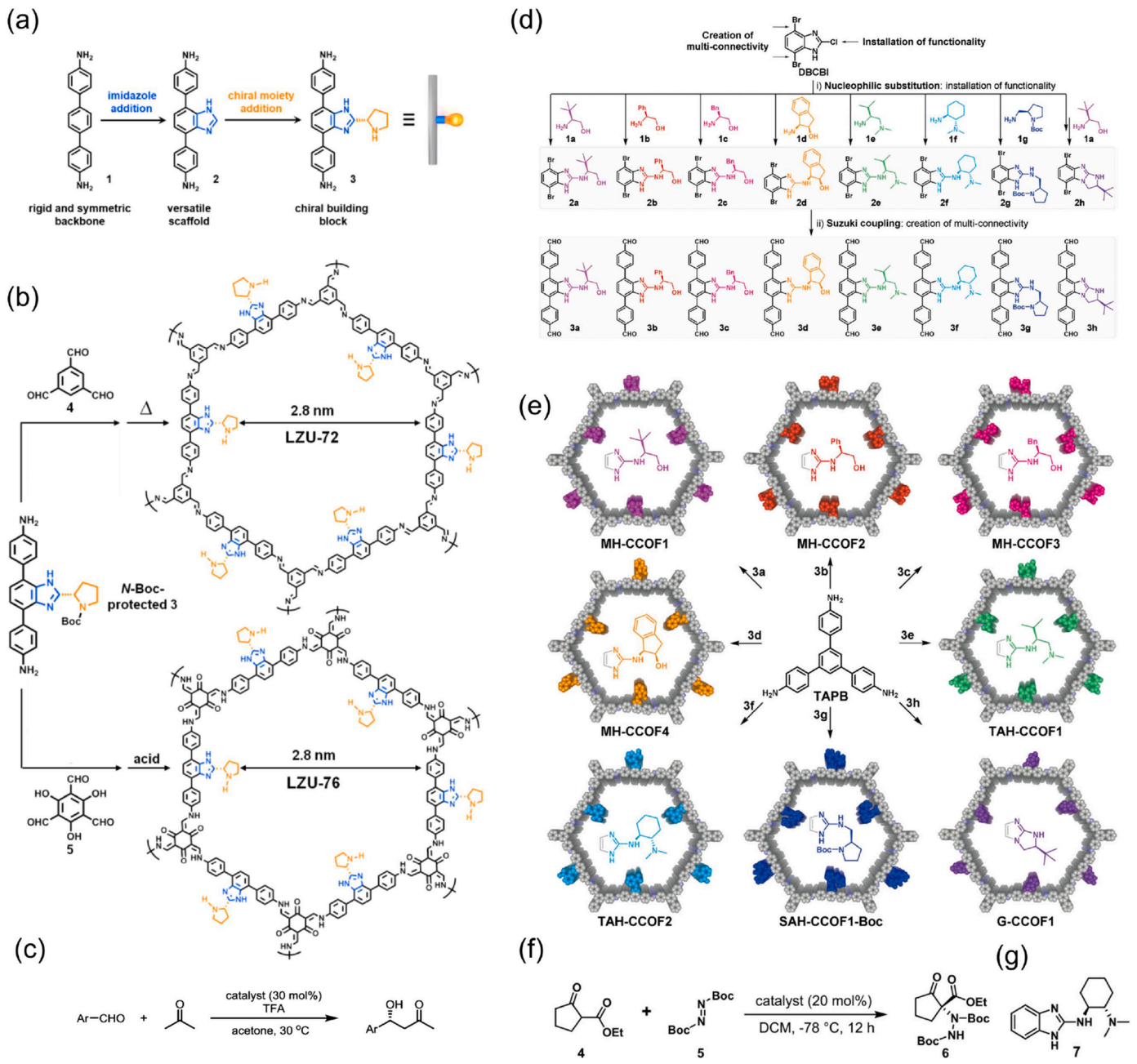

Fig. 12. (a) The design and synthesis of the rigid chiral building blocks with the chiral-pyrrolidine moiety. (b) Synthesis of **LZU-72** and **LZU-76** through direct construction. (c) Catalytic asymmetric Aldol reaction. Reproduced with permission [102]. Copyright 2016, American Chemical Society. (d) The divergent synthesis of the platform molecule **DBCBI** and the chiral monomers. (e) Divergent synthesis of eight chiral COFs. (f) Catalytic asymmetric amination of β-ketoesters. (g) The structure of model catalyst **7**. Reproduced with permission [107]. Copyright 2019, Wiley-VCH.

evaluation of their catalytic activities were constructed [107]. The basic design requirements should be met in order to balance the conflict between asymmetry and crystallinity. The designed monomer should be rigid, symmetric, and readily modified with chiral functionality and connectivity by reliable transformations. Following this design rule, **DBCBI** as a platform molecule was synthesized. It could be easily modified with different chiral functional moieties to realize the divergent synthesis of chiral monomers (Fig. 12d). Subsequently, eight chiral COFs as a library were constructed through the reactions of **3a–h** with **TAPB** (Fig. 12e). The catalytic activities for the asymmetric amination reaction were further investigated (Fig. 12f). Taking the asymmetric amination reaction as the model reaction, **TAH—CCOF2** exhibited higher activity and enantioselectivity than other chiral COFs. Compared to the model catalyst **7** (Fig. 12g) as a small molecule, the reticulation of the chiral and hydrogen-bonding sites in the π-conjugated chiral COF framework may further weaken the intermolecular hydrogen-bonding and therefore improve the steric control and catalytic activity.

As we know, the introduction of bulky chiral active groups usually influences the balance of asymmetry and crystallinity and results in the failure of the preparation of chiral COFs. Cui and co-workers aimed to solve this problem by using a multivariate strategy [108]. The rigid *C*3-symmetric building block (**TPB**) was chosen as the basic backbone. The chiral proline and imidazolidine groups were attached at the central aromatic ring to afford the chiral scaffolds **TPBn** and **TPBn′** (n = 2–5) (Fig. 13a). By regulating the contents of mixtures of **TPB1, TPBn, TPBn′** as triamines, and the **DMTA** as dialdehyde, three binary chiral COFs (**DMTA—TPBn**) (n = 2–4), four ternary chiral COFs (**DMTA—TPB1-TPBn**) (n = 2–5), and the related deprotected

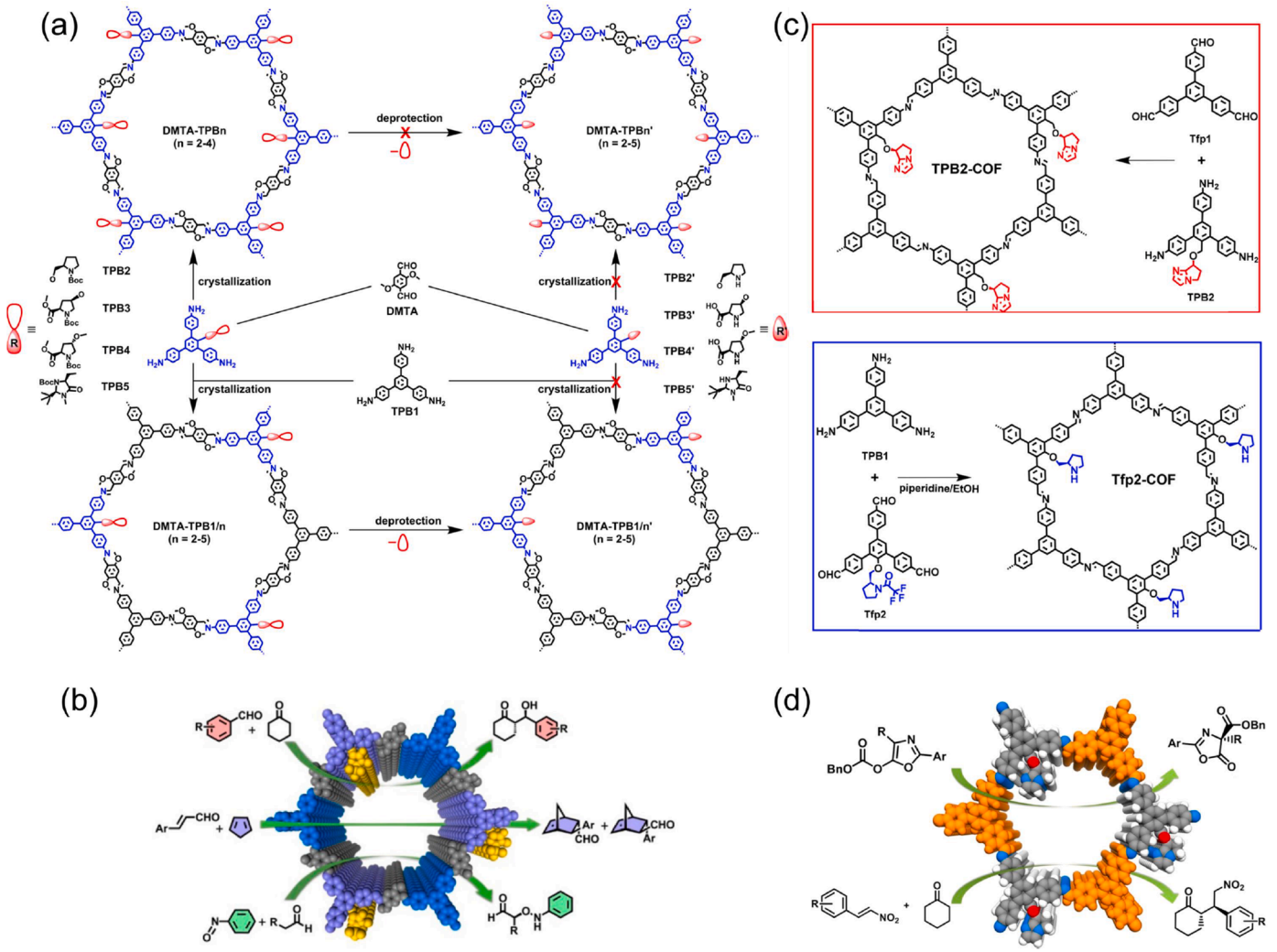

Fig. 13. (a) Synthesis of the chiral COFs through multivariate strategy. (b) Three types of asymmetric reactions catalyzed by chiral COFs. Reproduced with permission [108]. Copyright 2017, American Chemical Society. (c) Synthesis and structure of **TPB2-COF** and **Tfp2-COF**. (d) Asymmetric Steglich rearrangement and Michael addition reactions. Reproduced with permission [109]. Copyright 2019, American Chemical Society.

(**DMTA−TPB1-TPBn'**) (n = 2–5) were successfully obtained. Notably, direct synthesis of the binary and ternary COFs from the **TPBn′** monomers with unprotected proline or imidazolidine was unsuccessful. The weakened interlayered interactions by the presence of abundant deprotected functional groups are unfavorable for the crystallinity of the COFs. The introduction of the third building block (**TPB1**) decreased the number of chiral building blocks (**TPBn′**), and thus weakened the interlayer repulsion and facilitated the crystallization process. It was found that the multivariate strategy can not only control the crystallinity but also tune the chemical stability. Finally, three types of organic reactions (asymmetric aminooxylation reaction, aldol reaction, and Diels−Alder reaction) were chosen to test the catalytic activity of the obtained COFs (Fig. 13b). Pyrrolidine and imidazolidine groups as active asymmetric catalytic sites have been periodically appended on the channel walls in the crystalline chiral COFs. As a result, the ternary chiral COFs show excellent asymmetric catalytic activities with better stereoselectivity and diastereoselectivity compared to homogeneous analogues. In this work, the multivariate approach shows advantages for integrating chiral functionality, stability, and crystallinity in one chiral COFs. A wide range of chiral COFs holding interesting chirality properties is promising to be prepared.

By using a similar multivariate strategy, the same group soon after reported another two examples of chiral COFs (**TPB2-COF** and **Tfp2-COF**) by directly employing chiral organocatalysts as building units (Fig. 13c) [109]. The chiral 2,3-dihydroimidazolopyridine and pyrrolidine were used as active asymmetric catalytic sites. The precisely 1D channels with periodically appended chiral organocatalytic sites provide a microenvironment with activity, enantioselectivity, and diastereoselectivity for catalytic Steglich rearrangement and Michael addition (Fig. 13d).

These works first provided a possible solution to balance the conflict between asymmetry and crystallinity. This multivariate strategy may offer great potential for constructing a wide range of chiral COFs that will display interesting chirality properties, holding great promise for efficiently catalyzing a variety of asymmetric organic reactions.

The chiral active sites can either be attached to the rigid building blocks of the monomers (see the above examples) or be realized through the entire building block with chirality. Cui and co-workers reported two 2D imine-based chiral COFs (**CCOF-1** and **CCOF-2**) from enantiopure (*R,R*)-**TTA**, (*R,R*)-**TTPA)** and flexible diamine linker (**4,4′-DADPM**) (Fig. 14a) [110]. The chiral dihydroxy groups of **TADDOL** (tetraaryl-1, 3-dioxolane-4,5-dimethanols) units provide the chiral environment of the channels. Circular dichroism (CD) spectra of **CCOF-1** and **CCOF-2** made from the (*R,R*) and (*S,S*) enantiomers of the **TADDOL** monomers indicate their enantiomeric nature. By taking advantage of the chiral dihydroxy groups, the asymmetric catalytic performance of the addition of diethylzinc to aromatic aldehydes was examined. In the presence of excess $Ti(O^iPr)_4$, which provided the Lewis acidic units, up to 99%

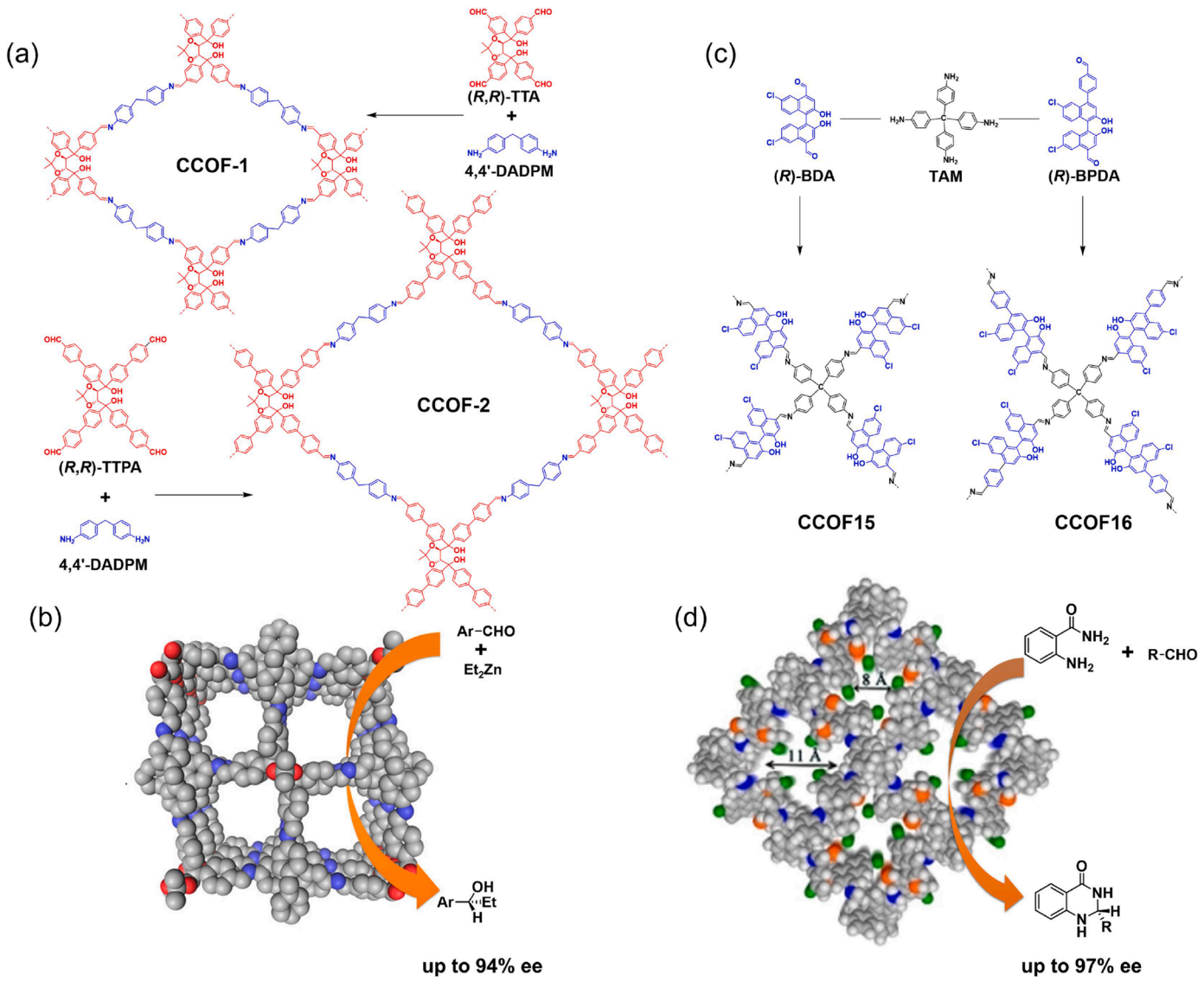

Fig. 14. (a) Synthesis of **CCOF-1** and **CCOF-2**. (b) Asymmetric catalysis of the addition from diethylzinc to aromatic aldehydes. Reproduced with permission [110]. Copyright 2016, American Chemical Society. (c) Synthesis of **CCOF15** and **CCOF16**. (d) Asymmetric acetalization of 2-aminobenzamide and aldehydes. Reproduced with permission [111]. Copyright 2021, Wiley-VCH.

conversion and 95% ee were obtained (Fig. 14b). This work demonstrates that the modular directed synthetic approach based on an enantiopure organic building block, even the flexible one, can be used to construct chiral COFs.

The same group recently reported another two 3D chiral COFs featuring chiral **BINOL** (1,1′-binaphthol) building blocks with different channel sizes (**CCOF15** and **CCOF16**) (Fig. 14c) [111]. Two chiral monomers, named as (*R*)-**BAD** and (*R*)-**BPDA** were chosen as active asymmetric catalytic building blocks to react with **TMA** yielding 3D chiral COFs with wide tubular channels of 8 Å and 11 Å (Fig. 14d). All **BINOL** hydroxyl units are periodically arranged within the channels of the frameworks. Due to the chiral confined microenvironment, **CCOF15** exhibits excellent activity for the condensation and cyclization of 2-aminobenzamide and aldehydes (91% yield and 97% ee) (Fig. 14d). In addition, the large-sized substrates lead to low yield, which is attributed to the unfavorable access of the substrates to the catalytical sites in the channels of **CCOF15**. Importantly, **CCOF 16**, with the isostructural porous structure, exhibited much lower enantioselectivity than **CCOF 15**. This is due to the larger channels with weaker enantioselective induction ability. The steric hindrance and confined effect provided by the microenvironment of the framework have been proven to play a key role in the enantioselectivity of BINOL groups. This study provided sufficient evidence that the reaction mainly occurs inside the pores of the chiral COFs. The confined effect for catalysis has also been efficiently utilized and discussed. The asymmetric catalysis from the chiral environment of the chiral COFs is similar to enzymatic catalysis in which the product selectivity is controlled by the enzyme pocket.

Dong and co-workers reported a chiral COF ((*R*)-**CuTAPBN-COF**), which consisted of Lewis acid (Cu(II)), chiral template ((*R*)-BINOL), and photothermal conversion (**Cu-TAPP**) species (Fig. 15) [112]. The chirality of the monomer (*R*)-**CuTAPBN-COF** is from the structure itself. This multifunctional integration endows this COF with both photothermal conversion and asymmetric catalytic properties. The asymmetric catalytic synthesis of (*S*)-**CIK** via photothermal converted Strecker reaction under visible-light irradiation was realized successfully. As high as 98% yield with 94% enantiomeric excess for the synthesis of (*S*)-**CIK** was obtained under visible-light irradiation. A multifunctional asymmetric catalytic material was constructed by integrating the functional groups of metalloporphyrin and chiral BINOL into the COFs structures. Multifunctionalities of catalysis, chiral templating,

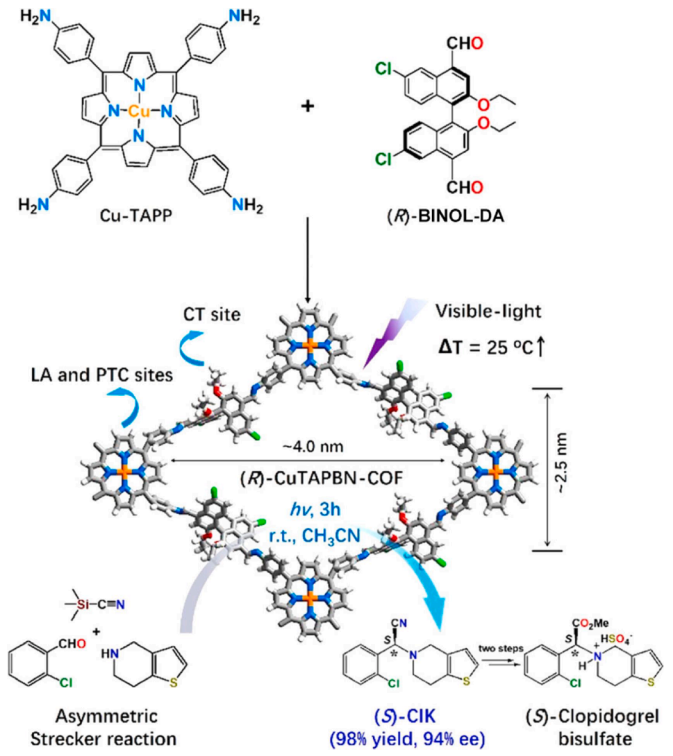

Fig. 15. Synthesis and structure of (*R*)-**CuTAPBN-COF**—, and diagram representation of the catalytic synthesis of (*S*)-**CIK**. Reproduced with permission [112]. Copyright 2020, American Chemical Society.

and photothermal conversion were then realized. Without copper as the photothermal functional group, only modest yields (17% and 18%) were obtained. The **Cu-TAAP** monomer only as the catalyst has no asymmetric catalytic activity. The mixture of the two monomers **Cu-TAPP** and **(*R*)-BINOL** as catalysts showed modest enantioselectivity (32% ee). Therefore, the confined environment in the COF structure plays a key role in enantioselectivity and yield for the Strecker reaction.

The chirality of the monomer is necessary during the design and synthesis of the monomer for most cases. It can be realized by either attaching chiral active groups to the monomers or using the chiral monomer itself. Dong and co-workers further developed a new route for constructing the chiral COFs from achiral monomers via catalytic asymmetric polymerization [113]. The asymmetric catalytic sites do not originally exist in the building blocks. The chiral COF was prepared through the asymmetric catalytic synthesis from **DMTP, TAPB, PA** in the presence of Cu(I)-(*S, S*)-pybox or Cu(I)-(*R, R*)-pybox as a highly efficient asymmetric catalyst for the synthesis of chiral propargylamines. Two chiral COFs ((*S*)-**DTP-COF** and (*R*)-**DTP-COF**) were successfully prepared (Fig. 16a). The chiral nature of the two chiral COFs was proved by the circular dichroism (CD) spectrum (Fig. 16b). The obtained chiral COFs exhibit excellent asymmetric catalytic activities towards asymmetric Michael addition reactions (Fig. 16c). The **DTP-COFs** possess chiral microenvironments that could regulate the product enantioselectivity by expediently tuning the chirality of the COFs. Most importantly, the asymmetric catalytic polymerization reported herein complements the existing approaches in the preparation of chiral COFs.

3.2. *Active sites installed via post-functionalization of COFs*

The post-synthetic strategy to construct chiral COFs is more efficient compared to direct construction. Keeping the high crystallinity and porosity of the COFs during the post-modification is the key for achieving high-performance chiral COFs. Another key factor is to ensure high conversion and the uniform distribution of the post-modified active catalytic chiral sites.

As we know, the post-synthetic strategy usually leads to an obvious change in the microenvironment of the COFs, such as the crystallinity, pore size, and shape of the channels. Jiang and co-workers have done representative studies to address this issue. The post-synthetic strategy (also called "pore surface engineering strategy") to install the chiral pendant groups onto the backbone of COFs was first demonstrated by Jiang and co-workers [114]. At first, the authors employed a three-component condensation system with **BPTA, DMTA**, and **TAPB** to synthesize the intermediate **[HC≡C]$_x$-TPB-DMTP-COFs**, where x is the percentage of functional groups (HC≡C) (Fig. 17a). Incorporating methoxy groups (**DMTA**) into the pore walls can reinforce the interlayer interactions for stability with high crystallinity and porosity. Subsequently, the achiral **[HC≡C]$_x$-TPB-DMTP-COFs** was converted into a chiral organocatalyst **[(*S*)-Py]$_x$-TPB-DMTP-COFs** through the introduction of (*S*)-pyrrolidine to the channel walls via a quantitative azide–ethynyl click reaction (Fig. 17a). It has been well recognized that the click reaction has the advantages of high yield, fast rate, and mild reaction conditions. In addition, the IR spectroscopy confirmed the completion of the click reactions. The almost identical PXRD profile of the **[(*S*)-Py]$_x$-TPB-DMTP-COFs** to **[HC≡C]$_x$-TPB-DMTP-COFs** indicates the lattice structure was not affected by the introduction of chiral catalytic sites on the walls of the pores. The porosity also retains through the measurement of BET surface areas. **[(*S*)-Py]$_x$-TPB-DMTP-COFs** shows high catalytic activity and enantioselectivity (up to 92% enantioselectivity and 90/10 diastereoselectivity) for asymmetric Michael addition reaction. Notably, two interesting results should be paid attention to. First, the amount of chiral catalytic sites has a significant influence on the reaction rate. The higher density of catalytic sites on the channel walls unexpectedly results in lower catalytic activity. The face-on attack by nitrostyrenes at the catalytic sites is inhibited by the overlap of the catalytic sites, which induces inefficient utilization of them (Fig. 17b). Second, the pore size was found to be an important factor for catalysis. The decrease in the pore size leads to an obvious suppression of the Michael reactions. These important observations indicate that the catalytic reaction does occur inside the channel of the chiral COFs.

The same group further reported another chiral COF example through a three-component reaction system consisting **BPTA, DHTA** and **H_2P** (Fig. 17c) [115]. The molar ratios between **BPTA** and **DHTA** can be adjusted by changing the value of X%. **[HC≡C]$_x$-H_2P-COFs** was successfully prepared and further converted into the chiral **[Pyr]$_x$-H_2P--COFs** through the introduction of pyrrolidine via click reaction. The desired chiral active groups (pyrrolidine) were anchored to the pore walls. The catalytic activities of **[Pyr]$_x$-H_2P-COFs** for the asymmetric Michael addition reaction were further investigated. **[Pyr]$_x$-H_2P-COFs** exhibits much better catalytic performance than the monomeric, amorphous, and nonporous catalyst. Notably, the large number of pyrrolidine units in the porous channels leads to steric congestion and obstructs the reagent's transport through the channels. This observation is similar to the example above. The crystallinity and porosity of COFs, together with the catalytically active sites, function collectively to realize the asymmetric catalytic process.

Similar to the normal catalytic COFs discussed in Section 1, the preparation of chiral COFs with reactive chiral pendant groups can be achieved by either direct synthesis (bottom-up) or post-synthetic approaches (top-down). Both advantages and disadvantages exist for these two approaches, just like the normal catalytic COFs discussed above. The realization of the chiral functionalities in chiral COFs usually depends on either dangling active sites on the framework or the embedded ones in the skeleton. The synergism with the channels and the highly ordered structures is equally important for catalysis.

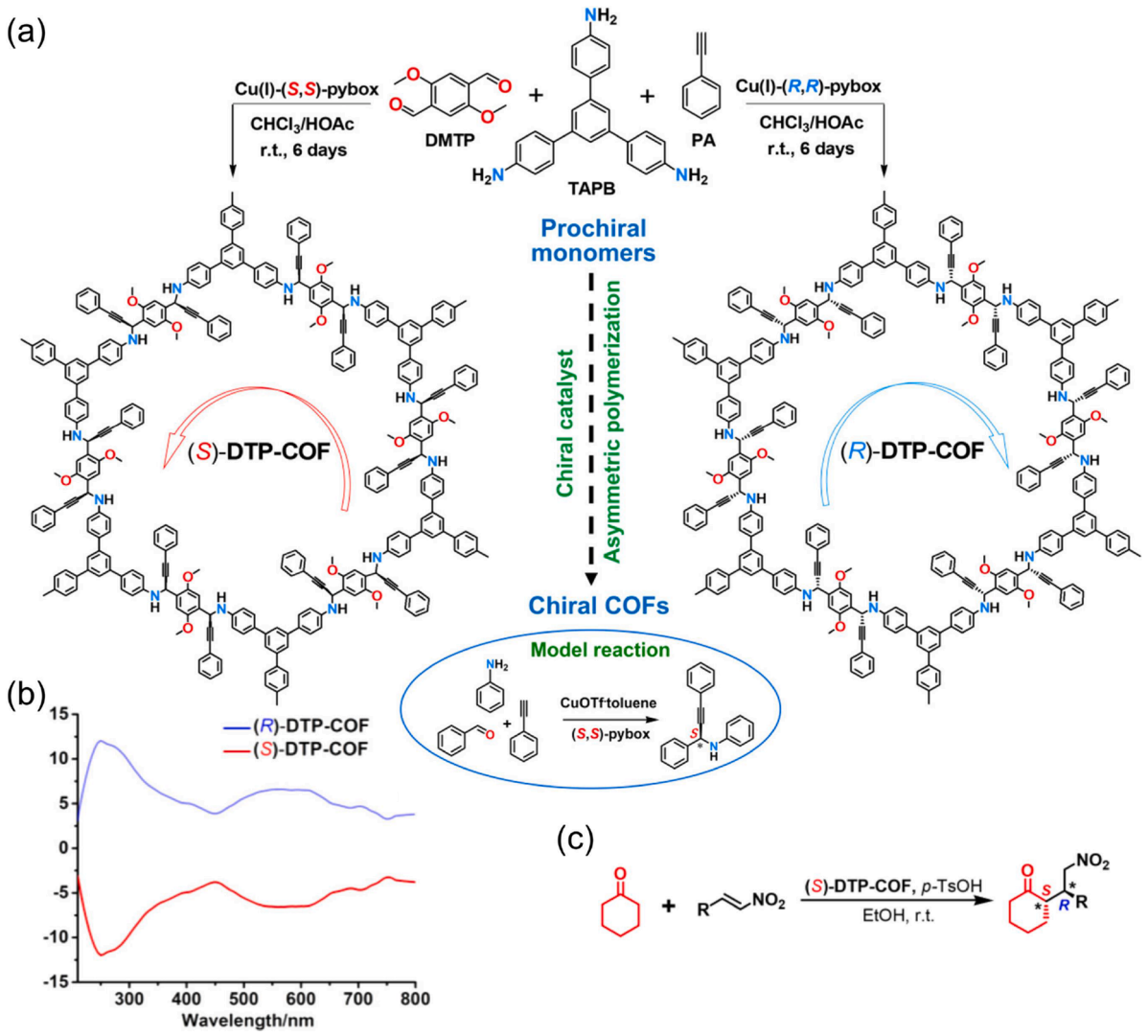

Fig. 16. (a) Synthesis of (*S*)- and (*R*)-**DTP-COFs** via catalytic asymmetric polymerization and the corresponding model reaction. (b) CD spectra of (*S*)- and (*R*)-**DTP-COFs**. (c) Asymmetric Michael addition reactions catalyzed by (*S*)-**DTP-COF**. Reproduced with permission [113]. Copyright 2020, American Chemical Society.

4. Metal-supported catalysis

It is well known that highly active MNPs can experience reduced catalytic activity due to the aggregation induced by their high surface energy. One solution to address this issue is to load active MNPs in porous materials containing chelate sites. The inherent advantages of COFs, such as the highly ordered porous structures and easy introduction of the chelate site for the active metal species, make them excellent supports for immobilizing catalytical MNPs. In addition, due to the relatively robust covalent bonds within the framework structures, COFs are fairly stable under most experimental conditions, making them potential scaffolds for catalysis applications. And there are a variety of chelate sites, such as imine linkage, salen, bipyridine, heteroatoms et al., which can be installed in the COF channels, which can strongly bind the metal species. Similar to the organocatalysis discussed in Sections 1 and 2, the COFs-based metal-supported catalysts can also be classified into direct synthesis and post-modification according to the preparation strategy. However, due to the limited number of building blocks inherently containing active metal species, successful examples through direct synthesis are rare. Alternatively, post-synthetic chemical modification of COFs provides more opportunities for docking various active metal species. This approach allows for the incorporation of metal species in the form of ions or nanoparticles. And both two forms of metals can enable efficient catalysis. The microenvironment created by the well-defined channels of the COFs is manifested in two aspects. First, the confined microenvironment enables control over the ultra-small size and the high dispersion of the MNPs during the growth of the MNPs. Second, the COF platform provides a confined reaction microenvironment that can make catalytic selectivity and activity similar to the enzyme pocket.

4.1. Metal ions-decorated COFs

4.1.1. Active metal ions pre-installed in monomers

The direct construction of the metal ions-decorated COFs is limited by the scarcity of building blocks containing active metal ions. Most of the metal ions-decorated COF catalysts are prepared by introducing catalytically active metal ions into COFs via post-synthetic modifications. There may be issues with the low loading amount and ununiform distributions of the post-introduced catalytic metal ions due to the non-quantitative conversion, especially for the large-sized active metal ions. Dong and co-workers designed an *N*-heterocyclic-carbene-metal (**NHC-M**) involved COF (**NHC-AuCl-COF**) by direct polymerization from the **NHC-M** organometallic monomer **TPDCA-NHC-Au** and **TAPT** through imine condensation (Fig. 18) [116]. As high as 23.40 wt% Au loading content (almost equal to the theoretical value) and uniform distribution

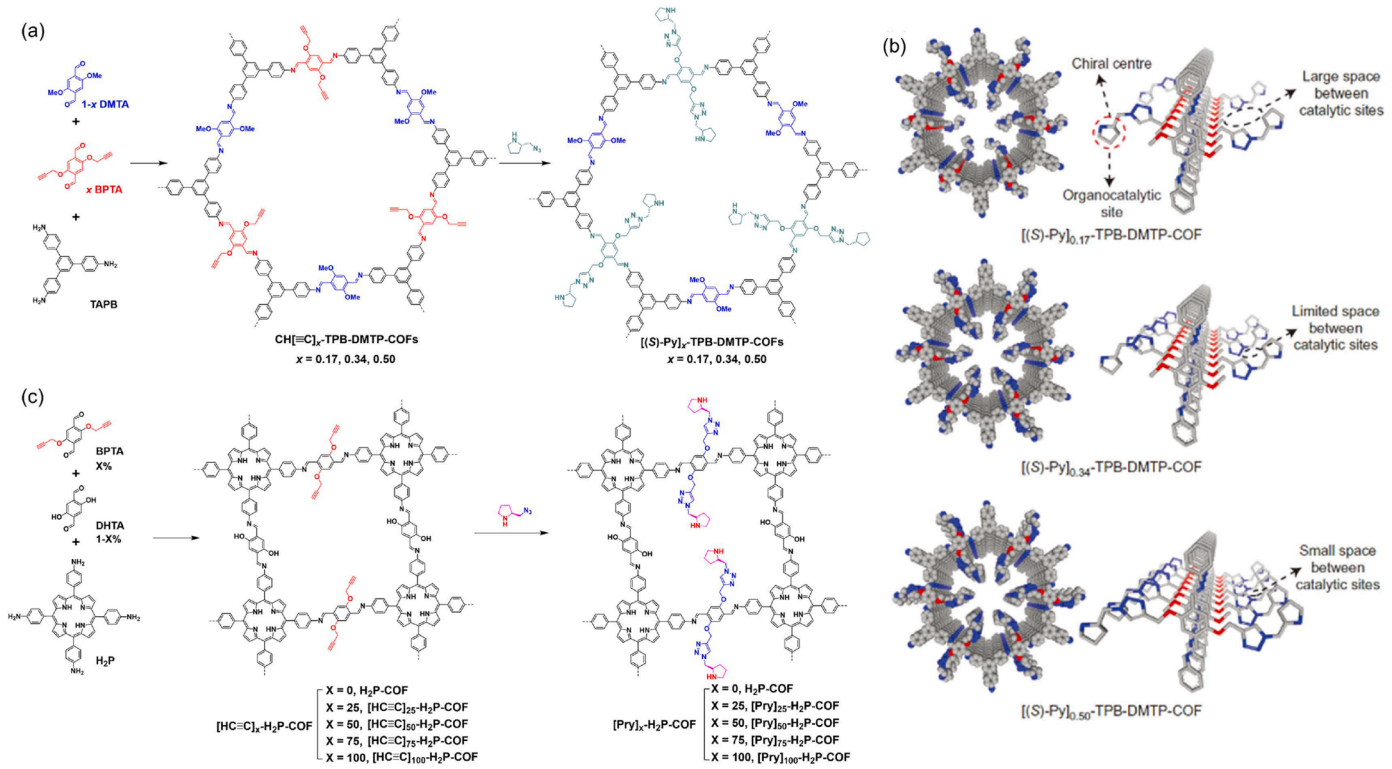

Fig. 17. (a) Synthesis of **[HC≡C]$_X$-H$_2$P-COF** and corresponding post-synthetic chiral **[(*S*)-Py]$_x$-TPB-DMTP-COFs**. (b) Channel-wall structure of the chiral organocatalytic **[(*S*)-Py]$_x$-TPB-DMTP-COFs**. Reproduced with permission [114]. Copyright 2015, Springer Nature. (c) The synthesis of the imine-linked **[HC≡C]$_X$-H$_2$P-COF** and the corresponding post-synthetic **[Pry]$_x$-H$_2$P-COF** through click chemistry. Reproduced with permission [115]. Copyright 2014, Royal Society of Chemistry.

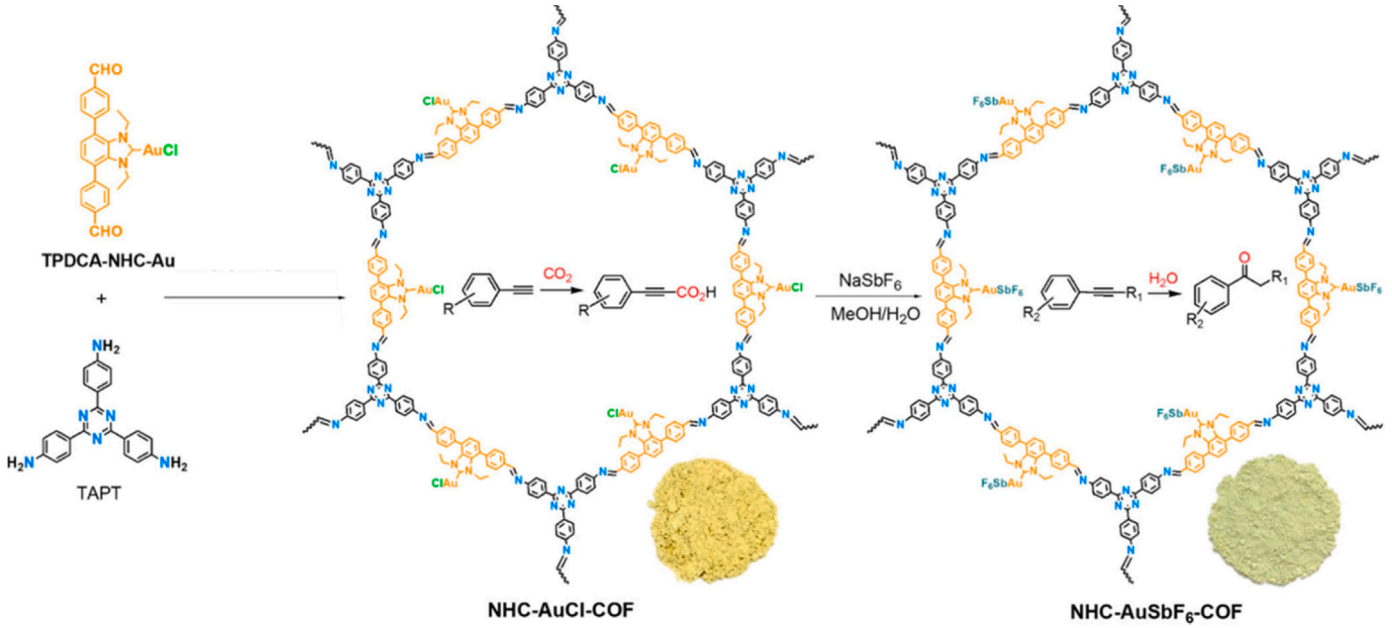

Fig. 18. Synthesis of **NHC-AuX-COF** (**X** = **Cl**$^-$, **SbF$_6^-$**) and its catalytic reactions. Reproduced with permission [116]. Copyright 2020, American Chemical Society.

in COFs were obtained. **NHC-AuSbF$_{6\text{-COF}}$** with SbF_6^- counterion can be easily realized via anion exchange. The different counterions in **NHC-AuX-COF** can catalyze different reactions. **NHC-AuCl-COF** shows high catalytic activity for terminal alkyne carboxylation with CO_2, while **NHC-AuSbF$_6$-COF** is a good catalyst for alkyne hydration. The obtained COFs possess capacious and expedited channels which can facilitate the transport of reactants to the catalytic sites, provided by the abundant active metal ions in the channels of the COFs.

Besides the direct introduction of metal ions to the monomer, metal ions can be used as a template during the preparation of the COFs, and thus stay in the COFs structure. Cui and co-workers synthesized two Salen-based chiral COFs by using the enantiopure 1,2-diaminocyclohexane as the building block (Fig. 19) [117]. The introduction of Zn^{2+} during the imine-condensations realized the metal-directed synthesis,

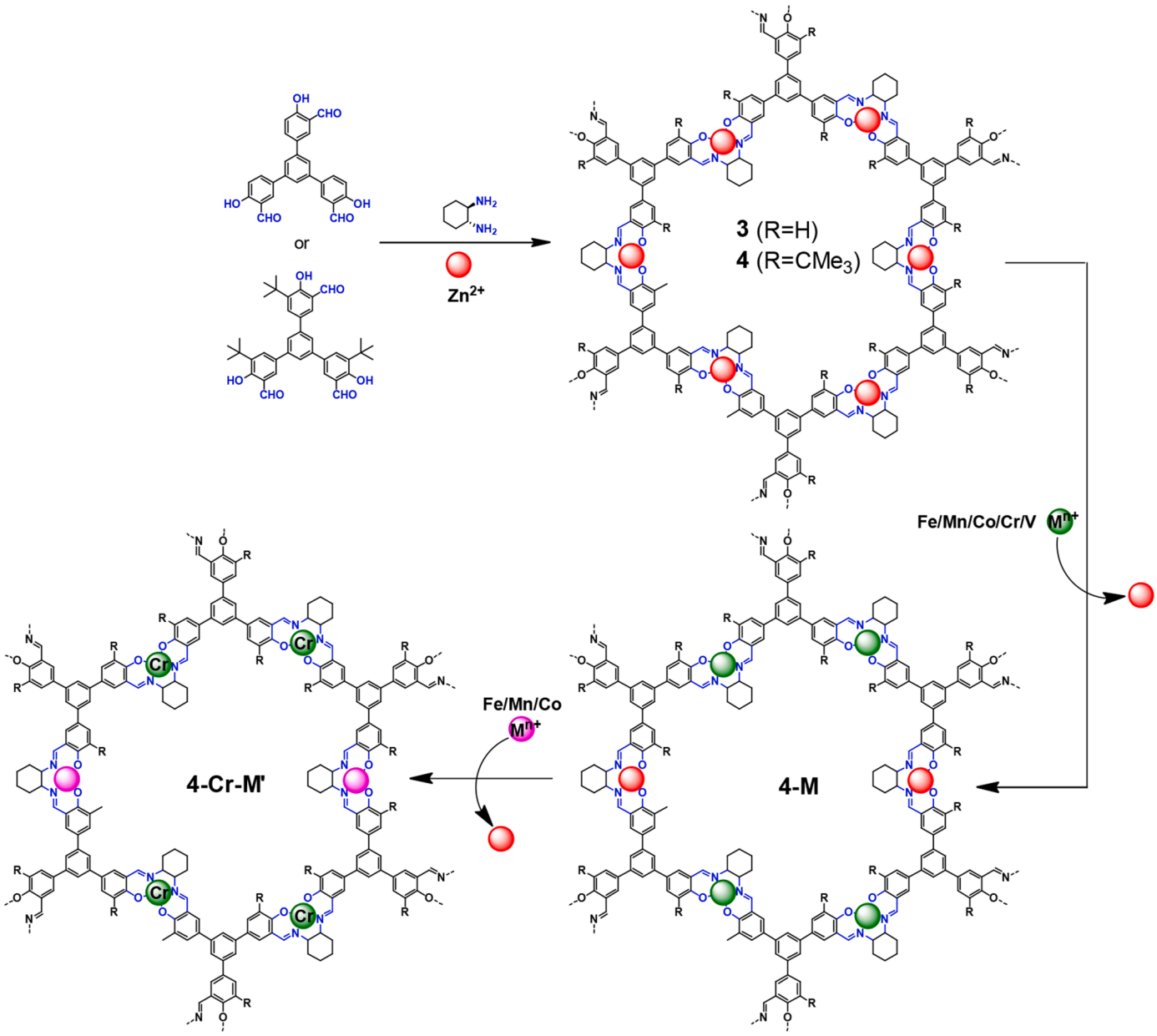

Fig. 19. Synthesis of chiral COFs through Zn-directed synthesis and multivariate metal ions installation into chiral COFs by the post-synthetic metal ions exchange. Reproduced with permission [117]. Copyright 2017, American Chemical Society.

which is the highlight of this work. The Zn (salen)-based chiral COFs (**3** and **4**) were successfully prepared. The metal ion exchange that occurs in COFs **3** and **4** leads to **3-M** or **4-M** without a change in structural integrities and loss in crystallinities. Notably, bimetallic or trimetallic chiral COFs can be obtained by controlling the metal-exchanging process. The bimetallic COFs exhibited excellent catalytic performance for asymmetric cyanation of aldehydes, Diels–Alder reaction, alkene epoxidation, and epoxide ring-opening reactions. The construction of the Zn-based COFs **3** and **4** experienced a direct synthesis. However, the introduction of active catalytic metal ions such as Mn or Cr went through the post-synthetic strategy.

Constructing metal-COF catalyst for capturing CO_2 and simultaneously converting it to chemical fuels is a promising approach to address the energy crisis. Huang reported a charged imidazolium functionalized porphyrin-based COF, **Co-iBFBim-COF-X** ($X = F^-$, Cl^-, Br^-or I^-), for electrocatalytic CO_2RR (Fig. 20a). [86] The imidazolium groups with free halogen counter ions were integrated into Co-porphyrin-based COFs. Thus, the catalytic pockets with a **Co-TAPP** centers and halogen counter ions were constructed, where the X^- of imidazolium nearby the active Co-porphyrin sites can stabilize the key intermediate *COOH and can interact with water to reduce the binding energy between H_2O and Co-porphyrin, thus inhibiting HER. Among them, **Co-iBFBim-COF-I$^-$** showed the best significant enhancement of kinetic activity for CO_2RR. This work achieved such delicate control of catalytic pockets with free anions in heterogeneous catalysts.

The electrochemical NRR under ambient conditions is attractive in sustainable ammonia production. An *in-situ* synthesis of COFs with transition metal centers as NRR electrocatalysts was developed by Jin and Xiang (Fig. 20b). [85] They introduced ordered quasi-phthalocyanine N-coordinated transition metal (Ti, Cu, or Co) centers into a **2D COF** trough a pyrolysis-free synthetic method. During the NRR process, the N-coordinated Ti center has stronger adsorption and activation ability for N_2 than those of Co and Cu. So the as-prepared **Ti-COF** exhibited the highest catalytic activity and selectivity for the electrocatalytic NRR. Besides, Feng and Dong reported a series of 2D conjugated covalent organic frameworks (**2D *c*-COFs**) with $M-N_4-C$

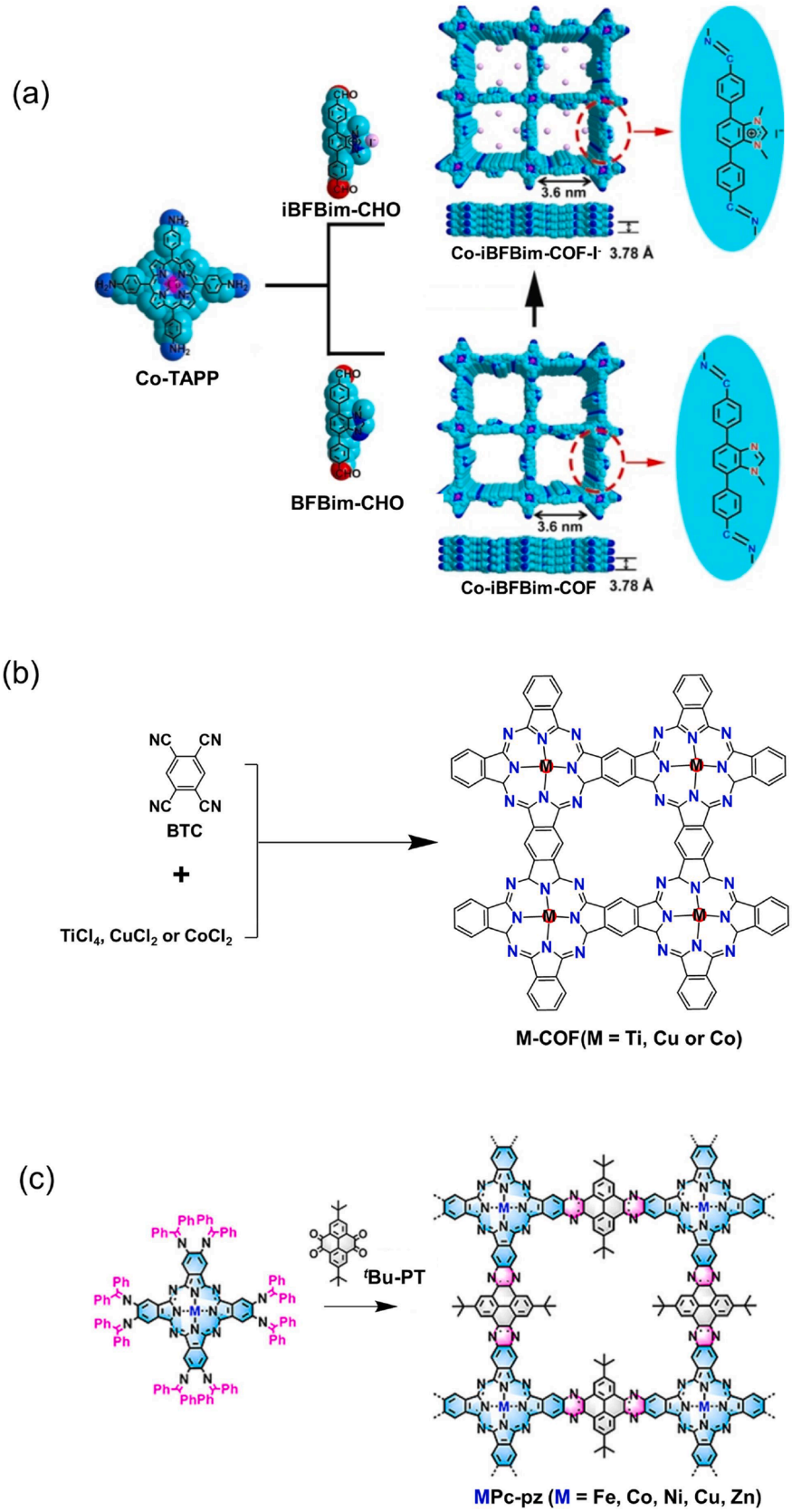

Fig. 20. (a) The synthesis route of **Co-iBFBim-COF-I⁻** and **Co-BFBim-COF**. Reproduced with permission [86]. Copyright 2022, Wiley-VCH. (b) The synthesis route of **2D M-COF** (M = Ti, Cu, or Co). Reproduced with permission [85]. Copyright 2022, American Chemical Society. (c) The synthetic route of **MPc-pz** (M = Fe, Co, Ni, Cu, and Zn). Reproduced with permission [83]. Copyright 2021, American Chemical Society.

center active sites (M= Fe, Co, Ni, Mn, Zn, and Cu) constructed by metal phthalocyanine (MPc) and pyrazine linkages ((Fig. 20c). The **2D *c*-COFs** with Fe−N_4−C center (act as catalytic sites) exhibit higher ammonia yield rate and Faradaic efficiency. [83] It follows that precisely tailoring metal-active sites can be designed into building blocks, thus forming MOFs and COFs materials. These works demonstrate the potential of COFs as next-generation organic catalysts and electrocatalysts for CO_2RR and NRR.

4.1.2. *Active metal ions installed via post-functionalization of COFs*

4.1.2.1. Imine linkage. In coordination chemistry, it has been well demonstrated that the imine linkages can incorporate a variety of metal ions [122]. Thus, exploring the large amount of imine-linked COFs for metal ion incorporation is very likely to achieve the functionality of catalysis. The pioneering work of metal ions-docked COF through the imine bonds was reported by Wang and co-workers [118]. The imine-linked 2D **COF-LZU1** was first obtained through an imine-condensation reaction (Fig. 21a). The distance of nitrogen atoms in adjacent layers is around 3.7 Å This makes **COF-LZU1** an ideal scaffold for incorporating metal ions. Through a simple post-treatment, Pd (II) decorated **Pd/COF-LZU1** was successfully prepared without losing the crystallinity. The coordinated Pd(II) is proposed to be located in between the two layers of **COF-LZU1**. A clear decrease in the BET surface area accompanied by a slight change in the pore size distribution of **Pd/COF-LZU1** after the post-modification were observed. This demonstrates that the presence of Pd(II) does not block the channels of the **COF-LZU1. Pd/COF-LZU1** exhibited excellent catalytic performance for

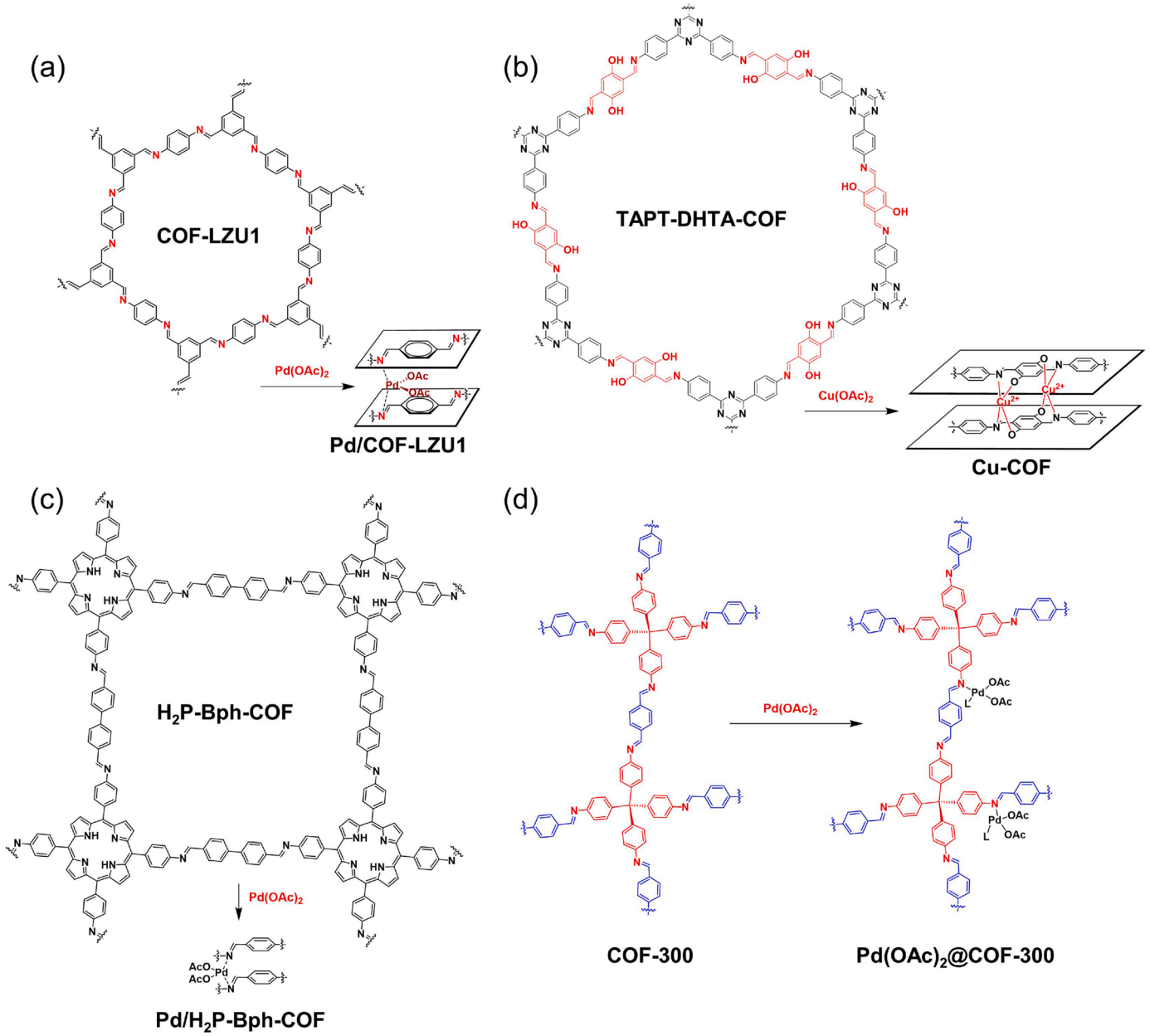

Fig. 21. (a) The structure of **Pd/COF-LZU1** through impregnation of $Pd(OAc)_2$ into **COF-LZU1**. Reproduced with permission [118]. Copyright 2011, American Chemical Society. (b) The structure of **Cu-COF** through impregnation of $Cu(OAc)_2$ into **TAPT-DHTA-COF**. Reproduced with permission [119]. Copyright 2017, American Chemical Society. (c) The structure of **Pd/H_2P-Bph-COF** through impregnation of $Pd(OAc)_2$ into **H_2P-Bph-COF**. Reproduced with permission [120]. Copyright 2015, Elsevier. (d) The structure of **Pd$(OAc)_2$@COF-300** through impregnation of $Pd(OAc)_2$ into **COF-300** pores. Reproduced with permission [121]. Copyright 2016, Wiley-VCH.

Suzuki-Miyaura coupling reaction. Due to the unique structure, **Pd/COF-LZU1** allows efficient access to the catalytic sites and fast mass transport of the reactants and products, thus resulting in excellent catalytic activity.

Chen and co-workers report another example of imine-linked **TAPT-DHTA-COF**, which can efficiently incorporate the copper ions through the coordination provided by hydroxyl groups and imine linkages (Fig. 21b) [119]. The obtained **Cu-COF** exhibited excellent catalytic performance toward the selective oxidation of styrene to benzaldehyde. Notably, the COF catalyst with superior crystallinity exhibits higher activity due to the facilitated diffusion of reactants induced by the highly ordered structure. In addition, the substrate scope study indicated that the larger steric hindrance from cyclo and olefins-substituents is unfavorable for the reactants to access the channels of **Cu-COF**, thus leading to poor catalytic efficiency.

Jiang and co-workers reported a porphyrin-based 2D COF (**H_2P-Bph-COF**) through imine condensation (Fig. 21c) [120]. The N atoms are either from the imine linkages or the porphyrin. Both of these two types of N atoms are periodically distributed in the COFs structure and play a key role in stabilizing and uniformly dispersing the Pd(II) within the structure of **H_2P-Bph-COF**. The thus-yielded **Pd/H_2P-Bph-COF** exhibits excellent catalytic activity for the Suzuki-coupling reaction with good selectivity.

The distances of the nitrogen atoms in adjacent layers of these 2D COFs are usually within the range of van der Waals forces, which make an ideal scaffold for incorporating metal ions. The interlayer distances are relatively small for the catalytic reactions to occur between the layers, so the catalytic reactions likely occur in the channels of COF instead of the space between adjacent layers.

Besides imine-based 2D COFs, Esteves, Buarque, and co-workers reported a $Pd(OAc)_2$ modified 3D COFs and its catalysis for different cross-coupling reactions (Fig. 21d) [121]. **COF-300** contains abundant imine groups in the skeleton of the COFs structure, which afford coordination sites for $Pd(OAc)_2$ on the walls of the nanochannels. **Pd$(OAc)_2$@COF-300** was easily obtained through post-synthetic modification. The **Pd$(OAc)_2$@COF-300** exhibits good catalytic performance for Sonogashira, Heck, and Suzuki cross-coupling reactions. Besides the active metal ions, the pore structure in the 3D COF shows a confined effect for the preorganization of the reactants, thus entropically facilitating the reaction.

4.1.2.2. Hydrazine linkage. Apart from imine linkage, hydrazine linkage was also explored in metal ions-functionalized COF catalysts. A molybdenum-doped COF (**Mo-COF**) was prepared by Jiang and co-workers by using a modified approach (Fig. 22a) [123]. This design facilitates the access of the reactants to the active metal ions through the channels of the COFs. The **Mo-COF** acts as a nanoreactor and shows excellent catalytic performance for the epoxidation of alkenes. Notably, the control experiment by using the pure COF without loading Mo and the pure $Mo(HSY)_2$ without the framework structure both show much lower catalytic activities. In addition, increasing the size of the substrates resulted in a lower yield. These observations demonstrate that the oxidation reaction indeed takes place inside the nanochannel of the framework, which provides a desirable microenvironment for selective oxidation.

Esteves and co-workers reported another example of hydrazine-based COFs (**RIO-12**) for nickel ions decoration [124]. **NiCl@RIO-12** was synthesized through post-synthetic modification (Fig. 22b). Interestingly, the amount of incorporated nickel ions could be tuned from 3.6 to 25 wt% by changing the loading conditions. The resulting nickel-decorated COFs preserved their crystallinity but with lower BET surface areas. **NiCl@RIO-12** showed excellent catalytic performance for Suzuki–Miyaura reaction.

4.1.2.3. Salen or Salphen linkage. The Salen (*N,N′*-Bis(salicylidene)ethylenediamine) unit, featuring stabilization of metal ions in various oxidation states, has been considered as one of the most important ligands to construct efficient catalysts for organic transformations. Wang, Ding, and co-workers successfully introduced the Salen moieties into COFs structures (Fig. 23a) [125]. The Salen-based COF was realized in one single step. And subsequent metalation of **Salen-COF** with different metal ions leads to the successful preparation of Metallo-Salen-based COFs (**M/Salen-COFs**), which preserve their crystallinities according to the PXRD patterns. The high metal loading contents from the ICP analysis indicate that most of the chelate sites in the Salen units have been occupied by the metal ions. The well-defined distribution of the active metals on the COF backbone enabled their high catalytic activity towards the Henry reaction.

Yang and co-workers synthesized another salen-based COF via *in-situ* salen unit formation through imine condensation (Fig. 23b) [126]. Hierarchical pores were obtained for **COF-salen** due to its AA stacking mode of the eclipsed structures. Metal-based **COF-salen-M** (M= Co, Mn,

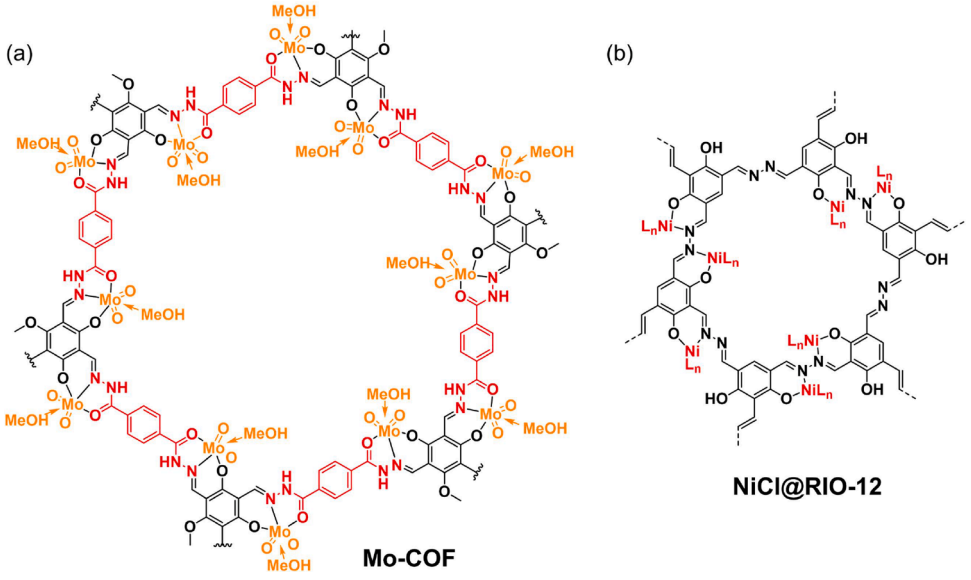

Fig. 22. (a) The structure of **Mo-COF**. Reproduced with permission [123]. Copyright 2014, Royal Society of Chemistry. (b) The structure of **NiCl@RIO-12**. Reproduced with permission [124]. Copyright 2019, Wiley-VCH.

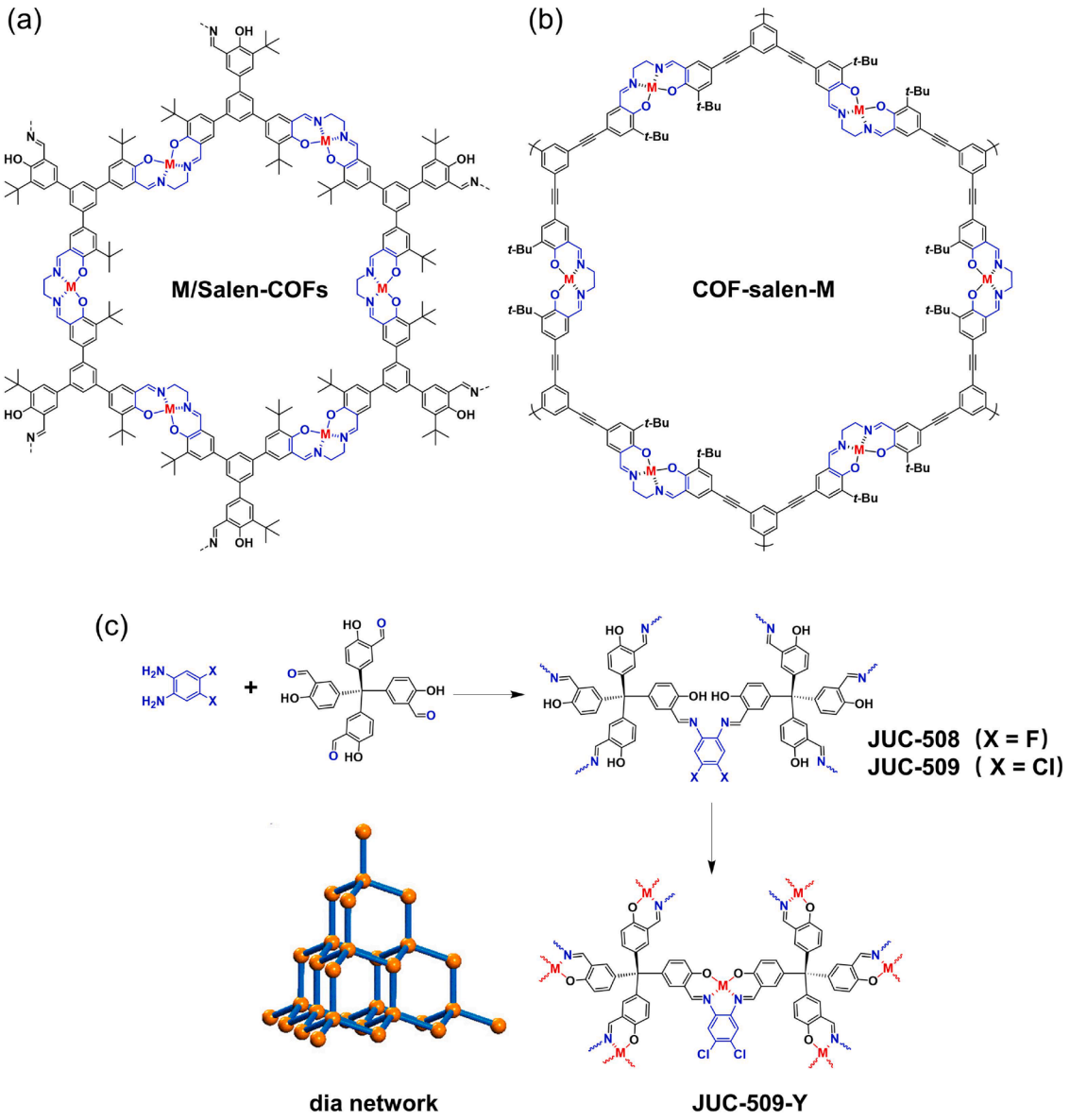

Fig. 23. (a) The structure of **M/Salen COFs**. Reproduced with permission [125]. Copyright 2019, Royal Society of Chemistry. (b) The structure of **COF-salen-M**. Reproduced with permission [126]. Copyright 2017, American Chemical Society. (c) The preparation of 3D-M-Salphen-COFs (**JUC-509-Y**) (Y = Mn, Cu or Eu) via the metal ions incorporation. Reproduced with permission [127]. Copyright 2019, American Chemical Society.

Cu, Zn) can be easily obtained by the treatment of different metal ions and maintained crystallinity. Notably, the metal loading content (>10%) is close to the theoretical value according to the ICP measurements. Most of the salen units have been coordinated by the metal ions due to the highly ordered channels in the COF structure. In addition, decreases in the pore volume and diameter were observed for the metal-modified **COF-salen–M**. This also suggests the occurrence of the coordination does happen inside of the channels of **COF-sale. COF-salen-Co** and **COF-salen-Mn** were then used as heterogeneous catalysts to successfully catalyze epoxide hydration and olefin epoxidation with a wide substrate scope. The lower catalytic activity of the corresponding amorphous polymers as control catalysts further demonstrated the advantages of the highly ordered COF structure. **COF-salen-M** can efficiently isolate the active sites encapsulated in the unique layered crystalline structures by restricting their mobility and generating cooperation between nearby active sites in adjacent layers.

Fang and co-workers extended the metal ions-decorated COFs from 2D to 3D. Salphen units were introduced into a tetrahedral tetraphenyl methane-based skeleton to construct two extended 3D Salphen-based COFs, named **JUC-508** and **JUC-509** (Fig. 23c) [127]. Furthermore, 3D M-Salphen-based COFs as metal ions-containing counterparts (**JUC-509-Y**) were acquired through the introduction of metal ions. The PXRD indicated that the crystalline structure remained after the metal ions incorporation. **JUC-509-Cu** exhibits high catalytic activity in the elimination of superoxide radicals. The high crystallinity and confined effect of porosity within COFs enhanced the high catalytic effect of the metal ion active sites.

4.1.2.4. Bipyridine linkage. A series of 2D COFs (**BPy COF**) containing imine and bipyridine units as two different types of nitrogen ligands were reported by Gao and co-workers (Fig. 24a) [128]. The contents of the bipyridine ligands can also be adjusted by using a three-component system through sophisticated design. The density of the imine groups is constant, while the contents of bipyridine could be adjusted according to the ratio of the two monomers. Pd (II) and Rh (I) were then simultaneously and uniformly distributed to the **BPy COF**. Pd (II) mainly occupies the imine sites between adjacent layers, while Rh (I) is mainly coordinated with bipyridine units. The bimetallic Rh (I)/Pd (II) based

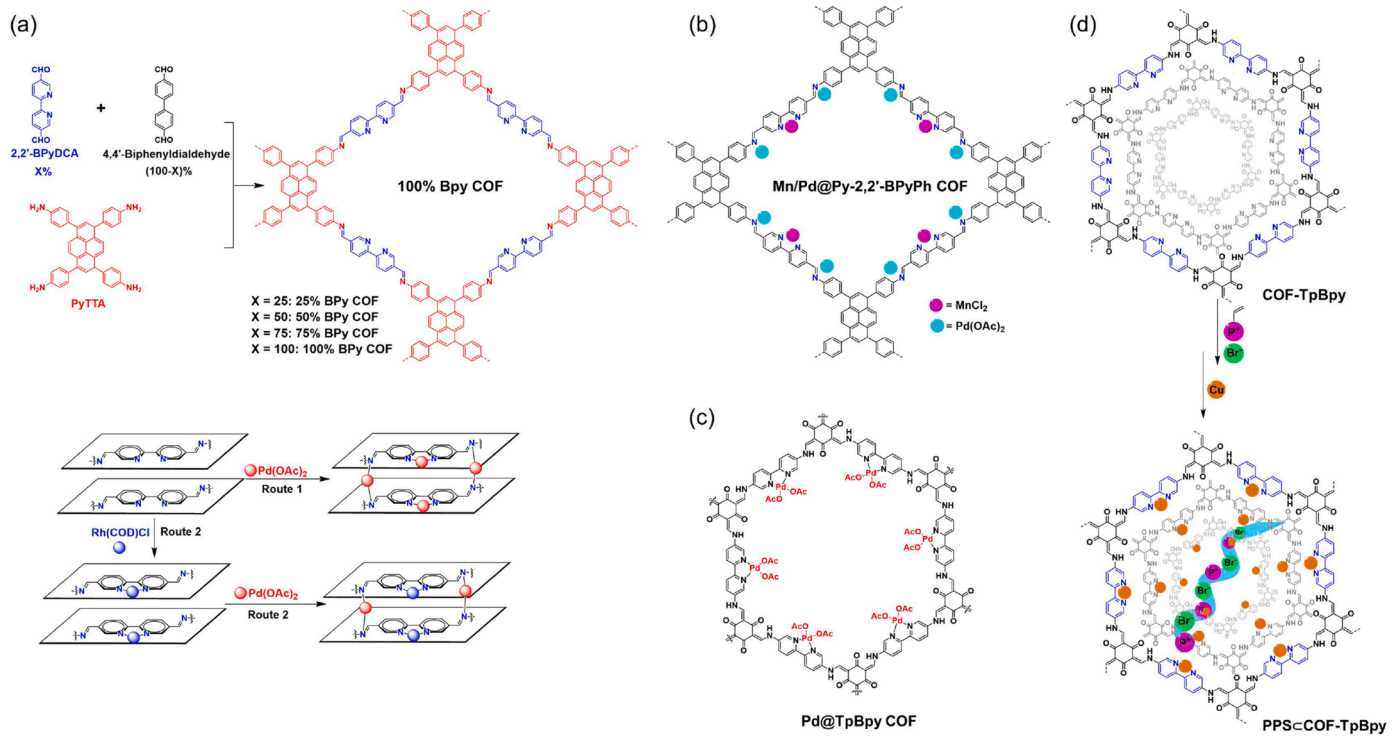

Fig. 24. (a) The three-component COFs and its bimetallic docked routes. Reproduced with permission [128]. Copyright 2016, Wiley-VCH. (b) The topology structures of Mn/Pd bimetallic docked COFs. Reproduced with permission [129]. Copyright 2016, Royal Society of Chemistry. (c) The topology structures of **Pd@TpBpy-COF**. Reproduced with permission [130]. Copyright 2019, Wiley-VCH. (d) The schematic of **PPS⊂COF-TpBpy-Cu** synthesis and topology structures of **COF-TpBpy** and **PPS⊂COF-TpBpy-Cu**. Reproduced with permission [131]. Copyright 2016, American Chemical Society.

COF can be obtained through a programmed synthetic procedure. The catalyst exhibited excellent catalytic performance in a one-pot addition–oxidation cascade reaction. The same group further fabricated a bimetallic docked COF via a post-synthetic procedure (Fig. 24b) [129]. **Py-2,2′-BPyPh COF** was first synthesized through imine condensation, which contained both bipyridine and imine ligands. Mn (II) and Pd (II) were then introduced into the COF sequentially to form **Mn/Pd@Py-2,2′-BPyPh COF**. Mn (II) usually coordinates with the bipyridine ligands, while Pd (II) would attach to the imine linkages. As we know, metal Pd could catalyze the Heck reaction to produce aromatic/aliphatic olefins, while Mn could catalyze the epoxidation reaction of olefins into epoxides. Therefore, the **Mn/Pd@Py-2,2′-BPyPh COF** exhibits superior catalytic activity towards a Heck-epoxidation tandem reaction.

Stanley and co-workers constructed a **Pd@TpBpy COF** by using the same COF parent **TpBpy COF** treated with $Pd(OAc)_2$ (Fig. 24c) [130]. **Pd@TpBpy COF** showed superior catalytic performance in catalyzing the additions of arylboronic acids to β,β-disubstituted enones. Notably, the lack of bipyridine units (biphenyl instead) as the reference catalyst is inactive. This demonstrated that the active catalysis is derived from the palladium coordination with the bipyridine linker within the COFs, not the coordination with the imine nitrogens.

Ma and co-workers confined the linear polymers featuring catalytically active components and Cu ions in the channels of the COFs and constructed a multifunctional catalyst (Fig. 24d) [131]. **COF-TpBpy** was first synthesized through imine condensation. An *in-situ* radical polymerization of the phosphonium salts (PS) as ionic monomers in the **COF-TpBpy** afforded **PPS⊂COF-TpBpy**. The polymeric phosphonium salts (PPS) were confined in the channels of **COF-TpBpy**. The Cu(II) was subsequently decorated to the channels of the **PPS⊂COF-TpBpy** through the strong chelation provided by the bipyridine units. The final composite catalyst **PPS⊂COF-TpBpy-Cu** was obtained, which maintained the crystallinity and porosity. Easy access of the reactants to the active catalytic site was thus realized. A significantly improved catalytic activity compared to every single component or the combination of the ionic component and metallated COF as the reference catalysts was obtained. The excellent catalytic activity of **PPS⊂COF-TpBpy-Cu** derived from the mobility of the active sites on the highly flexible PPS and their great potential cooperation with the Lewis acid sites (Cu species) anchored on the COF. The confined space provided by the COF enriched essential catalytic components in the microenvironment, thus leading to superior catalytic performance.

Similar to the above-mentioned strategy, a newly designed **2D COF** with incorporated Re complex (**Re-COF**) was used as photocatalysts for visible-light-driven CO_2RR (Fig. 25a). [87] The **2D COF** was synthesized via solvothermal reactions. Then, $Re(CO)_5Cl$ can coordinate with the bipyridine ligand in the COF to form **Re-COF**, which exhibits intrinsic light absorption and charge separation (CS) properties. **Re-COF** can be used as a photocatalyst for CO_2RR to reduce CO_2 to form CO under visible light illumination with high selectivity (98%). In another case, a bipyridine-containing covalent organic framework by way of engineering active Co(II) ions into its porous framework (**Co-TpBpy**) is utilized as an OER catalyst (Fig. 25b) [79]. The unusual catalytic stability arises from the synergetic effect of the inherent porosity and the presence of coordinating units in the **Co-TpBpy** skeleton.

4.1.2.5. Others. The hydroxyl group as a docking site within COFs was utilized to coordinate the transition-metal ions by Ma and co-workers (Fig. 26) [132]. They synthesized two 2D imine-linked COFs (**TAPT-2,3-DHTA** and **PyTTA-2,3-DHTA**) bearing hydroxyl functionalities. Next, the corresponding vanadium-docked COFs (**VO-TAPT-2,3-DHTA** and **VO-PyTTA-2,3-DHTA**) were successfully prepared through post-synthetic modification and maintained their framework crystallinities. The hydroxyl groups bind with vanadium to form activity sites, which were distributed in the 1D channels of the COFs. The vanadium-docked COFs as heterogeneous catalysts can catalyze the Mannich-type reaction with excellent catalytic performance for a wide range of substrates.

HER is of great significance for the popularization of clean H_2 energy,

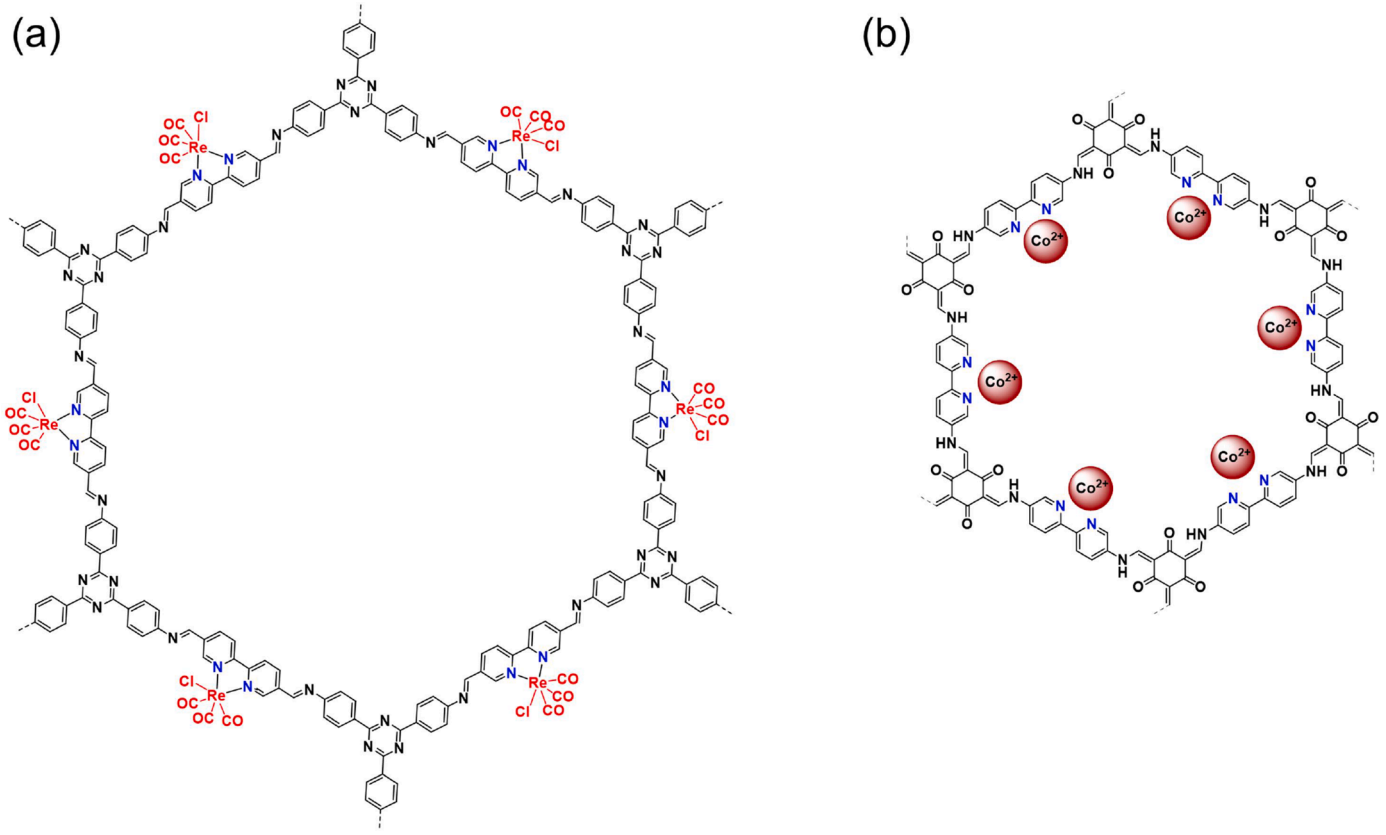

Fig. 25. (a) The chemical structure of **Re-COF**. Reproduced with permission [87]. Copyright 2018, American Chemical Society. (b) The chemical structure of **Co-TpBpy**. Reproduced with permission [79]. Copyright 2016, American Chemical Society.

but exploring new novel electrocatalysts with both lower overpotential and higher stability remains a challenge. As we know, the triazine-cored sp^2 carbon-conjugated COFs possess excellent semiconducting properties and photoelectrochemical activities, which can be used to construct electrocatalysts. Chen et al. reported a Ru complex of sp^2 carbon-conjugated COF as an efficient electrocatalyst for HER (Fig. 27a) [73]. The **COF-1** was synthesized via the Knoevenagel condensation reaction. The triazine moieties in COF can coordinate with many metal ions. Therefore, **Ru@COF-1** can be formed by adding **COF-1** and ruthenium (III) chloride to the methanol solution. Under the acidic condition, the nitrogen of triazine could be protonated and greatly improve the electrical conductivity of **Ru@COF-1**. Meanwhile, ruthenium ions, as active catalytic sites, can interact with hydrogen ions more easily and lead to excellent electrocatalytic performance in HER.

Porphyrin-based COF anchoring Au single atoms for photocatalytic NRR through a post-modification strategy was reported by Zhao and Jiang (Fig. 27b). [133] The porphyrin building blocks act as the docking sites to immobilize Au single atoms as well as light-harvesting antennae. The microenvironment of the Au catalytic center is precisely tuned by controlling the functional groups at the proximal and distal positions of porphyrin units. As a result, **COF1-Au** decorated with strong electron-withdrawing groups (benzothiadiazole) exhibits a high activity toward NH_3 production. From a more sustainable perspective, the foregrounds of COF-based catalysts are infinite. Its implementation has allowed access to new modes of reactivity and structural diversity from an organic point of view.

4.2. Ultrafine MNP-decorated COFs

MNPs have been widely used in heterogeneous catalysis because of their high surface areas and small size distribution, enabling high catalytic activities. However, due to the easy aggregation of MNPs [134], the formation of narrowly dispersed MNPs in the solid supports is difficult to realize. As mentioned above, the COFs possess highly ordered channel structures, porosity, and structure tunability, which make them ideal candidates as supports for loading and stabilizing catalytically active MNPs. The microenvironment of COFs provides coordination sites for uniform nucleation of MNPs inside the COFs channels. The confined effect of the microenvironment created by the highly ordered porous channels can realize the size control during the growth of nanoparticles. Different from the COFs decorated with metal ions, the formation of the MNPs in COFs usually needs an external reduction process. The use of an external reducing agent may change the internal structure of COFs, which usually affects their crystallinity and porosity. Therefore, a relatively robust structure is needed before the post-functionalization. Most of the reported examples are prepared through post-modification processes where MNPs are decorated on pre-synthesized COF materials.

4.2.1. Catalytically active metal ions pre-installed in monomers

Banerjee, Balarman, and co-workers developed an *in-situ* generation of metal (Pd) NPs-loaded COF (**Pd@TpBpy**) through the condensation reaction of a predesigned Pd-metal-anchored tailored building block (**Bpy-PdCl$_2$**) and **Tp** (Fig. 28) [135]. The Pd NPs were formed during the formation of the COFs via breaking the Pd-N bond without using conventional reducing agents. More importantly, the formation of Pd NPs has no influence on the structural integrity of the COF (**TpBpy**). Both the BET surface area and the pore size decrease compared to the pristine **TpBpy**. The average size of the Pd NPs was found to be 12 ± 4 nm, which suggested that the Pd NPs distributed at the surface and interlayer spacing of the COF. The **Pd@TpBpy** showed superior catalytic performance in the synthesis of 2-substituted benzofuran derivatives via a tandem process. This is due to the uniform NPs within the internal microenvironment as active catalytic sites, as well as the high porosity and ordered structure of COFs.

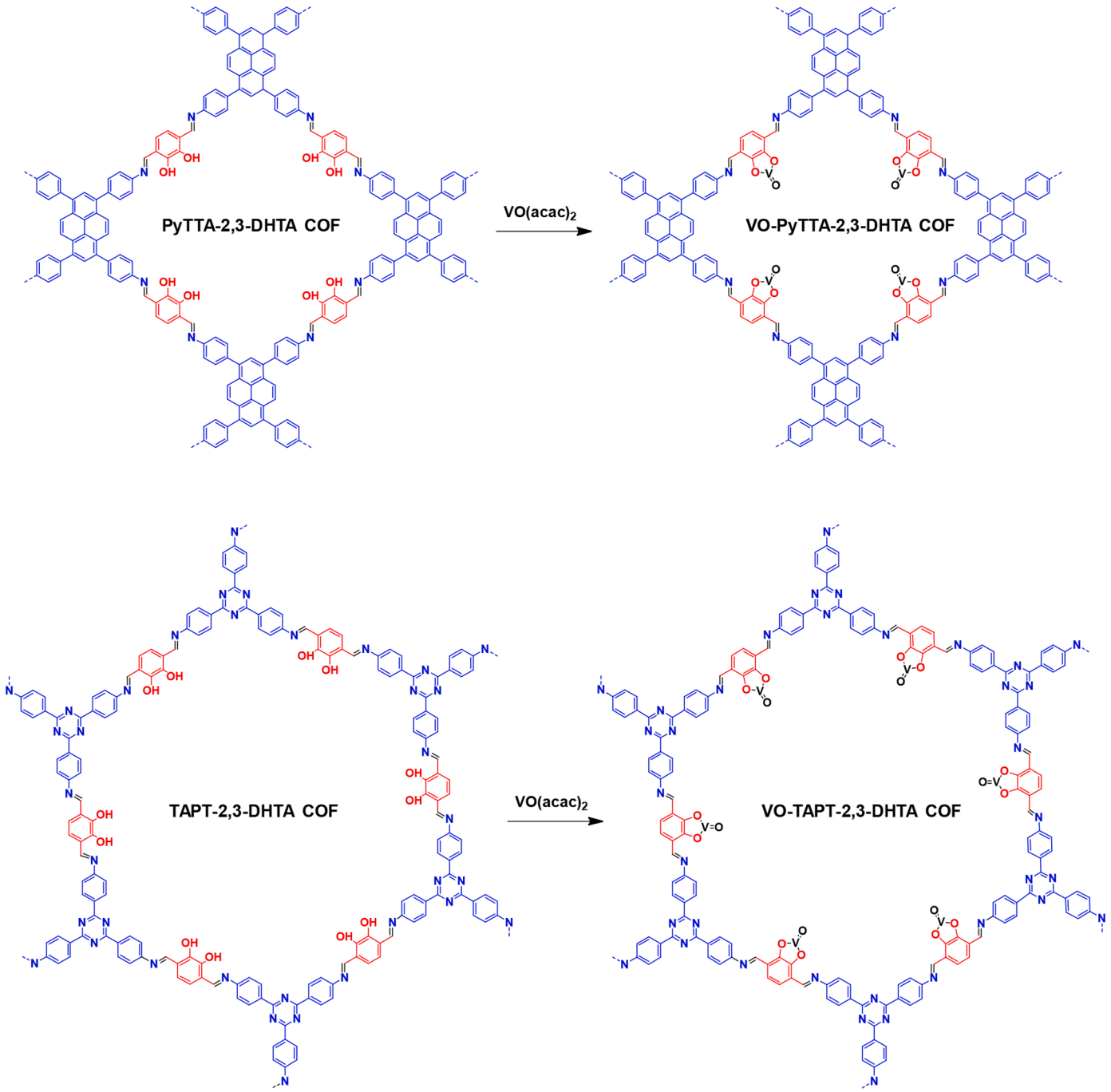

Fig. 26. The structures of **2D TAPT-2,3-DHTA COF, PyTTA-2,3-DHTA COF**, and vanadium docked **VO-TAPT-2,3-DHTA COF, VO-PyTTA-2,3-DHTA COF**. Reproduced with permission [132]. Copyright 2019, American Chemical Society.

4.2.2. Catalytically active metal ions installed via post-functionalization of COFs

4.2.2.1. β-ketoenamine linkage. To achieve COF-supported MNPs, the first challenge that needs to be overcome is their moderate stability under catalytic conditions. Banerjee and co-workers reported a highly stable β-ketoenamine linked COFs (**TpPa-1**) by introducing an irreversible keto−enol tautomerization within the COF backbone (Fig. 29a) [136,137]. Au(0), Pd(0) NPs can be easily immobilized into COF **TpPa-1** by a simple solution infiltration followed by $NaBH_4$ reduction. The excellent stability and crystallinity of **TpPa-1** make it a suitable support for MNPs. The obtained highly dispersed Au(0) and Pd(0) NPs exhibit superior reactivity towards nitrophenol reduction reaction, Cu-free Sonogashira, Heck, sequential one-pot Heck–Sonogashira cross-coupling reactions (Fig. 29a, b).

Murugavel and co-workers reported another example of β-ketoenamine linked stable COF (**TAT-TFP 2**) [138]. The nitrogen sites provide excellent affinity toward Pd(II). Post-treatment of **TAT-TFP 2** with Pd $(AcO)_2$ gives $\mathbf{Pd^{II}}$**/TAT-TFP**. Further reduction by $NaBH_4$ yields $\mathbf{Pd^0}$**/TAT-TFP**. Uniform distributions of Pd(II) and Pd(0) sites in the COFs were observed. Ultra-small MNPs within the COF cavities benefit from the confined synthesis approach. $\mathbf{Pd^0}$**/TAT-TFP** exhibits superior catalytic activity towards Suzuki–Miyaura reaction (Fig. 29c).

4.2.2.2. Imine linkage. Imine-linked COFs have acted as excellent supports for the immobilization of metal ions. This has been discussed in

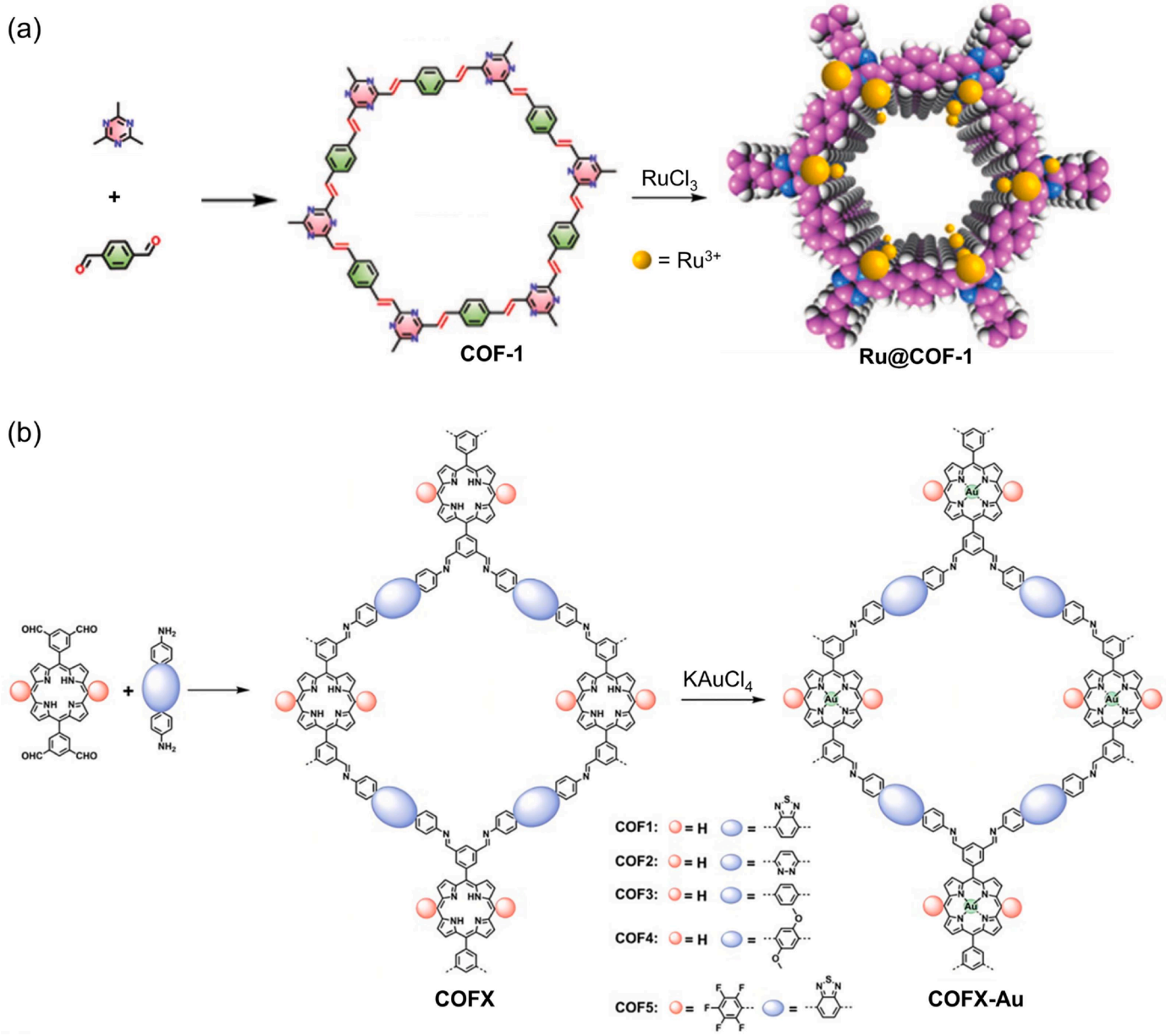

Fig. 27. (a) The synthesis route of **COF-1** and **Ru@COF-1**. Reproduced with permission [73]. Copyright 2022, Wiley-VCH. (b) The synthetic strategy of **COFX** and **COFX-Au**. Reproduced with permission [133]. Copyright 2023, American Chemical Society.

Section 3.1. Several examples of imine-based COFs have also been successfully decorated with metal nanoplates. Vaidhyanathan and co-workers reported a stable imine-based COF (**IISERP-COF5**), which can be loaded with Co^{2+}ions through sample wet chemistry. Further reduction with $NaBH_4$ yielded the composite (**Co@COF**) [139]. The loading content of Co was determined to be as high as 16 wt%. The sizes of the MNPs are in the range of 3–5 nm, indicating that the MNPs predominantly reside in the channels of the COF (Fig. 30a). The **Co@COF** exhibits excellent catalytic performance for the hydrogenation of nitro/nitrile compounds in the presence of $NaBH_4$ with good selectivity. The methoxy groups were designed next to the imine bonds to provide exceptional stability. The N-rich sites favor strong binding interactions with Co. The highly ordered COF channels can avoid the growth of MNPs outside the COF and thus lead to a stable heterogeneous MNP catalyst.

Murugavel and co-workers reported a similar 2D COF (**TAT-DHBD 1**) structure with OH groups installed instead of the methoxy groups [138]. The abundant imine groups and the phenolic OH groups are suitable for metal ions incorporation. Post-treatment of **TAT-DHBD 1** with $Pd(AcO)_2$ gives **Pd^{II}/TAT-DHBD**. Further reduction by $NaBH_4$ yields **Pd^0/TAT-DHBD**, which exhibits catalytic activity towards the Suzuki–Miyaura cross-coupling reaction (Fig. 30b).

Dong and co-workers reported a hydrazone-linked 2D COF (**COF-ASB**) through the imine condensation reaction [140]. The hydrazone linkage is similar to the imine linkage but with better stability. Thus, **COF-ASB** can act as an ideal support to upload Ru NPs to generate **Ru@COF-ASB** (Fig. 30c). **Ru@COF-ASB** exhibits high catalytic activity for the one-pot tandem synthesis of imine products from benzyl alcohols and amines.

4.2.2.3. Confined growth of nanoparticles in microenvironment. Encapsulation of MNPs inside the channels of COFs is essential for the confined growth of MNPs with controlled size. The chelate sites on the channels are necessary because they could facilitate the coordination of metal ion precursors and later formation of nucleation sites, thus realizing the confined growth of MNPs with controlled size.

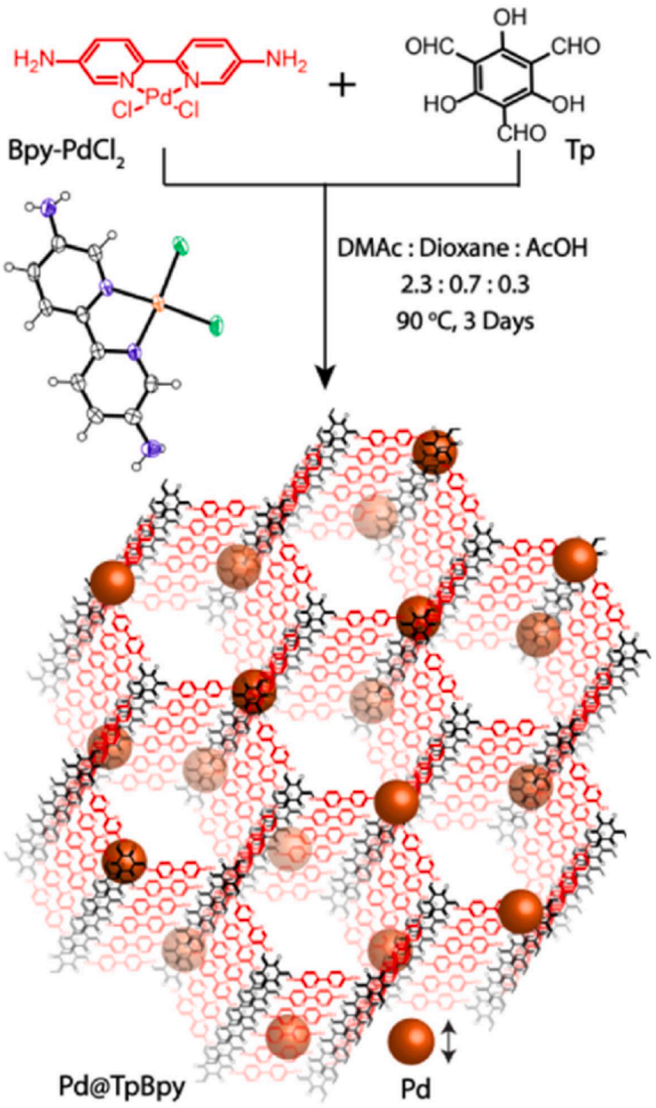

Fig. 28. Direction synthesis of **Pd@TpBpy** through *in-situ* generation of highly dispersed Pd NPs in the **TpBpy COF** skeleton. Reproduced with permission [135]. Copyright 2017, American Chemical Society.

Zhang, Gu, and co-workers synthesized a thieoether-containg COF (**Thio-COF**) and used it for the confined growth of ultrafine Pt and Pd NPs [141]. The thioether groups exhibit strong binding interactions with metal ions and point inside the cavity of the COFs (Fig. 31a). Thus, they can act as nucleation sites for the confined growth of NPs in the well-defined channels of the COF. The evenly distributed thioether groups on the highly ordered porous channels enabled the formation of ultrafine Pt or Pd NPs (1.7 ± 0.2 nm). The as-prepared COF-supported ultrafine Pt NPs and Pd NPs (**PtNPs@COF** and **PdNPs@COF**) showed excellent catalytic activity in nitrophenol reduction and Suzuki−Miyaura coupling reaction. Notably, ultrafine MNPs likely reside in the pore of the COFs structures rather than the surface. In addition, the well-defined cavities of the COFs provide a protecting shell ensuring a good stability of the MNPs.

Dong and co-workers reported a paraffin-chain quaternary ammonium salt-based Pd NP COF (**Pd@COF-QA**) [142]. The loaded Pd NPs were well dispersed in the cavity of the **COF-QA** with an average size of 2.4 nm, which is due to the well-defined channels of **COF-QA** (Fig. 31b). The obtained **Pd@COF-QA**, as a phase transfer catalyst, shows high catalytic activity for the aqueous Suzuki–Miyaura coupling reaction.

Zhao, Zhang, Li, and co-workers reported another example of ultrafine and highly dispersed Pd NPs grown in the channels of a highly rigid 3D COF (**SP-3D-COF-BPY**) as support [143]. Bipyridine units in the skeleton of the 3D COFs are used for anchoring the Pd ion precursors inside the channels (Fig. 31c). The uniform unobstructed 1D channels provided by the **SP-3D-COF-BPY** maximize the accessibility of the active sites. **Pd(II)@SP-3D-COF-BPY** with Pd(II) chelating to the bipyridine moieties was then prepared through a simple wet-chemistry approach. Pd NPs with an average diameter of 1.28 nm were observed from TEM. The Pd-decorated COFs exhibited superior catalytic efficiency in catalyzing the Suzuki–Miyaura coupling reaction.

Deng, Li, and co-workers developed the **PY-DHBD-COF** through a Schiff-base condensation reaction, which bears an adjacent hydroxyl group and imine bond in each constitutional unit (Fig. 32). [144] In the system of photocatalytic HER, the adsorption of $PtCl_6^{2-}$ on a specific site near the hydroxyl group and imine-N and the subsequent photoreduction lead to *in-situ* photo deposition of Pt clusters on the 2D COF surface layer with high dispersion. Pt exists in the form of both single atoms and small clusters (from ~ 1 nm to ~5 nm), which depends on the loading amount of H_2PtCl_6. These uniformly dispersed Pt co-catalysts can help easily trap localized photogenerated electrons on **PY-DHBD-COF**, thus suppressing charge combination during the long-distance transfer process, therefore leading to excellent HER performance. The Pt cluster-loaded COF established a micro-environment for co-catalyst

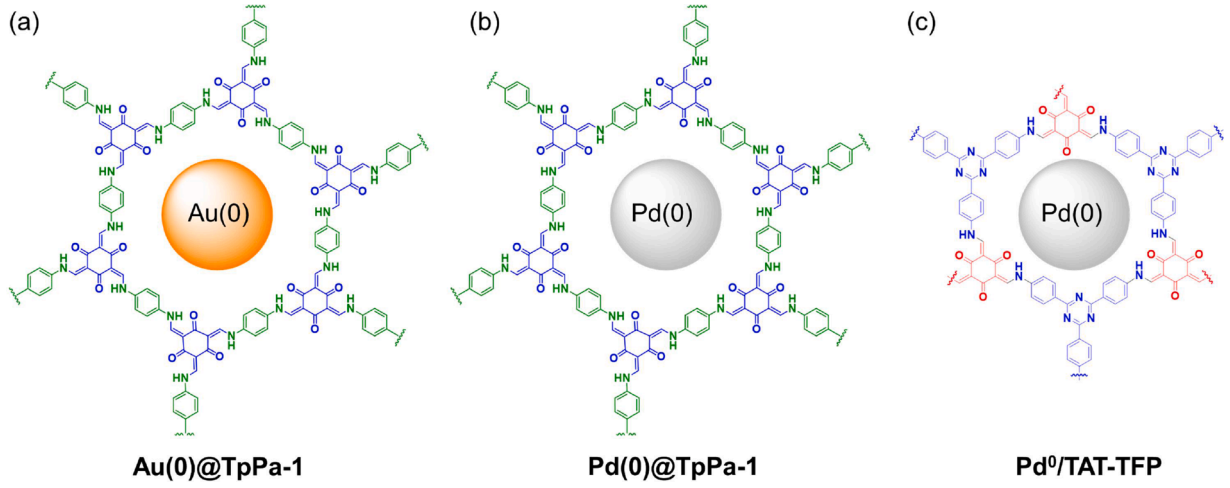

Fig. 29. The topology structures of (a) the **Au(0)@TpPa-1**, (b) **Pd(0)@TpPa-1** [136,137] and (c) **Pd(0)@TAT-TFP** [138]. Reproduced with permission [136]. Copyright 2014, Royal Society of Chemistry. Reproduced with permission [137]. Copyright 2014, Royal Society of Chemistry. Reproduced with permission [138]. Copyright 2017, Wiley-VCH.

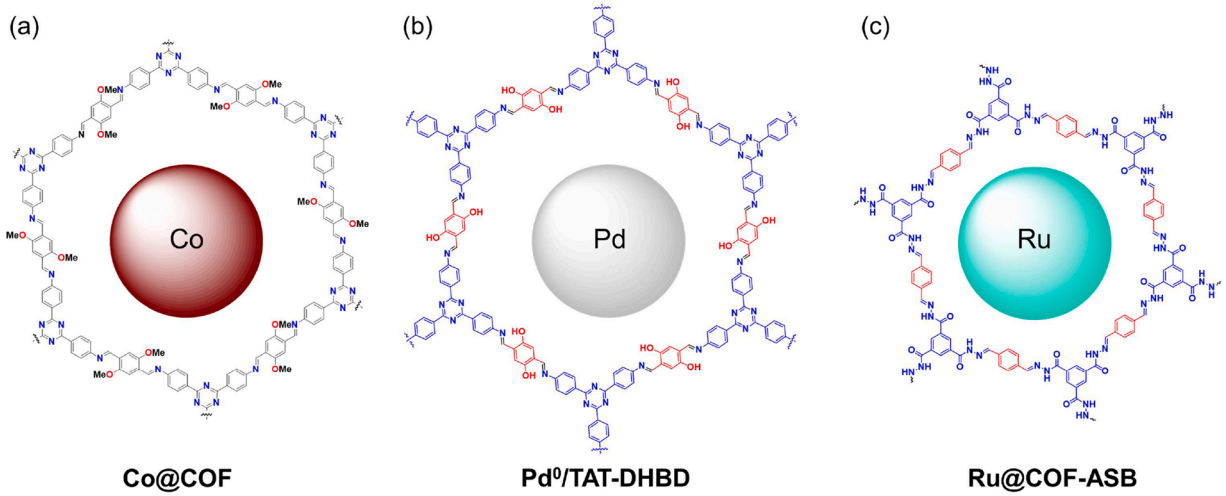

Fig. 30. The structures of (a) **Co@COF** [139], (b) **Pd(0)@TAT-DHBD** [138], and (c) **Ru@COF-ASB** [140]. Reproduced with permission [138]. Copyright 2017, Wiley-VCH; Reproduced with permission [139]. Copyright 2018, Wiley-VCH; Reproduced with permission [140]. Copyright 2018, American Chemical Society.

deposition on a photocatalyst for more efficient photocatalysis.

4.2.2.4. Chiral COFs support. Chiral COFs can be the asymmetric template to arrange the reaction substrates in specific spatial orientations. Chiral COFs with binding sites should be able to load and stabilize MNPs and realize the dual functions of the MNPs and the frameworks.

Dong and co-workers reported a Pd NPs loaded homochiral COF (**Pd@CCOF-MPC**) [145]. The chiral COF support (**CCOF-MPC**) was first synthesized by the combination of cyanuric chloride and *S*-(+)−2-methylpiperazine. The introduction of Pd(II) and sequential $NaBH_4$ reduction resulted in the successful preparation of **Pd@CCOF-MPC** (Fig. 33a). The optically pure chiral COFs act as the asymmetric template to guide the substrates. The active MNPs act as the active catalytic centers to accelerate the reaction. Considering the chiral feature and the embedded highly active Pd NPs within chiral COFs, **Pd@CCOF-MPC** showed excellent catalytic activity and stereoselectivity for the Henry reaction and reductive Heck reaction under the optimized reaction conditions. The larger-sized substrates were notably found unfavorable for the reaction with low yields and inactive enantioselectivity, further indicating that the asymmetric catalytic process occurs inside the COFs channels.

The same research group reported bimetallic NPs-loaded and porphyrin-based homochiral COFs (**Au@CCOF-CuTPP** and **Pd@CCOF-CuTPP**), which show excellent catalytic performance in the thermally-driven asymmetric one-pot Henry and A^3-coupling reactions [146]. The rigid homochiral host framework of the chiral COFs provides a suitable microenvironment to arrange the substrates in specific spatial orientation within the chiral COF confined space (Fig. 33b). Cu-porphyrin involved in the chiral COFs supplies the energy through the photothermal conversion process. The MNPs play the role of active catalytic sites. The synergy of chiral COF confined effect, Cu-porphyrin with enhanced photothermal conversion, and MNPs catalytic activation realize the asymmetric catalysis with high efficiency. In addition, the larger-sized substrates were unfavorable for the reaction with low yields. The pore size of the COF is not large enough for the larger-sized substrate to easily enter the cavity. This also demonstrated that the asymmetric reaction is an inner pore catalytic process.

The availability of the coordination sites within the internal microenvironment makes COFs ideal supports for anchoring various active metal species. Both metal ions and MNPs can be incorporated into COFs. The presence of binding sites is necessary since they can facilitate the loading of the metal species at specific positions, leading to improved loading amount and dispersibility. The metal loading content, dispersibility, uniformity, and stability are important factors for evaluating the quality of the obtained metal-decorated COFs.

Most of the examples discussed in this section focus on the role of active metal species in catalysis. The microenvironment of the COFs is mainly used for increasing the dispersion of metal ions and the confined growth of MNPs. Different from the examples in Sections 1 and 2, the choice of the catalytic reactions in this Section depends on the species of the supported metals, not the COFs structures themselves. The effect of the synergy between the active metal species and the porous channels in the COFs on catalysis would be an interesting topic and can be explored further.

5. Summary

In summary, owing to the powerful tools of organic synthesis, a rich diversity of building blocks could be designed and synthesized, creating a colorful world for COFs. The COFs as catalysts can combine the advantages of both small molecules and polymers, providing a new approach combining the advantages of "homogeneous" and "heterogeneous" catalysts into one single material. The unique and uniform pores in COFs function as nanoreactors that provide a special microenvironment either for the reaction itself or growing MNPs for applications in catalysis. The effect of the confined microenvironment can significantly improve the activity, selectivity, and durability of the catalysts.

There are still many open questions, particularly regarding the stability of the materials and the catalytic mechanisms, that need to be addressed. The stability of COFs still needs to be enhanced as they usually experience a decrease in structural integrity when exposed to harsh conditions, particularly for long reaction times. In traditional COF synthesis, keto-enol tautomerization has been widely used to improve the structure stability. In addition, new linkages beyond B-O bonds and C = N bonds have been developed, such as vinylene, sp^2 carbon−carbon bond, oxazole, thiazole, pyrazine, dioxin, imidazole, aromatic thieno [3,2-*c*]pyridine et al., which could help solve this problem since they exhibit superior stabilities even under harsh conditions. Besides the cleavage of the linkages, another important factor impacting the stability of COF materials is the exfoliation that occurs during catalytic processes. The relatively weak van der Waals force between the adjacent 2D layers sometimes causes the dislocation glide of the layers and influences the regularity of the 2D COF structures. Although the development of 3D COFs could address this issue, the reported 3D COFs for chemical catalysis are still rare. Based on the collected examples, the number of 3D COFs for chemical catalysis is only ~10% of 2D COFs, which indicates that this area may hold promise for future research opportunities that have yet to be explored.

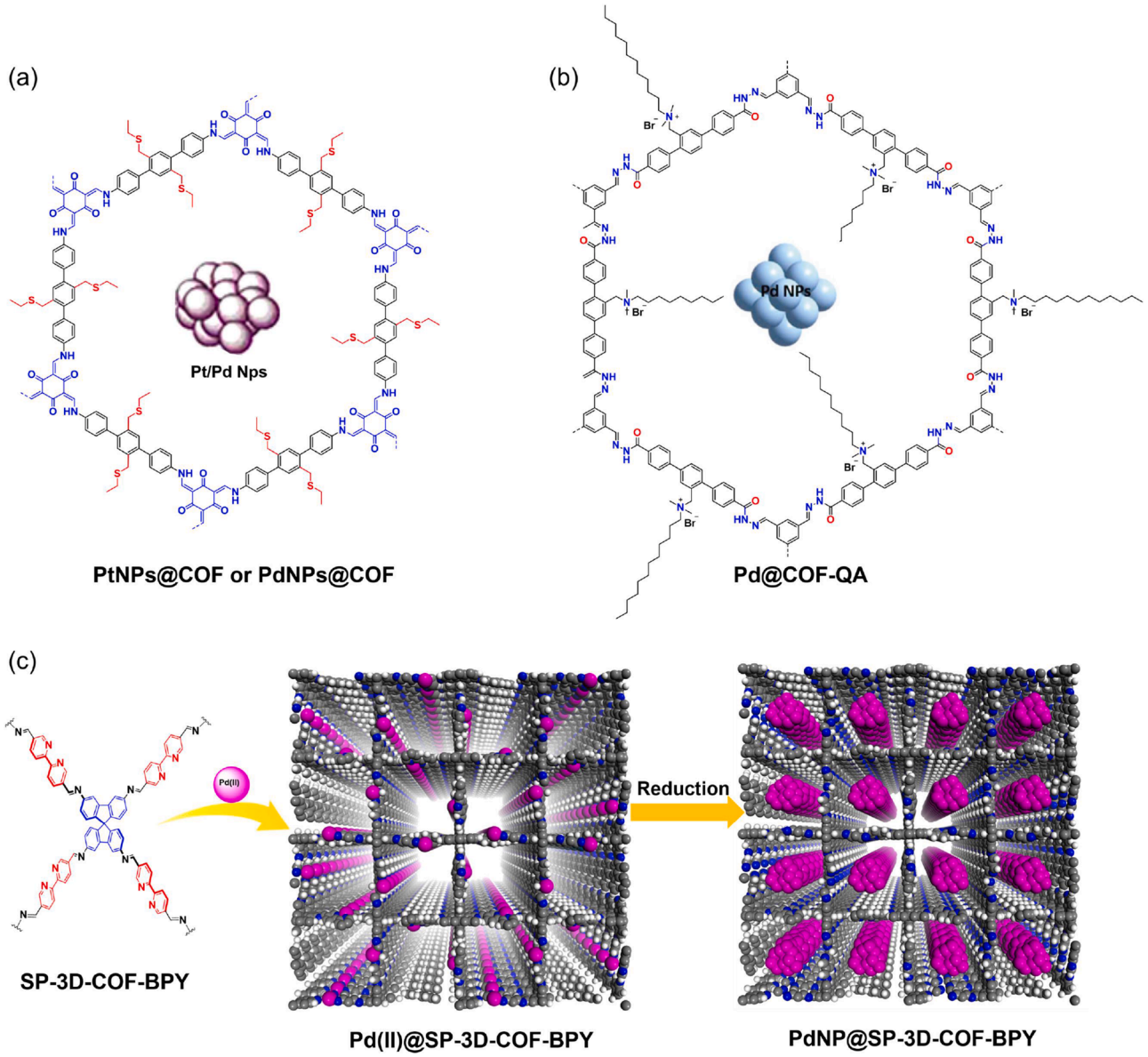

Fig. 31. (a) Schematic representation of the **Thio-COF** supported **PtNPs@COF** or **PdNPs@COF**. Reproduced with permission [141]. Copyright 2017, American Chemical Society. (b) The structure of **Pd@COF-QA**. Reproduced with permission [142]. Copyright 2020, Royal Society of Chemistry. (c) Schematic representation of Pd(II) or Pd NPs impregnation to the **SP-3D-COF-BPY**. Reproduced with permission [143]. Copyright 2020, Chinese Chemical Society.

Moreover, developing more catalytic systems with a clear microenvironment effect during the catalytic process is essential to understanding the mechanism of catalysis in COFs. For example, capturing some active intermediates? Stabilizing transition states? Does the catalytic reaction really proceed inside the COF channels or just on the surface? In addition, how does the cascade reaction proceed in the porous channels? Reasonable control experiments are also crucial in this type of research. The design of similar structures of control COFs and small molecules can verify the roles of the confined channel and the active catalytic sites. Besides, the substrate scope exploration will be helpful in understanding the mechanism. The diverse substrates with different sizes can be used to demonstrate the effect of shape-selectivity, confinement, steric hindrance, and mass transfer process. Different substrates may lead to different catalytic activities due to the microenvironment effect provided by the catalyst, which would help understand the catalytic mechanism.

The uniqueness of these COF-based catalysts compared with small molecule catalysts is their high substrate selectivity at the molecular level. The easy construction of the chiral microenvironment in COFs offers a great advantage in recognizing chiral organic substrates. The combination of the confined effect and enantioselective moieties within COFs may provide a new opportunity for heterogeneous asymmetric catalysis. In most cases, the chiral functions are achieved by the active sites of the enantioselective moieties dangling from the framework, such as proline with the chiral activity. Chiral frameworks with active chiral sites embedded in their backbones rather than attached to their backbones are still less reported but would be highly desirable. Exploring novel chiral functional moieties for the direct construction of a chiral microenvironment, or utilizing achiral molecules to create such an environment, would be of significant interest.

As for the metal-decorated catalytic COFs, it has been widely accepted that active metal species usually play a very important role in catalysis. Achieving precise positioning for the active metal sites within the COF channels remains a great challenge. Surface-adsorbed metal species can also exhibit catalytic activity, which can complicate the assessment. The precise installation of active metal sites in a uniform

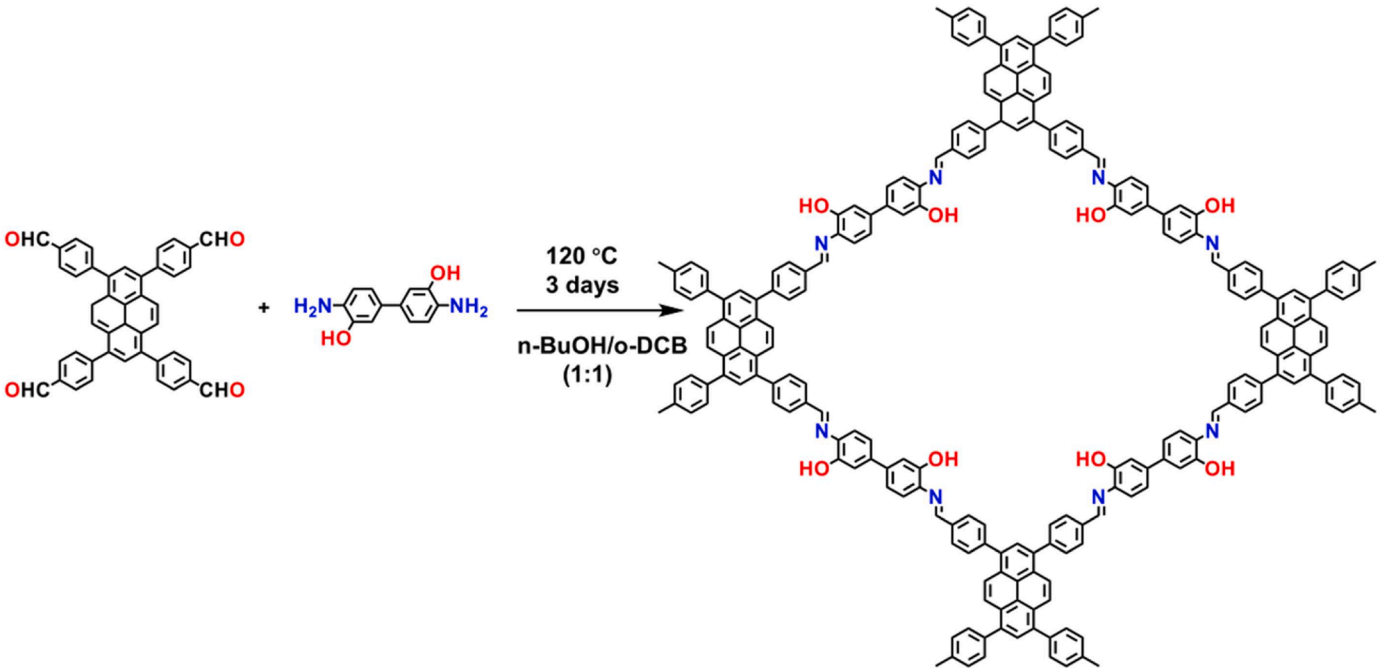

Fig. 32. The synthesis route and structure of **PY-DHBD-COF**. Reproduced with permission [144]. Copyright 2022, Springer Nature.

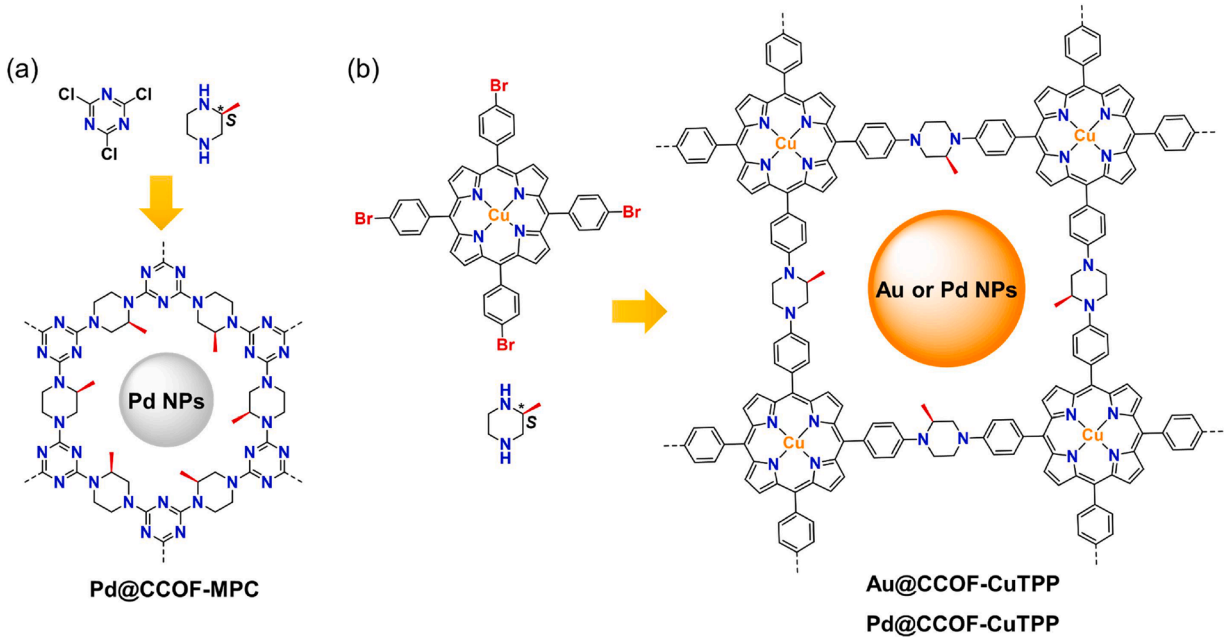

Fig. 33. (a) The structures of monomers and corresponding **Pd@CCOF-MPC**. Reproduced with permission [145]. Copyright 2017, American Chemical Society. (b) The structures of monomers and corresponding **Au@CCOF-CuTPP** and **Pd@CCOF-CuTPP.** Reproduced with permission [146]. Copyright 2019, Springer Nature.

microenvironment is still the goal actively pursued. A promising solution may be directly synthesizing metal-decorated COFs with well-defined structures using the pre-designed monomers with metal binding sites on them. Besides, the recently reported metal-coordinated 3D woven structures provide new insights for the implementation of precise decoration of the frameworks with metal species [147].

Currently, the catalytic study of these metal-decorated COFs focuses only on active metal species. The microenvironment in the COFs plays an important role in well dispersing the metal species by the confined effect. The synergistic catalytic effect enabled by both the microenvironment and the metal species has been paid less attention to. As expected, the cavity in the COFs should not only be used to load metal species but also provide an enabling microenvironment to facilitate catalysis.

In addition, single-atom metal catalysts, where metal atoms are highly dispersed on the support, have seen an explosion in the study of catalysis. The monodispersed metal atoms can be loaded to the support by defect introduction, in-plane atoms replacement, and in-plane atoms coordination. Some electro/photo-catalysis examples have been achieved by single-atom-based COF catalysts [133,148-150]. COFs, with highly ordered structures and large surface areas, have shown promising potential in organocatalysis and chemical energy conversation as precise

structural supports for single-atom catalysis. In the catalytic pockets, the active sites can effectively adsorb and activate substrate molecules, which is conducive to the occurrence of the catalytic reaction process. In addition, the porous channels in the microenvironment can facilitate the rapid transport of reactants and products.

Lastly, in enzyme catalysis, the core of the catalytic process is formed by a pocket with varied pore sizes, shapes, and catalytically active sites. COFs can serve as valuable models for biomimetic enzyme catalysis and recognition due to their "pocket-like" porous structures. Despite their great potential, the use of COF-based emulating enzymes is currently limited and merits further exploration.

The microenvironment in the COF materials is clearly an essential factor for their catalytic activity among all catalytic components, given their precise channel structures and tunable functional groups. Taking advantage of the microenvironment effect, it would address broad interests in developing novel catalytic systems that do not rely on traditional catalysts. Research efforts devoted to this direction would bring the field of developing high-performance heterogeneous catalysts to the next level.

Author contributions

Y.Z and W.Z initiated the concept. Q.P, Z.L, Y.Z and W.Z wrote the review together.

Declaration of Competing Interest

The authors declare that they have no known competing financial interests or personal relationships that could have appeared to influence the work reported in this paper.

Data availability

No data was used for the research described in the article.

Acknowledgments

This work was supported by the University of Colorado Boulder, the National Science Foundation (CHE-2108197), National Natural Science Foundation of China (22175101, 22105112), and the Natural Science Foundation of Shandong Province (ZR2020ZD38).

References

[1] R. Breslo, Biomimetic chemistry and artificial enzymes catalysis by design, Acc. Chem. Res. 28 (1995) 146–153.
[2] Y. Zhang, J. Ge, Z. Liu, Enhanced activity of immobilized or chemically modified enzymes, ACS Catal 5 (2015) 4503–4513.
[3] T. Ennaert, J. Van Aelst, J. Dijkmans, R. De Clercq, W. Schutyser, M. Dusselier, D. Verboekend, B.F. Sels, Potential and challenges of zeolite chemistry in the catalytic conversion of biomass, Chem. Soc. Rev. 45 (2016) 584–611.
[4] M.V. Opanasenko, W.J. Roth, J. Čejka, Two-dimensional zeolites in catalysis: current status and perspectives, Catal. Sci. Technol. 6 (2016) 2467–2484.
[5] M. Dusselier, M.E. Davis, Small-pore zeolites: synthesis and catalysis, Chem. Rev. 118 (2018) 5265–5329.
[6] J. Zhang, L. Wang, Y. Shao, Y. Wang, B.C. Gates, F.S. Xiao, A Pd@Zeolite catalyst for nitroarene hydrogenation with high product selectivity by sterically controlled adsorption in the zeolite micropores, Angew. Chem. Int. Ed. 56 (2017) 9747–9751.
[7] X. Yu, C.T. Williams, Recent advances in the applications of mesoporous silica in heterogeneous catalysis, Catal. Sci. Technol. 12 (2022) 5765–5794.
[8] M. Davidson, Y. Ji, G.J. Leong, N.C. Kovach, B.G. Trewyn, R.M. Richards, Hybrid mesoporous silica/noble-metal nanoparticle materials—synthesis and catalytic applications, ACS Appl. Nano Mater. 1 (2018) 4386–4400.
[9] R. De Clercq, M. Dusselier, E. Makshina, B.F. Sels, Catalytic gas-phase production of lactide from renewable alkyl lactates, Angew. Chem. Int. Ed. 57 (2018) 3074–3078.
[10] C.T. Kresge, M.E. Leonowicz, W.J. Roth, J.C. Vartuli, J.S. Beck, Ordered mesoporous molecular sieves synthesized by a liquid-crystal template mechanism, Nature 359 (1992) 710–712.
[11] X. Yan, L. Chen, H. Song, Z. Gao, H. Wei, W. Ren, W. Wang, Metal–organic framework (MOF)-derived catalysts for chemoselective hydrogenation of nitroarenes, New J. Chem. 45 (2021) 18268–18276.
[12] S. Ko, F. Gao, X. Yao, H. Yi, X. Tang, C. Wang, H. Liu, N. Luo, Z. Qi, Synthesis of metal–organic frameworks (MOFs) and their application in the selective catalytic reduction of NOx with NH3, New J. Chem. 46 (2022) 15758–15775.
[13] R. Matsuda, R. Kitaura, S. Kitagawa, Y. Kubota, R.V. Belosludov, T.C. Kobayashi, H. Sakamoto, T. Chiba, M. Takata, Y. Kawazoe, Y. Mita, Highly controlled acetylene accommodation in a metal-organic microporous material, Nature 436 (2005) 238–241.
[14] T. Uemura, R. Kitaura, Y. Ohta, M. Nagaoka, S. Kitagawa, Nanochannel-promoted polymerization of substituted acetylenes in porous coordination polymers, Angew. Chem. Int. Ed. 45 (2006) 4112–4116.
[15] T. Uemura, D. Hiramatsu, Y. Kubota, M. Takata, S. Kitagawa, Topotactic linear radical polymerization of divinylbenzenes in porous coordination polymers, Angew. Chem. Int. Ed. 46 (2007) 4987–4990.
[16] S. Opelt, V. Krug, J. Sonntag, M. Hunger, E. Klemm, Investigations on stability and reusability of [Pd(2-pymo)2]n as hydrogenation catalyst, Micropor. Mesopor. Mat. 147 (2012) 327–333.
[17] M. Hartmann, M. Fischer, Amino-functionalized basic catalysts with MIL-101 structure, Micropor. Mesopor. Mat. 164 (2012) 38–43.
[18] P. Wu, J. Wang, Y. Li, C. He, Z. Xie, C. Duan, Luminescent sensing and catalytic performances of a multifunctional lanthanide-organic framework comprising a triphenylamine moiety, Adv. Funct. Mater. 21 (2011) 2788–2794.
[19] M. Zheng, Y. Liu, C. Wang, S. Liu, W. Lin, Cavity-induced enantioselectivity reversal in a chiral metal–organic framework Brønsted acid catalyst, Chem. Sci. 3 (2012) 2623–2627.
[20] C. Tan, K. Yang, J. Dong, Y. Liu, Y. Liu, J. Jiang, Y. Cui, Boosting enantioselectivity of chiral organocatalysts with ultrathin two-dimensional metal-organic framework nanosheets, J. Am. Chem. Soc. 141 (2019) 17685–17695.
[21] S.H. Cho, B. Ma, S.T. Nguyen, J.T. Hupp, T.E. Albrecht-Schmitt, A metal-organic framework material that functions as an enantioselective catalyst for olefin epoxidation, Chem. Commun. (2006) 2563–2565.
[22] Y.N. Takayabu, T. Iguchi, M. Kachi, A. Shibata, H.i. Kanzawa, Design and synthesis of an exceptionally stable and highly porous metal-organic framework, Nature 402 (1999) 276–279.
[23] Y. Jin, Y. Hu, W. Zhang, Tessellated multiporous two-dimensional covalent organic frameworks, Nat. Rev. Chem. 1 (2017) 0056.
[24] X. Feng, X. Ding, D. Jiang, Covalent organic frameworks, Chem. Soc. Rev. 41 (2012) 6010–6022.
[25] S.Y. Ding, W. Wang, Covalent organic frameworks (COFs): from design to applications, Chem. Soc. Rev. 42 (2013) 548–568.
[26] Y. Hu, L.J. Wayment, C. Haslam, X. Yang, S.-h. Lee, Y. Jin, W. Zhang, Covalent organic framework based lithium-ion battery: fundamental, design and characterization, EnergyChem 3 (2021), 100048.
[27] A.P. Cote, A.I. Benin, N.W. Ockwig, M. O'Keeffe, A.J. Matzger, O.M. Yaghi, Porous, crystalline, covalent organic frameworks, Science 310 (2005) 1166–1170.
[28] P.J. Waller, F. Gándara, O.M. Yaghi, Chemistry of covalent organic frameworks, Acc. Chem. Res. 48 (2015) 3053–3063.
[29] H.M. El-Kaderi, J.R. Hunt, J.L. Mendoza-Cortes, A.P. Cote, R.E. Taylor, M. O'Keeffe, O.M. Yaghi, Designed synthesis of 3D covalent organic frameworks, Science 316 (2007) 268–272.
[30] K. Geng, T. He, R. Liu, S. Dalapati, K.T. Tan, Z. Li, S. Tao, Y. Gong, Q. Jiang, D. Jiang, Covalent organic frameworks: design, synthesis, and functions, Chem. Rev. 120 (2020) 8814–8933.
[31] Hui Hu, Qianqian Yan, Rile Ge, Y. Gao, Covalent organic frameworks as heterogeneous catalysts, Chinese J. Catal. 39 (2018) 1167–1179.
[32] Y. Yusran, H. Li, X. Guan, Q. Fang, S. Qiu, Covalent organic frameworks for catalysis, EnergyChem 2 (2020), 100035.
[33] H.Y. Cheng, T. Wang, Covalent organic frameworks in catalytic organic synthesis, Adv. Synth. Catal. 363 (2020) 144–193.
[34] D. Ma, Y. Wang, A. Liu, S. Li, C. Lu, C. Chen, Covalent organic frameworks: promising materials as heterogeneous catalysts for C–C bond formations, Catalysts 8 (2018) 404.
[35] H.C. Ma, J. Zou, X.T. Li, G.J. Chen, Y.B. Dong, Homochiral covalent organic frameworks for asymmetric catalysis, Chem. Eur. J. 26 (2020) 13754–13770.
[36] Cha Li, Zining Qiu, H. Sun, Y. Yang, C.-P. Li, Recent progress in covalent organic frameworks (COFs) for electrocatalysis, Chin. J. Struct. Chem. 41 (2022) 2211084–2211099.
[37] A.M. Evans, M.J. Strauss, A.R. Corcos, Z. Hirani, W. Ji, L.S. Hamachi, X. Aguilar-Enriquez, A.D. Chavez, B.J. Smith, W.R. Dichtel, Two-dimensional polymers and polymerizations, Chem. Rev. 122 (2022) 442–564.
[38] J. Liu, N. Wang, L. Ma, Recent advances in covalent organic frameworks for catalysis, Chem. Asian J. 15 (2020) 338–351.
[39] R.K. Sharma, M. Yadav, R. Gupta, P. Rana, A. Srivastava, R. Zboril, R.S. Varma, M. Antonietti, M.B. Gawande, Recent development of covalent organic frameworks (COFs): synthesis and catalytic (organic-electro-photo) applications, Mater. Horiz. 7 (2020) 411–454.
[40] A. López-Magano, S. Daliran, A.R. Oveisi, R. Mas-Balleste, A. Dhakshinamoorthy, J. Alemán, H. Garcia, R. Luque, Recent advances in the use of covalent organic frameworks as heterogenous photocatalysts in organic synthesis, Adv. Mater. (2023), 220945.
[41] R. Schlogl, Heterogeneous catalysis, Angew. Chem. Int. Ed. 54 (2015) 3465–3520.

[42] P.M. Budd, B.S. Ghanem, S. Makhseed, N.B. McKeown, K.J. Msayib, C. E. Tattershall, Polymers of intrinsic microporosity (PIMs): robust, solution-processable, organic nanoporous materials, Chem. Commun. (2004) 230–231.
[43] J.-X. Jiang, F. Su, A. Trewin, C.D. Wood, N.L. Campbell, H. Niu, C. Dickinson, A. Y. Ganin, M.J. Rosseinsky, Y.Z. Khimyak, A.I. Cooper, Conjugated microporous poly(aryleneethynylene) networks, Angew. Chem. Int. Ed. 46 (2007) 8574–8578.
[44] J. Guo, D. Jiang, Covalent organic frameworks for heterogeneous catalysis: principle, current status, and challenges, ACS. Cent. Sci. 6 (2020) 869–879.
[45] Y. Jin, C. Yu, R.J. Denman, W. Zhang, Recent advances in dynamic covalent chemistry, Chem. Soc. Rev. 42 (2013) 6634–6654.
[46] Y. Jin, Y. Zhu, W. Zhang, Development of organic porous materials through Schiff-base chemistry, CrystEngComm 15 (2013) 1484–1499.
[47] A.M. Evans, L.R. Parent, N.C. Flanders, R.P. Bisbey, E. Vitaku, M.S. Kirschner, R. D. Schaller, L.X. Chen, N.C. Gianneschi, W.R. Dichtel, Seeded growth of single-crystal two-dimensional covalent organic frameworks, Science 361 (2018) 52–57.
[48] Y. Du, H. Yang, J.M. Whiteley, S. Wan, Y. Jin, S.H. Lee, W. Zhang, Ionic covalent organic frameworks with spiroborate linkage, Angew. Chem. Int. Ed. 55 (2016) 1737–1741.
[49] Y. Hu, S.J. Teat, W. Gong, Z. Zhou, Y. Jin, H. Chen, J. Wu, Y. Cui, T. Jiang, X. Cheng, W. Zhang, Single crystals of mechanically entwined helical covalent polymers, Nat. Chem. 13 (2021) 660–665.
[50] N. Keller, D. Bessinger, S. Reuter, M. Calik, L. Ascherl, F.C. Hanusch, F. Auras, T. Bein, Oligothiophene-bridged conjugated covalent organic frameworks, J. Am. Chem. Soc. 139 (2017) 8194–8199.
[51] J.X. Ma, J. Li, Y.F. Chen, R. Ning, Y.F. Ao, J.M. Liu, J. Sun, D.X. Wang, Q. Q. Wang, Cage based crystalline covalent organic frameworks, J. Am. Chem. Soc. 141 (2019) 3843–3848.
[52] P.F. Wei, M.Z. Qi, Z.P. Wang, S.Y. Ding, W. Yu, Q. Liu, L.K. Wang, H.Z. Wang, W. K. An, W. Wang, Benzoxazole-linked ultrastable covalent organic frameworks for photocatalysis, J. Am. Chem. Soc. 140 (2018) 4623–4631.
[53] J.M. Seo, H.J. Noh, H.Y. Jeong, J.B. Baek, Converting unstable imine-linked network into stable aromatic benzoxazole-linked one via post-oxidative cyclization, J. Am. Chem. Soc. 141 (2019) 11786–11790.
[54] P.J. Waller, Y.S. AlFaraj, C.S. Diercks, N.N. Jarenwattananon, O.M. Yaghi, Conversion of imine to oxazole and thiazole linkages in covalent organic frameworks, J. Am. Chem. Soc. 140 (2018) 9099–9103.
[55] F. Haase, E. Troschke, G. Savasci, T. Banerjee, V. Duppel, S. Dorfler, M.M. J. Grundei, A.M. Burow, C. Ochsenfeld, S. Kaskel, B.V. Lotsch, Topochemical conversion of an imine- into a thiazole-linked covalent organic framework enabling real structure analysis, Nat. Commun. 9 (2018) 2600.
[56] J. Xu, Y. He, S. Bi, M. Wang, P. Yang, D. Wu, J. Wang, F. Zhang, An olefin-linked covalent organic framework as a flexible thin-film electrode for a high-performance micro-supercapacitor, Angew. Chem. Int. Ed. 58 (2019) 12065–12069.
[57] S. Bi, C. Yang, W. Zhang, J. Xu, L. Liu, D. Wu, X. Wang, Y. Han, Q. Liang, F. Zhang, Two-dimensional semiconducting covalent organic frameworks via condensation at arylmethyl carbon atoms, Nat. Commun. 10 (2019) 2467.
[58] Y. Zhao, H. Liu, C. Wu, Z. Zhang, Q. Pan, F. Hu, R. Wang, P. Li, X. Huang, Z. Li, Fully Conjugated two-dimensional sp(2) -carbon covalent organic frameworks as artificial photosystem i with high efficiency, Angew. Chem. Int. Ed. 58 (2019) 5376–5381.
[59] Y. Wang, W. Hao, H. Liu, R. Chen, Q. Pan, Z. Li, Y. Zhao, Facile construction of fully sp2-carbon conjugated two-dimensional covalent organic frameworks containing benzobisthiazole units, Nat. Commun. 13 (2022) 100.
[60] S. Kandambeth, A. Mallick, B. Lukose, M.V. Mane, T. Heine, R. Banerjee, Construction of crystalline 2D covalent organic frameworks with remarkable chemical (acid/base) stability via a combined reversible and irreversible route, J. Am. Chem. Soc. 134 (2012) 19524–19527.
[61] S. Mitra, S. Kandambeth, B.P. Biswal, M.A. Khayum, C.K. Choudhury, M. Mehta, G. Kaur, S. Banerjee, A. Prabhune, S. Verma, S. Roy, U.K. Kharul, R. Banerjee, Self-exfoliated guanidinium-based ionic covalent organic nanosheets (iCONs), J. Am. Chem. Soc. 138 (2016) 2823–2828.
[62] M.R. Rao, Y. Fang, S. De Feyter, D.F. Perepichka, Conjugated covalent organic frameworks via michael addition-elimination, J. Am. Chem. Soc. 139 (2017) 2421–2427.
[63] X. Guan, H. Li, Y. Ma, M. Xue, Q. Fang, Y. Yan, V. Valtchev, S. Qiu, Chemically stable polyarylether-based covalent organic frameworks, Nat. Chem. 11 (2019) 587–594.
[64] J. Guo, Y. Xu, S. Jin, L. Chen, T. Kaji, Y. Honsho, M.A. Addicoat, J. Kim, A. Saeki, H. Ihee, S. Seki, S. Irle, M. Hiramoto, J. Gao, D. Jiang, Conjugated organic framework with three-dimensionally ordered stable structure and delocalized pi clouds, Nat. Commun. 4 (2013) 2736.
[65] M. Wang, M. Ballabio, M. Wang, H.H. Lin, B.P. Biswal, X. Han, S. Paasch, E. Brunner, P. Liu, M. Chen, M. Bonn, T. Heine, S. Zhou, E. Canovas, R. Dong, X. Feng, Unveiling electronic properties in metal-phthalocyanine-based pyrazine-linked conjugated two-dimensional covalent organic frameworks, J. Am. Chem. Soc. 141 (2019) 16810–16816.
[66] B. Zhang, M. Wei, H. Mao, X. Pei, S.A. Alshmimri, J.A. Reimer, O.M. Yaghi, Crystalline dioxin-linked covalent organic frameworks from irreversible reactions, J. Am. Chem. Soc. 140 (2018) 12715–12719.
[67] P.L. Wang, S.Y. Ding, Z.C. Zhang, Z.P. Wang, W. Wang, Constructing robust covalent organic frameworks via multicomponent reactions, J. Am. Chem. Soc. 141 (2019) 18004–18008.
[68] Y. Wang, H. Liu, Q. Pan, C. Wu, W. Hao, J. Xu, R. Chen, J. Liu, Z. Li, Y. Zhao, Construction of fully conjugated covalent organic frameworks via facile linkage conversion for efficient photoenzymatic catalysis, J. Am. Chem. Soc. 142 (2020) 5958–5963.
[69] Z. Lei, L.J. Wayment, J.R. Cahn, H. Chen, S. Huang, X. Wang, Y. Jin, S. Sharma, W. Zhang, Cyanurate-linked covalent organic frameworks enabled by dynamic nucleophilic aromatic substitution, J. Am. Chem. Soc. 144 (2022) 17737–17742.
[70] C.J. Wu, X.Y. Li, T.R. Li, M.Z. Shao, L.J. Niu, X.F. Lu, J.L. Kan, Y. Geng, Y.B. Dong, Natural sunlight photocatalytic synthesis of benzoxazole-bridged covalent organic framework for photocatalysis, J. Am. Chem. Soc. 144 (2022) 18750–18755.
[71] M. Bhadra, S. Kandambeth, M.K. Sahoo, M. Addicoat, E. Balaraman, R. Banerjee, Triazine functionalized porous covalent organic framework for photo-organocatalytic E- Z isomerization of olefins, J. Am. Chem. Soc. 141 (2019) 6152–6156.
[72] X. Wang, L. Chen, S.Y. Chong, M.A. Little, Y. Wu, W.H. Zhu, R. Clowes, Y. Yan, M. A. Zwijnenburg, R.S. Sprick, A.I. Cooper, Sulfone-containing covalent organic frameworks for photocatalytic hydrogen evolution from water, Nat. Chem. 10 (2018) 1180–1189.
[73] Y. Zhao, Y. Liang, D. Wu, H. Tian, T. Xia, W. Wang, W. Xie, X.M. Hu, X. Tian, Q. Chen, Ruthenium complex of sp(2) carbon-conjugated covalent organic frameworks as an efficient electrocatalyst for hydrogen evolution, Small 18 (2022), 2107750.
[74] M. Liu, Q. Xu, Q. Miao, S. Yang, P. Wu, G. Liu, J. He, C. Yu, G. Zeng, Atomic Co–N4 and Co nanoparticles confined in COF@ZIF-67 derived core–shell carbon frameworks: bifunctional non-precious metal catalysts toward the ORR and HER, J. Mater. Chem. A 10 (2022) 228–233.
[75] B.C. Patra, S. Khilari, R.N. Manna, S. Mondal, D. Pradhan, A. Pradhan, A. Bhaumik, A metal-free covalent organic polymer for electrocatalytic hydrogen evolution, ACS Catal 7 (2017) 6120–6127.
[76] R. Kamai, K. Kamiya, K. Hashimoto, S. Nakanishi, Oxygen-tolerant electrodes with platinum-loaded covalent triazine frameworks for the hydrogen oxidation reaction, Angew. Chem. Int. Ed. 55 (2016) 13184–13188.
[77] P. Das, G. Chakraborty, J. Roeser, S. Vogl, J. Rabeah, A. Thomas, Integrating bifunctionality and chemical stability in covalent organic frameworks via one-pot multicomponent reactions for solar-driven H(2)O(2) production, J. Am. Chem. Soc. 145 (2023) 2975–2984.
[78] S. Mondal, B. Mohanty, M. Nurhuda, S. Dalapati, R. Jana, M. Addicoat, A. Datta, B.K. Jena, A. Bhaumik, A thiadiazole-based covalent organic framework: a metal-free electrocatalyst toward oxygen evolution reaction, ACS Catal. 10 (2020) 5623–5630.
[79] H.B. Aiyappa, J. Thote, D.B. Shinde, R. Banerjee, S. Kurungot, Cobalt-modified covalent organic framework as a robust water oxidation electrocatalyst, Chem. Mater. 28 (2016) 4375–4379.
[80] Z. Xiang, D. Cao, L. Huang, J. Shui, M. Wang, L. Dai, Nitrogen-doped holey graphitic carbon from 2D covalent organic polymers for oxygen reduction, Adv. Mater. 26 (2014) 3315–3320.
[81] D. Li, C. Li, L. Zhang, H. Li, L. Zhu, D. Yang, Q. Fang, S. Qiu, X. Yao, Metal-free thiophene-sulfur covalent organic frameworks: precise and controllable synthesis of catalytic active sites for oxygen reduction, J. Am. Chem. Soc. 142 (2020) 8104–8108.
[82] Q. Zuo, G. Cheng, W. Luo, A reduced graphene oxide/covalent cobalt porphyrin framework for efficient oxygen reduction reaction, Dalton. Trans. 46 (2017) 9344–9348.
[83] H. Zhong, M. Wang, M. Ghorbani-Asl, J. Zhang, K.H. Ly, Z. Liao, G. Chen, Y. Wei, B.P. Biswal, E. Zschech, I.M. Weidinger, A.V. Krasheninnikov, R. Dong, X. Feng, Boosting the electrocatalytic conversion of nitrogen to ammonia on metal-phthalocyanine-based two-dimensional conjugated covalent organic frameworks, J. Am. Chem. Soc. 143 (2021) 19992–20000.
[84] S. Liu, M. Wang, T. Qian, H. Ji, J. Liu, C. Yan, Facilitating nitrogen accessibility to boron-rich covalent organic frameworks via electrochemical excitation for efficient nitrogen fixation, Nat. Commun. 10 (2019) 3898.
[85] M. Jiang, L. Han, P. Peng, Y. Hu, Y. Xiong, C. Mi, Z. Tie, Z. Xiang, Z. Jin, Quasi-phthalocyanine conjugated covalent organic frameworks with nitrogen-coordinated transition metal centers for high-efficiency electrocatalytic ammonia synthesis, Nano Lett 22 (2022) 372–379.
[86] Q.J. Wu, D.H. Si, Q. Wu, Y.L. Dong, R. Cao, Y.B. Huang, Boosting electroreduction of CO(2) over cationic covalent organic frameworks: hydrogen bonding effects of halogen ions, Angew. Chem. Int. Ed. 62 (2023), 202215687.
[87] S. Yang, W. Hu, X. Zhang, P. He, B. Pattengale, C. Liu, M. Cendejas, I. Hermans, X. Zhang, J. Zhang, J. Huang, 2D covalent organic frameworks as intrinsic photocatalysts for visible light-driven CO(2) reduction, J. Am. Chem. Soc. 140 (2018) 14614–14618.
[88] Q. Wu, R.-K. Xie, M.-J. Mao, G.-L. Chai, J.-D. Yi, S.-S. Zhao, Y.-B. Huang, R. Cao, Integration of strong electron transporter tetrathiafulvalene into metalloporphyrin-based covalent organic framework for highly efficient electroreduction of CO2, ACS Energy Lett 5 (2020) 1005–1012.
[89] Q. Fang, S. Gu, J. Zheng, Z. Zhuang, S. Qiu, Y. Yan, 3D microporous base-functionalized covalent organic frameworks for size-selective catalysis, Angew. Chem. Int. Ed. 53 (2014) 2878–2882.**The imine-based 3D COFs show excellent size selectivity in catalyzing Knoevenagel condensation reactions due to the well-defined channels and the base-functionalized groups in the channels**
[90] H. Li, Q. Pan, Y. Ma, X. Guan, M. Xue, Q. Fang, Y. Yan, V. Valtchev, S. Qiu, Three-dimensional covalent organic frameworks with dual linkages for bifunctional cascade catalysis, J. Am. Chem. Soc. 138 (2016) 14783–14788.
[91] D.B. Shinde, S. Kandambeth, P. Pachfule, R.R. Kumar, R. Banerjee, Bifunctional covalent organic frameworks with two dimensional organocatalytic micropores, Chem. Commun. 51 (2015) 310–313.

[92] X. Li, Z. Wang, J. Sun, J. Gao, Y. Zhao, P. Cheng, B. Aguila, S. Ma, Y. Chen, Z. Zhang, Squaramide-decorated covalent organic framework as a new platform for biomimetic hydrogen-bonding organocatalysis, Chem. Commun. 55 (2019) 5423–5426.

[93] Y. Wu, H. Xu, X. Chen, J. Gao, D. Jiang, A pi-electronic covalent organic framework catalyst: pi-walls as catalytic beds for Diels-Alder reactions under ambient conditions, Chem. Commun. 51 (2015) 10096–10098.

[94] Y. Peng, Z. Hu, Y. Gao, D. Yuan, Z. Kang, Y. Qian, N. Yan, D. Zhao, Synthesis of a sulfonated two-dimensional covalent organic framework as an efficient solid acid catalyst for biobased chemical conversion, ChemSusChem 8 (2015) 3208–3212.

[95] J. Zhao, G. Guo, D. Wang, H. Liu, Z. Zhang, L. Sun, N. Ding, Z. Li, Y. Zhao, A "one-step" approach to the highly efficient synthesis of lactide through the confinement catalysis of covalent organic frameworks, Green Chem 25 (2023) 3103–3110.**The precision confinement effect and the functional moieties covered on the channels inside of the obtained 2D COFs allow the highly efficient synthesis of lactide**

[96] L.-G. Ding, B.-J. Yao, F. Li, S.-C. Shi, N. Huang, H.-B. Yin, Q. Guan, Y.-B. Dong, Ionic liquid-decorated COF and its covalent composite aerogel for selective CO2 adsorption and catalytic conversion, J. Mater. Chem. A 7 (2019) 4689–4698.

[97] A. Nagai, Z. Guo, X. Feng, S. Jin, X. Chen, X. Ding, D. Jiang, Pore surface engineering in covalent organic frameworks, Nat. Commun. 2 (2011) 536.

[98] B. Dong, L. Wang, S. Zhao, R. Ge, X. Song, Y. Wang, Y. Gao, Immobilization of ionic liquids to covalent organic frameworks for catalyzing the formylation of amines with CO2 and phenylsilane, Chem. Commun. 52 (2016) 7082–7085.

[99] Z.J. Mu, X. Ding, Z.Y. Chen, B.H. Han, Zwitterionic covalent organic frameworks as catalysts for hierarchical reduction of CO(2) with amine and hydrosilane, ACS Appl. Mater. Interfaces 10 (2018) 41350–41358.

[100] B.J. Yao, W.X. Wu, L.G. Ding, Y.B. Dong, Sulfonic acid and ionic liquid functionalized covalent organic framework for efficient catalysis of the biginelli reaction, J. Org. Chem. 86 (2021) 3024–3032.

[101] C. Xing, P. Mei, Z. Mu, B. Li, X. Feng, Y. Zhang, B. Wang, Enhancing enzyme activity by the modulation of covalent interactions in the confined channels of covalent organic frameworks, Angew. Chem. Int. Ed. 61 (2022), 202201378.

[102] H.S. Xu, S.Y. Ding, W.K. An, H. Wu, W. Wang, Constructing crystalline covalent organic frameworks from chiral building blocks, J. Am. Chem. Soc. 138 (2016) 11489–11492.

[103] C.A. Wang, Z.K. Zhang, T. Yue, Y.L. Sun, L. Wang, W.D. Wang, Y. Zhang, C. Liu, W. Wang, Bottom-up" embedding of the Jorgensen-Hayashi catalyst into a chiral porous polymer for highly efficient heterogeneous asymmetric organocatalysis, Chem. Eur. J. 18 (2012) 6718–6723.

[104] W.K. An, M.Y. Han, C.A. Wang, S.M. Yu, Y. Zhang, S. Bai, W. Wang, Insights into the asymmetric heterogeneous catalysis in porous organic polymers: constructing a TADDOL-embedded chiral catalyst for studying the structure-activity relationship, Chem. Eur. J. 20 (2014) 11019–11028.

[105] D. Wu, F. Xu, B. Sun, R. Fu, H. He, K. Matyjaszewski, Design and preparation of porous polymers, Chem. Rev. 112 (2012) 3959–4015.

[106] P. Kaur, J.T. Hupp, S.T. Nguyen, Porous organic polymers in catalysis: opportunities and challenges, ACS Catal 1 (2011) 819–835.

[107] L.K. Wang, J.J. Zhou, Y.B. Lan, S.Y. Ding, W. Yu, W. Wang, Divergent synthesis of chiral covalent organic frameworks, Angew. Chem. Int. Ed. 58 (2019) 9443–9447.

[108] J. Zhang, X. Han, X. Wu, Y. Liu, Y. Cui, Multivariate chiral covalent organic frameworks with controlled crystallinity and stability for asymmetric catalysis, J. Am. Chem. Soc. 139 (2017) 8277–8285.

[109] J. Zhang, X. Han, X. Wu, Y. Liu, Y. Cui, Chiral DHIP- and pyrrolidine-based covalent organic frameworks for asymmetric catalysis, ACS Sustainable Chem. Eng. 7 (2019) 5065–5071.

[110] X. Wang, X. Han, J. Zhang, X. Wu, Y. Liu, Y. Cui, Homochiral 2D porous covalent organic frameworks for heterogeneous asymmetric catalysis, J. Am. Chem. Soc. 138 (2016) 12332–12335.

[111] B. Hou, S. Yang, K. Yang, X. Han, X. Tang, Y. Liu, J. Jiang, Y. Cui, Confinement-driven enantioselectivity in 3d porous chiral covalent organic frameworks, Angew. Chem. Int. Ed. 60 (2021) 6086–6093.

[112] H.C. Ma, G.J. Chen, F. Huang, Y.B. Dong, Homochiral covalent organic framework for catalytic asymmetric synthesis of a drug intermediate, J. Am. Chem. Soc. 142 (2020) 12574–12578.

[113] J.C. Wang, X. Kan, J.Y. Shang, H. Qiao, Y.B. Dong, Catalytic asymmetric synthesis of chiral covalent organic frameworks from prochiral monomers for heterogeneous asymmetric catalysis, J. Am. Chem. Soc. 142 (2020) 16915–16920.**Chiral COFs were constructed from prochiral monomers via catalytic asymmetric polymerization and promoted asymmetric Michael addition reactions**

[114] H. Xu, J. Gao, D. Jiang, Stable, crystalline, porous, covalent organic frameworks as a platform for chiral organocatalysts, Nat. Chem. 7 (2015) 905–912.**Chiral COFs were prepared through the post-introduction of chiral pyrrolidine units into the pore walls of COFs and are attractive in heterogeneous organocatalysis due to their catalytic activity, enantioselectivity, and recyclability**

[115] H. Xu, X. Chen, J. Gao, J. Lin, M. Addicoat, S. Irle, D. Jiang, Catalytic covalent organic frameworks via pore surface engineering, Chem. Commun. 50 (2014) 1292–1294.

[116] Y. Li, Y. Dong, J.L. Kan, X. Wu, Y.B. Dong, Synthesis and catalytic properties of metal-N-heterocyclic-carbene-decorated covalent organic framework, Org. Lett. 22 (2020) 7363–7368.

[117] X. Han, Q. Xia, J. Huang, Y. Liu, C. Tan, Y. Cui, Chiral covalent organic frameworks with high chemical stability for heterogeneous asymmetric catalysis, J. Am. Chem. Soc. 139 (2017) 8693–8697.**Two chiral COFs were constructed through metal-directed synthesis and serve as efficient heterogeneous catalysts for various asymmetric reactions**

[118] S.Y. Ding, J. Gao, Q. Wang, Y. Zhang, W.G. Song, C.Y. Su, W. Wang, Construction of covalent organic framework for catalysis: pd/COF-LZU1 in Suzuki–Miyaura coupling reaction, J. Am. Chem. Soc. 133 (2011) 19816–19822.**A Pd(II)-containing COFs was successfully constructed through a simple post-treatment and first utilized for highly efficient catalysis**

[119] M. Mu, Y. Wang, Y. Qin, X. Yan, Y. Li, L. Chen, Two-dimensional imine-linked covalent organic frameworks as a platform for selective oxidation of olefins, ACS Appl. Mater. Interfaces 9 (2017) 22856–22863.

[120] Y. Hou, X. Zhang, J. Sun, S. Lin, D. Qi, R. Hong, D. Li, X. Xiao, J. Jiang, Good Suzuki-coupling reaction performance of Pd immobilized at the metal-free porphyrin-based covalent organic framework, Micropor. Mesopor. Mat. 214 (2015) 108–114.

[121] R.S.B. Gonçalves, A.B.V. de Oliveira, H.C. Sindra, B.S. Archanjo, M.E. Mendoza, L.S.A. Carneiro, C.D. Buarque, P.M. Esteves, Heterogeneous catalysis by covalent organic frameworks (COF): pd(OAc)2@COF-300 in cross-coupling reactions, ChemCatChem 8 (2016) 743–750.

[122] R.R. Coombs, M.K. Ringer, J.M. Blacquiere, J.C. Smith, J.S. Neilsen, Y.-S. Uh, J. B. Gilbert, L.J. Leger, H. Zhang, A.M. Irving, S.L. Wheaton, C.M. Vogels, S. A. Westcott, A. Decken, F.J. Baerlocher, Palladium(II) Schiff base complexes derived from sulfanilamides and aminobenzothiazoles, Transit. Metal Chem. 30 (2005) 411–418.

[123] W. Zhang, P. Jiang, Y. Wang, J. Zhang, Y. Gao, P. Zhang, Bottom-up approach to engineer a molybdenum-doped covalent-organic framework catalyst for selective oxidation reaction, RSC Adv 4 (2014) 51544–51547.

[124] R.A. Maia, F. Berg, V. Ritleng, B. Louis, P.M. Esteves, Design, synthesis and characterization of nickel-functionalized covalent organic framework NiCl@RIO-12 for heterogeneous suzuki-miyaura catalysis, Chem. Eur. J. 26 (2020) 2051–2059.

[125] L.H. Li, X.L. Feng, X.H. Cui, Y.X. Ma, S.Y. Ding, W. Wang, Salen-based covalent organic framework, J. Am. Chem. Soc. 139 (2017) 6042–6045.

[126] H. Li, X. Feng, P. Shao, J. Chen, C. Li, S. Jayakumar, Q. Yang, Synthesis of covalent organic frameworks via *in situ* salen skeleton formation for catalytic applications, J. Mater. Chem. A 7 (2019) 5482–5492.

[127] S. Yan, X. Guan, H. Li, D. Li, M. Xue, Y. Yan, V. Valtchev, S. Qiu, Q. Fang, Three-dimensional salphen-based covalent-organic frameworks as catalytic antioxidants, J. Am. Chem. Soc. 141 (2019) 2920–2924.

[128] W. Leng, Y. Peng, J. Zhang, H. Lu, X. Feng, R. Ge, B. Dong, B. Wang, X. Hu, Y. Gao, Sophisticated design of covalent organic frameworks with controllable bimetallic docking for a cascade reaction, Chem. Eur. J. 22 (2016) 9087–9091.

[129] W. Leng, R. Ge, B. Dong, C. Wang, Y. Gao, Bimetallic docked covalent organic frameworks with high catalytic performance towards tandem reactions, RSC Adv 6 (2016) 37403–37406.

[130] P.M. Heintz, B.P. Schumacher, M. Chen, W. Huang, L.M. Stanley, A Pd(II)-functionalized covalent organic framework for catalytic conjugate additions of arylboronic acids to β,β-disubstituted enones, ChemCatChem 11 (2019) 4286–4290.

[131] Q. Sun, B. Aguila, J. Perman, N. Nguyen, S. Ma, Flexibility matters: cooperative active sites in covalent organic framework and threaded ionic polymer, J. Am. Chem. Soc. 138 (2016) 15790–15796.

[132] H. Vardhan, L. Hou, E. Yee, A. Nafady, M.A. Al-Abdrabalnabi, A.M. Al-Enizi, Y. Pan, Z. Yang, S. Ma, Vanadium docked covalent-organic frameworks: an effective heterogeneous catalyst for modified mannich-type reaction, ACS Sustainable Chem. Eng. 7 (2019) 4878–4888.

[133] T. He, Z. Zhao, R. Liu, X. Liu, B. Ni, Y. Wei, Y. Wu, W. Yuan, H. Peng, Z. Jiang, Y. Zhao, Porphyrin-based covalent organic frameworks anchoring au single atoms for photocatalytic nitrogen fixation, J. Am. Chem. Soc. 145 (2023) 6057–6066.

[134] H. Hu, S. Lu, T. Li, Y. Zhang, C. Guo, H. Zhu, Y. Jin, M. Du, W. Zhang, Controlled growth of ultrafine metal nanoparticles mediated by solid supports, Nanoscale Adv 3 (2021) 1865–1886.

[135] M. Bhadra, H.S. Sasmal, A. Basu, S.P. Midya, S. Kandambeth, P. Pachfule, E. Balaraman, R. Banerjee, Predesigned metal-anchored building block for in situ generation of pd nanoparticles in porous covalent organic framework: application in heterogeneous tandem catalysis, ACS Appl. Mater. Interfaces 9 (2017) 13785–13792.

[136] P. Pachfule, S. Kandambeth, D.Diaz Diaz, R. Banerjee, Highly stable covalent organic framework-Au nanoparticles hybrids for enhanced activity for nitrophenol reduction, Chem. Commun. 50 (2014) 3169–3172.

[137] P. Pachfule, M.K. Panda, S. Kandambeth, S.M. Shivaprasad, D.D. Díaz, R. Banerjee, Multifunctional and robust covalent organic framework–nanoparticle hybrids, J. Mater. Chem. A 2 (2014) 7944–7952.

[138] D. Kaleeswaran, R. Antony, A. Sharma, A. Malani, R. Murugavel, Catalysis and CO2 capture by palladium-incorporated covalent organic frameworks, Chempluschem 82 (2017) 1253–1265.

[139] D. Mullangi, D. Chakraborty, A. Pradeep, V. Koshti, C.P. Vinod, S. Panja, S. Nair, R. Vaidhyanathan, Highly stable COF-supported Co/Co(OH)(2) nanoparticles heterogeneous catalyst for reduction of nitrile/nitro compounds under mild conditions, Small 14 (2018), 1801233.

[140] G.J. Chen, X.B. Li, C.C. Zhao, H.C. Ma, J.L. Kan, Y.B. Xin, C.X. Chen, Y.B. Dong, Ru Nanoparticles-loaded covalent organic framework for solvent-free one-pot tandem reactions in air, Inorg. Chem. 57 (2018) 2678–2685.

[141] S. Lu, Y. Hu, S. Wan, R. McCaffrey, Y. Jin, H. Gu, W. Zhang, Synthesis of ultrafine and highly dispersed metal nanoparticles confined in a thioether-containing covalent organic framework and their catalytic applications, J. Am. Chem. Soc.

139 (2017) 17082–17088.**A thioether-containing COF was constructed for the confined growth and size-controlled synthesis of ultrafine NPs for highly efficient catalysis**
[142] J.-C. Wang, C.-X. Liu, X. Kan, X.-W. Wu, J.-L. Kan, Y.-B. Dong, Pd@COF-QA: a phase transfer composite catalyst for aqueous Suzuki–Miyaura coupling reaction, Green Chem 22 (2020) 1150–1155.
[143] Y. Liu, C. Wu, Q. Sun, F. Hu, Q. Pan, J. Sun, Y. Jin, Z. Li, W. Zhang, Y. Zhao, Spirobifluorene-based three-dimensional covalent organic frameworks with rigid topological channels as efficient heterogeneous catalyst, CCS Chem 3 (2021) 2418–2427.
[144] Y. Li, L. Yang, H. He, L. Sun, H. Wang, X. Fang, Y. Zhao, D. Zheng, Y. Qi, Z. Li, W. Deng, In situ photodeposition of platinum clusters on a covalent organic framework for photocatalytic hydrogen production, Nat. Commun. 13 (2022) 1355.
[145] H.-C. Ma, J.-L. Kan, G.-J. Chen, C.-X. Chen, Y.-B. Dong, Pd NPs-loaded homochiral covalent organic framework for heterogeneous asymmetric catalysis, Chem. Mater. 29 (2017) 6518–6524.
[146] H.C. Ma, C.C. Zhao, G.J. Chen, Y.B. Dong, Photothermal conversion triggered thermal asymmetric catalysis within metal nanoparticles loaded homochiral covalent organic framework, Nat. Commun. 10 (2019) 3368.
[147] Y. Liu, Y. Ma, Y. Zhao, X. Sun, F. Gándara, H. Furukawa, Z. Liu, H. Zhu, C. Zhu, K. Suenaga, P. Oleynikov, A.S. Alshammari, X. Zhang, O. Terasaki, O.M. Yaghi, Weaving of organic threads into a crystalline covalent organic framework, Science 351 (2016) 365–369.
[148] P. Dong, Y. Wang, A. Zhang, T. Cheng, X. Xi, J. Zhang, Platinum single atoms anchored on a covalent organic framework: boosting active sites for photocatalytic hydrogen evolution, ACS Catal. 11 (2021) 13266–13279.
[149] L. Ran, Z. Li, B. Ran, J. Cao, Y. Zhao, T. Shao, Y. Song, M.K.H. Leung, L. Sun, J. Hou, Engineering single-atom active sites on covalent organic frameworks for boosting CO(2) photoreduction, J. Am. Chem. Soc. 144 (2022) 17097–17109.
[150] W. Weng, J. Guo, The effect of enantioselective chiral covalent organic frameworks and cysteine sacrificial donors on photocatalytic hydrogen evolution, Nat. Commun. 13 (2022) 5768.

Qingyan Pan received her Ph.D. degree from Qingdao University of Science and Technology (QUST) in 2020. She is now working in Prof. Yingjie Zhao's group as a research assistant professor at QUST. Her research interest is the design and synthesis of porous nanomaterials based on covalent organic frameworks and graphdiyne for energy storage and conversion applications.

Zepeng Lei earned his B.S. degree in Chemistry from Fudan University in 2017 and completed his Ph.D. in Chemistry at the University of Colorado Boulder in 2023. Currently, he is serving as a post-doctoral research fellow in Prof. Wei Zhang's research group at the University of Colorado Boulder. His-primary research interests revolve around the creation of innovative polymeric materials utilizing dynamic covalent chemistry.

Yingjie Zhao obtained his PhD from the Institute of Chemistry, Chinese Academy of Sciences, in 2011. From 2011 to 2016, he did post-doctoral research at the University of Geneva and ETH Zürich, successively. In 2016, he joined Qingdao University of Science and Technology to start his independent research and was promoted to Full Professor in the same year. The main research interests of Zhao are crystalline nanoporous materials and supramolecular chemistry.

Wei Zhang received his B.S. in Chemistry from Peking University in 2000, and his Ph.D. in Chemistry from University of Illinois at Urbana-Champaign (UIUC) in 2005. After a postdoc stint at MIT, he started his independent career at University of Colorado Boulder in 2008. Currently he is a full professor and serves as the Chair of the Department. His-research is focused on utilizing dynamic covalent chemistry to develop novel organic and hybrid functional materials targeting a broad range of environmental, energy and biological applications.